Title

Properties of the ▯' Meson

Permalink

https://escholarship.org/uc/item/9b17q88j

Author

Rittenberg, Alan

Publication Date

1969-06-01

UCRL-18863

PROPERTIES OF THE η' MESON

Alan Rittenberg
(Ph.D. Thesis)

June 4, 1969

AEC Contract No. W-7405-eng-48

[illegible] Sept. 1969

UCRL-18863

LAWRENCE RADIATION LABORATORY
UNIVERSITY of CALIFORNIA BERKELEY

PROPERTIES OF THE η' MESON

Contents

PROPERTIES OF THE η' MESON

Alan Rittenberg

Lawrence Radiation Laboratory
University of California
Berkeley, California

June 4, 1969

ABSTRACT

The $\eta'(958)$ meson has been studied in the reaction $K^-p \rightarrow \Lambda\eta'$, with K^- beam momenta ranging from 1.70 to 2.65 Gev/c. The Dalitz plots of η' decay into $\pi^+\pi^-\eta$ and $\pi^+\pi^-\gamma$ have been examined, and from them we have determined that the most likely quantum numbers of the η' are $I^GJ^P = 0^+0^-$, although $J^P = 2^-$ cannot be completely ruled out. We have also shown that the decay into $\pi^+\pi^-\gamma$ is mediated by the decay $\eta' \rightarrow \rho^0\gamma$. An examination of the production process has yielded further evidence for the $J^P = 0^-$ assignment and suggested that the process takes place via $K^*(891)$ exchange in the t channel. Branching fractions and cross sections have been determined, and finally a search for a negatively charged η' in the deuterium reaction $K^-d \rightarrow p\Lambda\eta'^-$ has confirmed the $I = 0$ assignment for the η'.

I. INTRODUCTION

The η' meson, originally called X^o and sometimes referred to as η^*, was discovered independently in 1964 by two groups.[1,2] It was found to have a mass of about 960 Mev and a width $\Gamma \lesssim 10$ Mev. The reactions in which the meson was observed were

$$\begin{aligned} K^- p \rightarrow\ & \Lambda + \text{neutrals}\ , \\ & \Lambda\, \pi^+ \pi^- + \text{neutrals}\ , \\ \text{and}\qquad & \Lambda\, \pi^+ \pi^+ \pi^- \pi^- \pi^o\ , \end{aligned}$$

where, in each reaction, the effective mass of the particles recoiling against the Λ exhibited an enhancement in the 960 Mev region. In addition, it was observed that the latter two reactions contained an η in the final state, indicating that $\pi^+\pi^-\eta$ was a preferred mode of decay of the η'. Studies analyzing the $\pi\pi\eta$ Dalitz plot and taking into account the apparent absence of a $\pi^+\pi^-\pi^o$ decay mode[1,3,4] suggested the quantum number assignments $I^G J^P = 0^+ 0^-$. A $\pi^+\pi^-\gamma$ mode of decay, consisting primarily of $\rho^o\gamma$, was subsequently found and gave further evidence for these assignments.[3-6]

It is the purpose of this paper to present additional data on the η', thereby hopefully establishing its quantum numbers and branching fractions more firmly.

II. DATA PRODUCTION AND REDUCTION

A. The Beam and Exposure

The data for this experiment were obtained during the years 1963-1965 from an exposure of the Alvarez Group 72" bubble chamber to a separated K^- beam extracted from the Lawrence Radiation Laboratory's Bevatron.

The beam particles were produced on an internal flip target exposed to $\sim 10^{12}$ protons per pulse, at a proton kinetic energy of 6 Gev. The extracted particles passed through a beam transport system designed primarily by Dr. Joseph J. Murray.[7] This system, depicted in Figure 1, consisted of two stages of electrostatic separation, which will be briefly described here.

The initial momentum selection was performed by the Bevatron field. The quadrupoles Q1 - Q3 then served to produce a parallel beam in the first electrostatic separator S1, operated at a field of 100kV/cm. Upon exiting from S1, the particles were refocused by quadrupoles Q4 - Q6 to form an image of the target at the first mass slit. Additional momentum selection and beam steering were obtained by use of bending magnet M3. The mass slit, of a special shape and tilted with respect to the beam to take account of momentum dispersion and chromatic aberration, produced a π/K rejection ratio of ~ 100. The above process was then repeated in the second stage, yielding a total π/K rejection of $\sim 10^5$. Since the "rejected" π's were not actually stopped by the slits, but rather had their momentum degraded, the final bending magnet M4 was used to sweep out these degraded π's.

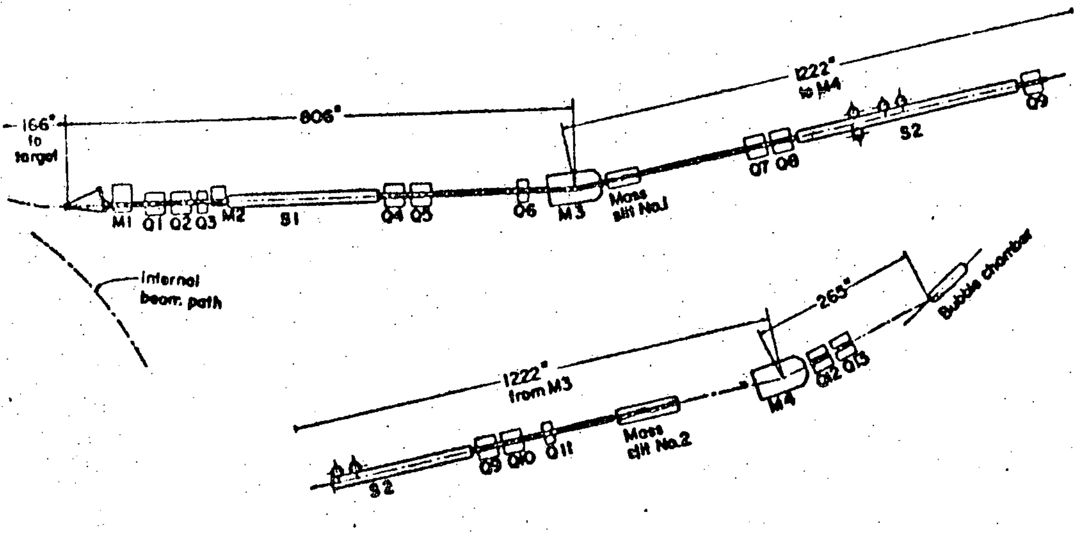

MU-36827

Figure 1. Schematic diagram of the beam layout for this experiment.

Finally, quadrupoles Q12 and Q13 served to align and focus the beam for entrance into the chamber.

The typical yield of this transport system was 6 - 10 K^- per pulse, with a π^- contamination which varied from $\sim 5\%$ at lower momenta to $\sim 20\%$ at higher momenta. The momentum bite was $\Delta p/p \approx \pm 1\frac{1}{2}\%$.

The 72" bubble chamber was filled with hydrogen for most of the running, but an exposure was also made with deuterium. Table I gives the number of pictures taken at each setting. Because of their closeness, the 2.59, 2.64, and 2.73 Gev/c settings will be combined for the purposes of this paper, producing a sample of data with central momentum 2.65 Gev/c.

Figure 2 shows a plot of the beam momentum of a selected sample of our events.

B. Scanning

All of the film listed in Table I was scanned once for every event topology possible, with the exception of simple 0, 1, and 2 prongs with no associated decay. Each event found, of which there were some 370,000 in hydrogen and 160,000 in deuterium, together with a code number for its topology, its location in the chamber, and any special information such as associated electron pairs or secondary scatters, was recorded on a magnetic tape "master list." This master list then provided a complete record of the history of each event as it passed through the various phases of data analysis. The Group A program LYRIC[8] was used for all the bookkeeping work of the experiment.

Table I. Exposure parameters.

P_{beam} (Gev/c)		Number of Pictures		Path Length (events/μb)	
Hydrogen					
1.70		155,000		3.28 ± 0.06	
2.10		145,000		5.76 ± 0.09	
2.47		70,000		1.76 ± 0.05	
2.59	2.65	160,000	510,000	3.44 ± 0.07	12.77 ± 0.16
2.64		220,000		6.15 ± 0.12	
2.73		130,000		3.18 ± 0.08	
Deuterium					
2.11		65,000		2.71 ± 0.14	
2.65		80,000		2.84 ± 0.14	

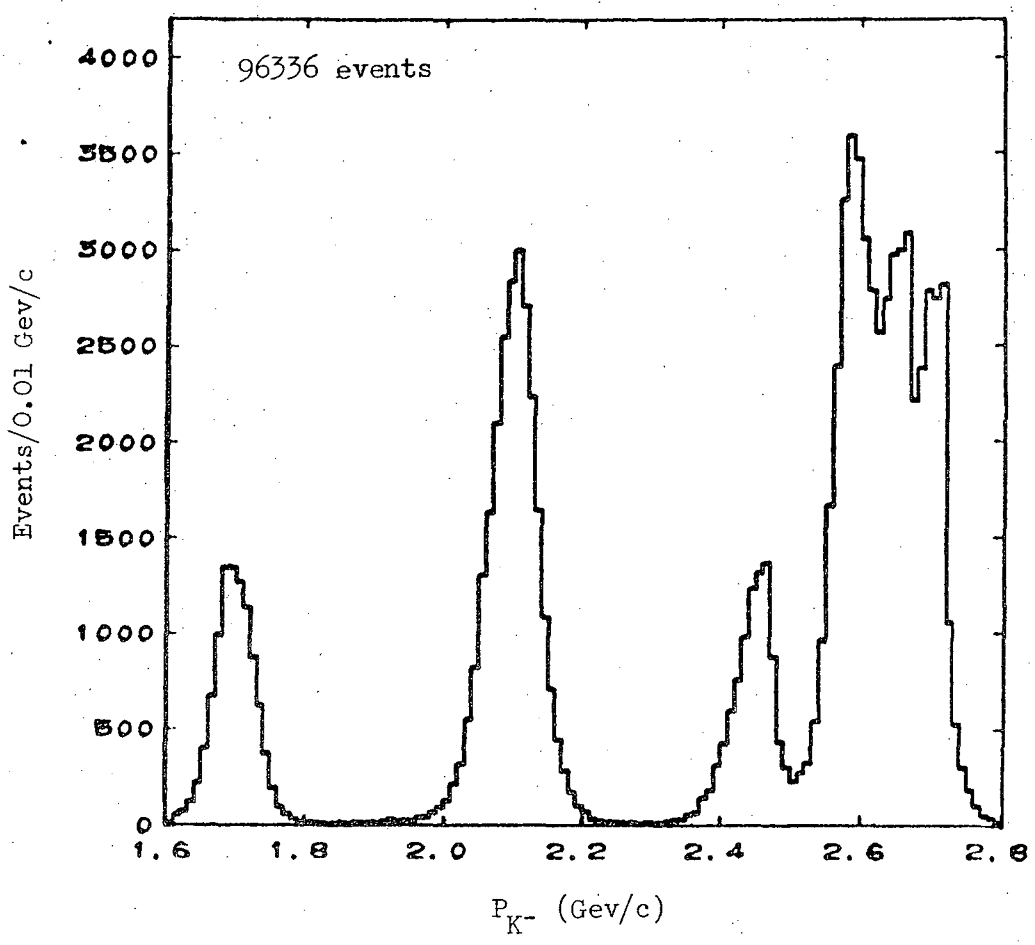

Figure 2. Plot of the fitted beam momentum, P_{K^-}, for a selected sample of K^-p events.

In order to determine the K^- path lengths at each of our momentum settings, use was made of the fact that a K^- of a given momentum has a known probability of decaying into $\pi^+\pi^-\pi^-$ while passing through the chamber. By counting the number N_τ of such τ decays, we can thus determine the number of K^- at each momentum setting. The path length λ, in events/μb is then given by the expression

$$\lambda = N \frac{\rho}{m_T} \frac{pc}{m_K} \frac{\tau_{K^-}}{f} \times 10^{-30} \quad ,$$

where τ_{K^-} is the mean life of a K^-, f is the branching fraction of K^- into $\pi^+\pi^-\pi^-$, ρ is the density of the liquid in grams/cm^3, m_T is the mass of the target atom in grams, m_K is the mass of a K^- in Gev, p is the momentum of the beam in Gev/c, and c is the speed of light in cm/sec. In actuality, because of the difficulty in distinguishing a τ decay from other 3-charged-body decays of the K^-, the total number of 3-charged-body decays was counted and the appropriate value of f was used. The path lengths thus determined are given in Table I. The values for the hydrogen data[9] are for a somewhat more restricted fiducial volume than that used for the deuterium data.

For this paper the topologies of interest are those with a Vee and 0, 2, or 4 prongs in the H_2 data, and those with a Vee and 1, 2, 3, or 4 prongs in the D_2 data. For the deuterium events, the scanners included in the topology code an indication as to whether there was a stopping proton, a probable (non-stopping) proton, or definitely no proton of momentum <500 Mev/c, at the primary vertex of the event. Since we will be concerned here only with interactions off the neutron, where the proton is thus a relatively slow "spectator" proton, only the first two classes of D_2 events have been considered. Table II gives the total number of events found on the initial scan in each of the topologies referred to above.

In addition to the primary scan, about 90% of the film was scanned a second time. For 10% of the hydrogen film and 3% of the deuterium film the first and second scans were compared, event by event. All discrepancies found were looked at on the scan table a third time and the discrepancy resolved. In this manner, we were able to calculate a scanning efficiency for each topology. This efficiency takes into account both events that were missed and those that were misidentified as to topology. Because the latter correction is included, the efficiency for a given topology may be greater than 100% if more events are falsely called that topology than are missed or falsely called another topology. The scanning efficiencies for the events of interest here are given in Table II. (For the hydrogen V-4 prongs and for all the deuterium topologies, all momenta were combined for the calculations because of limited statistics.) The overall efficiency for these events is 100 ± 3%, resulting from 5% of the events being missed and 5% spurious events being picked up. It should be noted that the efficiencies presented in Table II were calculated only for those events where the Vee was not too close to the primary interaction vertex. Events with close-in Vees are very likely to be misidentified on both scans, since the Vee may appear to be simply two more prongs at the interaction vertex. A correction for these events will be included separately when branching fractions, cross sections, and angular

Table II. Numbers of events scanned and scanning efficiencies for topologies of interest in this paper.

Hydrogen

P_{beam} (Gev/c)	V-0 Prongs		V-2 Prongs		V-4 Prongs	
	Number Scanned	Scanning Efficiency %	Number Scanned	Scanning Efficiency %	Number Scanned	Scanning Efficiency %
1.70	11860	99 ± 1	17339	102 ± 1	146	100 ± 2
2.10	14750	98 ± 1	29870	100 ± 1	642	100 ± 2
2.47	3964	95 ± 2	8914	100 ± 1	426	100 ± 2
2.65	26013	98 ± 1	62827	100 ± 1	3874	100 ± 2

Deuterium

P_{beam} (Gev/c)	V-1 and -2 Prongs		V-3 and -4 Prongs	
	Number Scanned	Scanning Efficiency %	Number Scanned	Scanning Efficiency %
2.11	11766	99 ± 4	2369	97 ± 6
2.65	9769	99 ± 4	3521	97 ± 6

distributions are discussed.

C. Measuring

After scanning, the events were measured on either a Franckenstein, an SMP, or a Spiral Reader measuring machine.[10] A large fraction of those events which subsequently failed in the geometric reconstruction or kinematic fitting programs, to be described below, were measured a second time, and a fraction of those still failing were measured one or more times. An average of $\sim 25\%$ of events in all categories failed to be successfully processed through the kinematics program (excluding the V-0 prongs at 1.70 Gev/c which were not measured at all). These events fall into three broad areas: 1) those which are difficult to measure because of obscured vertices, a small angle scatter on a track, a steeply dipping track, or other such problems; 2) those where there was a measuring operator mistake; and 3) those which were called the wrong topology by the original scanner and thus rejected by the measurer. Since cases 1) and 2) are bona fide events and case 3) is already accounted for by the scanning efficiency, we may calculate a measuring efficiency by dividing the number of events which have been successfully processed through the kinematics program by the corrected number of events scanned. The results of this calculation, with one modification, are presented in Table III. The modification consists of taking into account the fact that the final states we will be interested in have a slightly different probability for being successfully processed than the events as a whole. This results from the events of interest

Table III. Measuring efficiencies for the topologies of interest in this paper.

Hydrogen

P_{beam} (Gev/c)	V-0 Prongs %	V-2 Prongs %	V-4 Prongs %
1.70	0	77 ± 2	76 ± 7
2.10	46 ± 1	82 ± 2	78 ± 4
2.47	84 ± 3	88 ± 3	71 ± 4
2.65	65 ± 2	79 ± 2	80 ± 3

Deuterium

P_{beam} (Gev/c)	V-1 and -2 Prongs %	V-3 and -4 Prongs %
2.11	62 ± 3	78 ± 5
2.65	53 ± 3	78 ± 5

having different lab momenta, on the average, from the total sample, which in turn affects the success of the kinematic fitting procedure.

D. Geometric Reconstruction, Kinematic Fitting, and Hypothesis Decision Making

Those events measured on the Spiral Reader (the V-1 and -2 prongs from deuterium) were first processed through the filter program POOH[11] which picks out the tracks of the event from among the coordinate points digitized by the Reader. The output from POOH and the output from the Franckensteins and SMP's were put through PANAL,[12] a reformatting and gross-error-checking program.

The next step in the processing consisted of geometric reconstruction and kinematic fitting by the program PACKAGE.[13] PACKAGE reconstructs each track of the event in 3-dimensional space and then attempts fits to a number of specified hypotheses as to the identity of each particle in the event, requiring energy and momentum balance at each vertex. For each hypothesis tried, PACKAGE outputs the chi-square for the fit, the fitted momentum vector for each track, and the error matrix for the fit. Or, if no fit is possible, a reject code is produced. Also output by PACKAGE are the unfitted, or measured, momentum vectors.

The final decision as to the correct set of particles for the event was made in the program DSTEXAM,[14] which reads the output of PACKAGE as reduced and reformatted by WRING and AFREET.[15] DSTEXAM constructs a confidence level for each complete hypothesis in the following manner. Since PACKAGE generally fits each vertex in the event separately, DSTEXAM first determines which individual vertex fits are involved in the complete hypothesis. For example, in the reaction $K^- p \rightarrow \Lambda \pi^+ \pi^- \pi^o$ followed by the decay $\Lambda \rightarrow p \pi^-$, there are two vertices involved -- one for the production of $\Lambda \pi^+ \pi^- \pi^o$ and one for the decay of the Λ. The chi-squares χ_i^2 for the fits to all the vertices are summed, as are the constraint classes LC_i of the fits:

$$\chi^2_{total} = \Sigma \chi_i^2$$
$$LC_{total} = \Sigma LC_i \quad .$$

The constraint class of a vertex is the number of constraint equations at the vertex (which is always four, resulting from energy and vector momentum balance) minus the number of unmeasured momentum quantities, the latter resulting from either neutral particles or badly measured charged tracks. In actuality, because it is known that PACKAGE tends to under-estimate the errors of measured tracks, each χ_i^2 in the sum above is multiplied by a suitably determined correction factor which is dependent upon LC_i. A confidence level is then computed in the standard manner. It should be noted that this confidence level is not strictly correct, both because of the incorrect estimation of errors referred to above and because the vertices of the event are not fit completely independently; that is, PACKAGE does use the momentum of a decaying particle, as determined from the decay fit, in making the production fit. However, a plot of the confidence level obtained as above generally has the desired flat shape; there tends to be some peaking at very low values resulting from poorly measured events.

In addition to the over-constrained hypotheses discussed above, all topologies have a number of "missing mass" hypotheses. These consist of those cases where two or more neutral particles which do not decay visibly in the chamber are assumed to have been produced in the reaction. For these cases, no fit can be attempted and thus no genuine confidence level can be constructed. However, it was found that a pseudo-confidence level could be computed for such hypotheses, which served as a first order approximation in separating missing mass events from constrained events. This computation is based on an empirically determined expression which takes into account the extent to which the missing energy (excess of energy in the initial state over that of the measured particles in the final state) exceeds that which would be expected if only one non-visibly decaying neutral particle were produced. It also takes into account the quality of the corresponding fits with zero or one non-decaying neutral. The details of this calculation can be found in the reference cited above for DSTEXAM.

After calculating the confidence levels of all hypotheses in the above manner, the event is assigned to that hypothesis with the highest confidence level, provided this is greater than 0.005. If no hypothesis has a confidence level > 0.005, the event is put on the list to be remeasured.

For many events there will be two or more hypotheses which have acceptable fits. For events measured on a Franckenstein or SMP, about half of these ambiguous events were looked at on the scanning table and the ionization of the tracks was used to rule out certain hypotheses where possible. For those events measured on the Spiral Reader, the ionization of each track is output by the Reader, and where this information was reliable it was used rather than having the events looked at again. For those ambiguous events where the ambiguity was not resolvable or resolved, we assume that statistically the hypothesis with the highest confidence level is the correct one. Certain checks were made to see that biases introduced by this assumption were not significant.

III. OBSERVATION OF THE η' IN K^-p INTERACTIONS

The reactions with which we shall be most concerned here are the following

$$\begin{array}{lll} 1) & K^- p & \rightarrow \Lambda \pi^+ \pi^+ \pi^- \pi^- \pi^0 \\ 2) & & \rightarrow \Lambda \pi^+ \pi^- \, MM \\ 3) & & \rightarrow \Lambda \pi^+ \pi^- \pi^0 \\ 4) & & \rightarrow \Lambda \, MM \end{array}$$

where MM represents a missing mass, or in other words two or more non-decaying neutral particles. In all cases we consider only those events where the Λ has decayed into a proton and a π^-. Thus reaction 1) is a V-4 prong event, 2) and 3) are V-2 prongs, and 4) is a V-0 prong. The data to be shown are from the 2.10 to 2.65 Gev/c film.

A. The $\Lambda \pi^+ \pi^+ \pi^- \pi^- \pi^0$ Final State

We begin by discussing reaction 1). Figure 3 shows a plot of the effective mass of the 5π system, defined by

$$M_{5\pi} = \Big[(E_{\pi^+} + E_{\pi^+} + E_{\pi^-} + E_{\pi^-} + E_{\pi^0})^2 - (\vec{p}_{\pi^+} + \vec{p}_{\pi^+} + \vec{p}_{\pi^-} + \vec{p}_{\pi^-} + \vec{p}_{\pi^0})^2\Big]^{\frac{1}{2}} .$$

In the region of 960 Mev there is a pronounced enhancement, with a width of ~ 20 Mev, roughly comparable to our experimental resolution as determined from the fitted momentum vector errors. If we define the four-momentum transfer squared to the proton-Λ system (or,

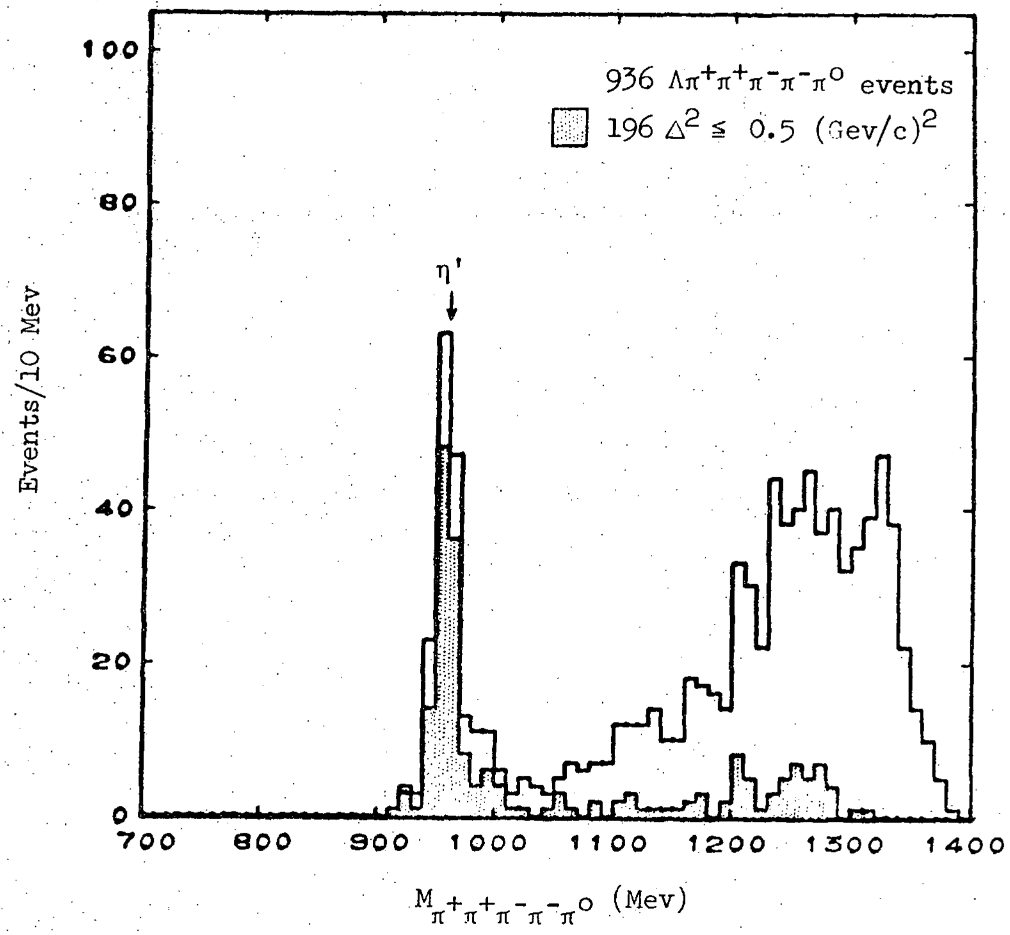

Figure 3. The $M_{\pi^+\pi^+\pi^-\pi^-\pi^0}$ mass spectrum for events fitting the reaction $K^-p \rightarrow \Lambda\pi^+\pi^+\pi^-\pi^-\pi^0$. The shaded events are those with $\Delta^2 \leqq 0.5$ (Gev/c)^2.

equivalently, to the K^--5π system) by

$$\Delta^2 = -t = \left[(\vec{p}_\Lambda - \vec{p}_p)^2 - (E_\Lambda - E_p)^2\right]$$
$$= \left[(\vec{p}_{5\pi} - \vec{p}_{K-})^2 - (E_{5\pi} - E_{K-})^2\right]$$

and make a Chew-Low plot of Δ^2 versus $M_{5\pi}$, Figure 4 results. It is clear that the 960 Mev region events prefer a low momentum transfer. The shaded portion of Figure 3 is a plot of those events which remain when a cut of $\Delta^2 \leqq 0.5$ $(\text{Gev/c})^2$ is applied. These two plots suggest that a resonance decaying into 5 pions is being produced by a peripheral mechanism. It is this resonance which is the η'.

It we next plot $M_{5\pi}$ versus the effective mass of each of the four $\pi^+\pi^-\pi^o$ combinations which can be formed among the 5 pions, as is done in Figure 5 for the low Δ^2 events, we see that $M_{\pi^+\pi^-\pi^o}$ tends to cluster near the η mass of 549 Mev. Figure 6 shows a histogram of $M_{\pi^+\pi^-\pi^o}$ (4 combinations) for events with $950 \leqq M_{5\pi} \leqq 970$ Mev and low Δ^2. The peak at the η mass is seen to contain roughly one-quarter of the event-combinations. Since each event is plotted four times, this indicates that essentially all of the η' events are of the form

$$\begin{array}{lll} K^- p \rightarrow \Lambda\ \eta' & & \\ \qquad\qquad\ \ \llcorner\!\!\rightarrow \pi^+\ \pi^-\ \eta & & \\ \qquad\qquad\qquad\qquad\quad \llcorner\!\!\rightarrow \pi^+\ \pi^-\ \pi^o\ . & & \end{array}$$

That is, the η' mode observed here is $\pi^+\pi^-\eta$. It should be noted that the resolution of our experiment is such that the "π^o" in some of these events may in fact be a γ from the η decay mode $\eta \rightarrow \pi^+\pi^-\gamma$.

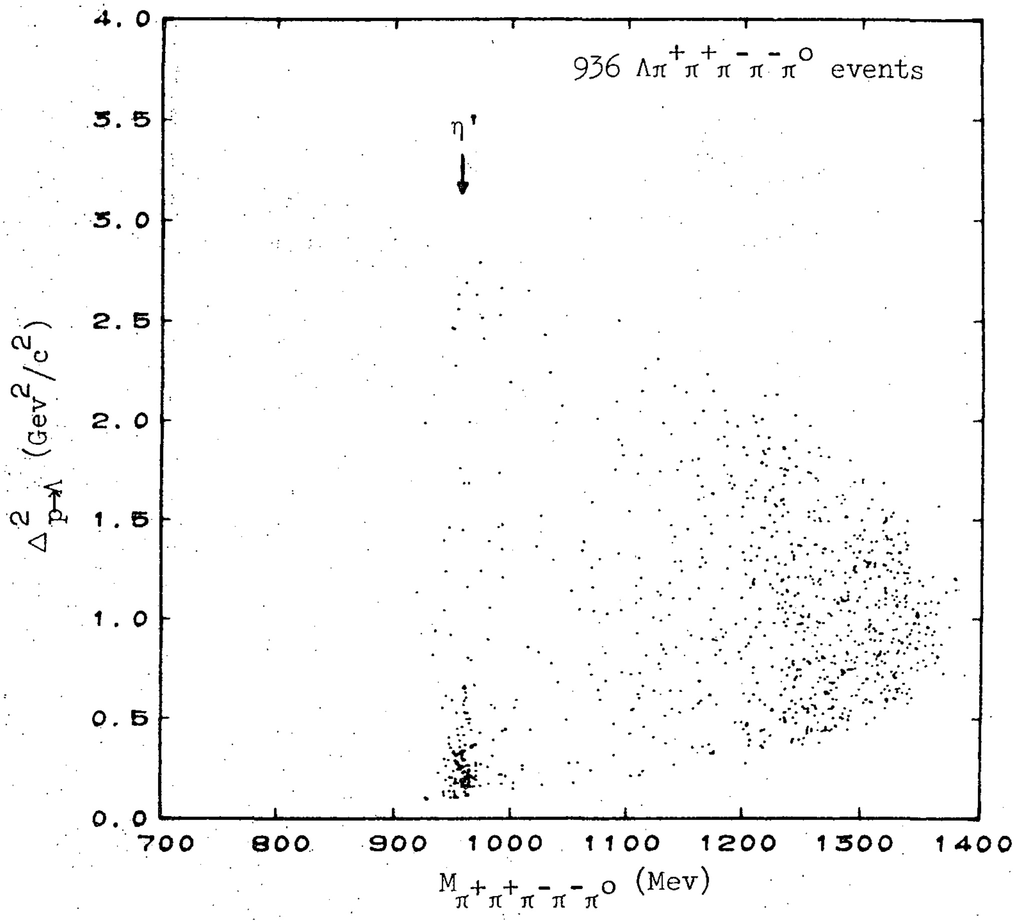

Figure 4. The Chew-Low plot for the $\Lambda\pi^+\pi^+\pi^-\pi^-\pi^0$ events of Figure 3, showing Δ^2 versus $M_{\pi^+\pi^+\pi^-\pi^-\pi^0}$.

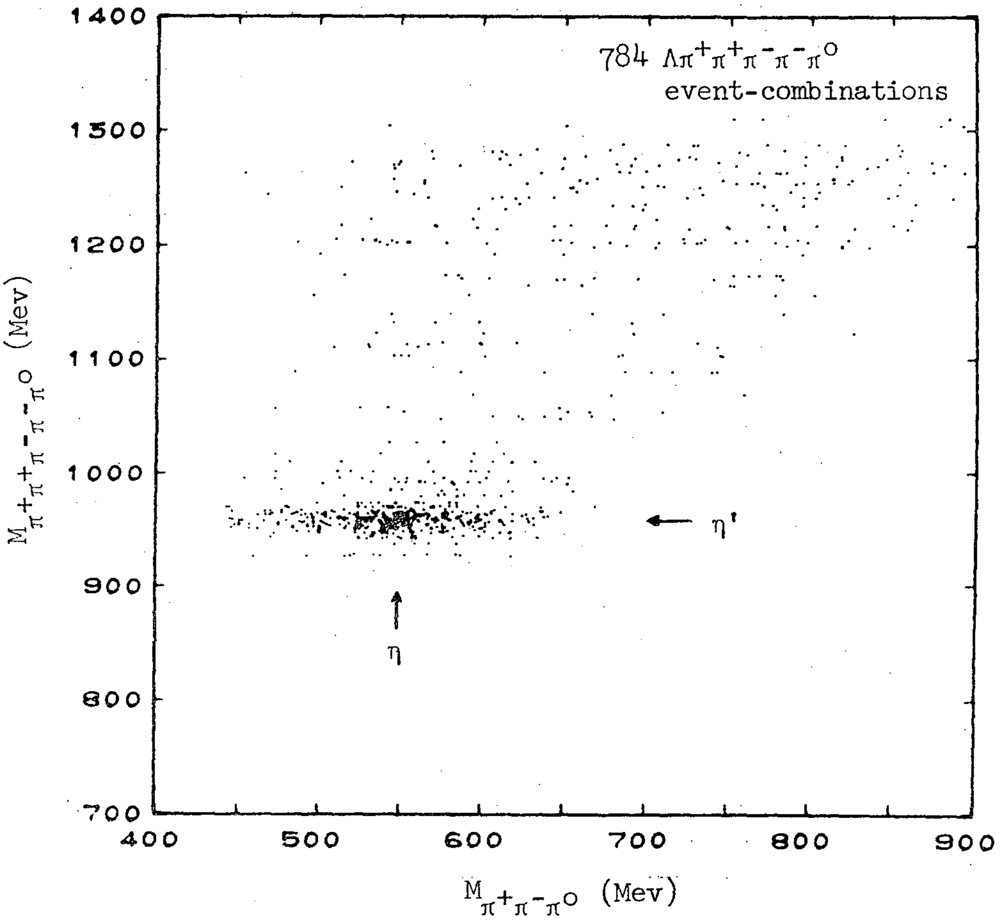

Figure 5. $M_{\pi^+\pi^+\pi^-\pi^-\pi^0}$ versus $M_{\pi^+\pi^-\pi^0}$ for $\Lambda\pi^+\pi^+\pi^-\pi^-\pi^0$ events with low Δ^2. Each event is plotted four times, representing the four $\pi^+\pi^-\pi^0$ combinations which can be formed.

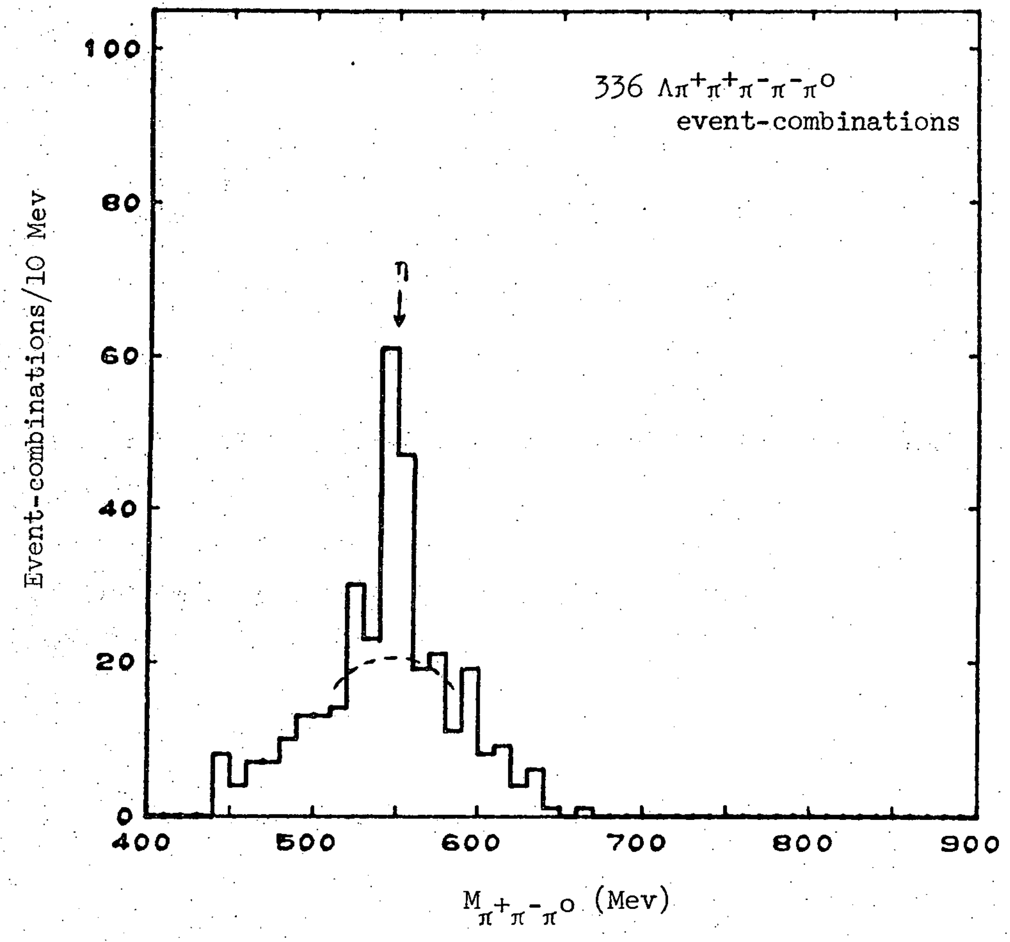

Figure 6. The projection of Figure 5 onto the $M_{\pi^+\pi^-\pi^0}$ axis for those $\Lambda\pi^+\pi^+\pi^-\pi^-\pi^0$ events with $950 \leq M_{\pi^+\pi^+\pi^-\pi^-\pi^0} \leq 970$ Mev. Again each event appears four times. The peak at the η mass, measured from the dashed line upward, contains one-quarter of the event-combinations.

B. The $\Lambda\, \pi^+ \pi^-$ MM Final State

We turn next to reaction 2): $K^- p \to \Lambda\pi^+\pi^-$MM. Figure 7 shows a histogram of the $\pi^+\pi^-$MM effective mass. Again we see an excess of events at a mass of ~960 Mev, and this excess is further enhanced by requiring that $\Delta^2 \leqq 0.5$ (Gev/c)^2 as seen in the shaded histogram. Here, as in the $\Lambda 5\pi$ final state, Δ^2 is the momentum transfer squared to the proton-Λ system. Figure 8 shows the relevant Chew-Low plot. If we make a scatter plot of $M_{\pi^+\pi^-MM}$ versus the missing mass MM for the low Δ^2 events, Figure 9 results. Figure 9, and its projection on the MM axis for $950 \leqq M_{\pi^+\pi^-MM} \leqq 970$ Mev shown in Figure 10, indicates that the missing mass for at least most of the 960 Mev events is that of an η. Thus we are again seeing the $\pi^+\pi^-\eta$ decay mode of the η', but here the η is decaying neutrally:

$$\begin{array}{l} K^- \; p \;\to\; \Lambda \; \eta' \\ \qquad\qquad\quad \hookrightarrow \pi^+ \; \pi^- \; \eta \\ \qquad\qquad\qquad\qquad\quad \hookrightarrow \text{all neutrals} \; . \end{array}$$

Figure 11 shows the $\pi^+\pi^-$MM effective mass, after a cut is applied to the missing mass to restrict it to the η region: $530 \leqq \text{MM} \leqq 570$ Mev. For the low Δ^2 events (shaded portion), the peak is seen to stand out extremely clearly.

C. The Λ MM Final State

For reaction 4), namely $K^- p \to \Lambda$MM, the quantity of interest is the missing mass. Figure 12 shows a plot of this mass, for all values of Δ^2, and for $\Delta^2 \leqq 0.5$ (Gev/c)^2. Although there is more background

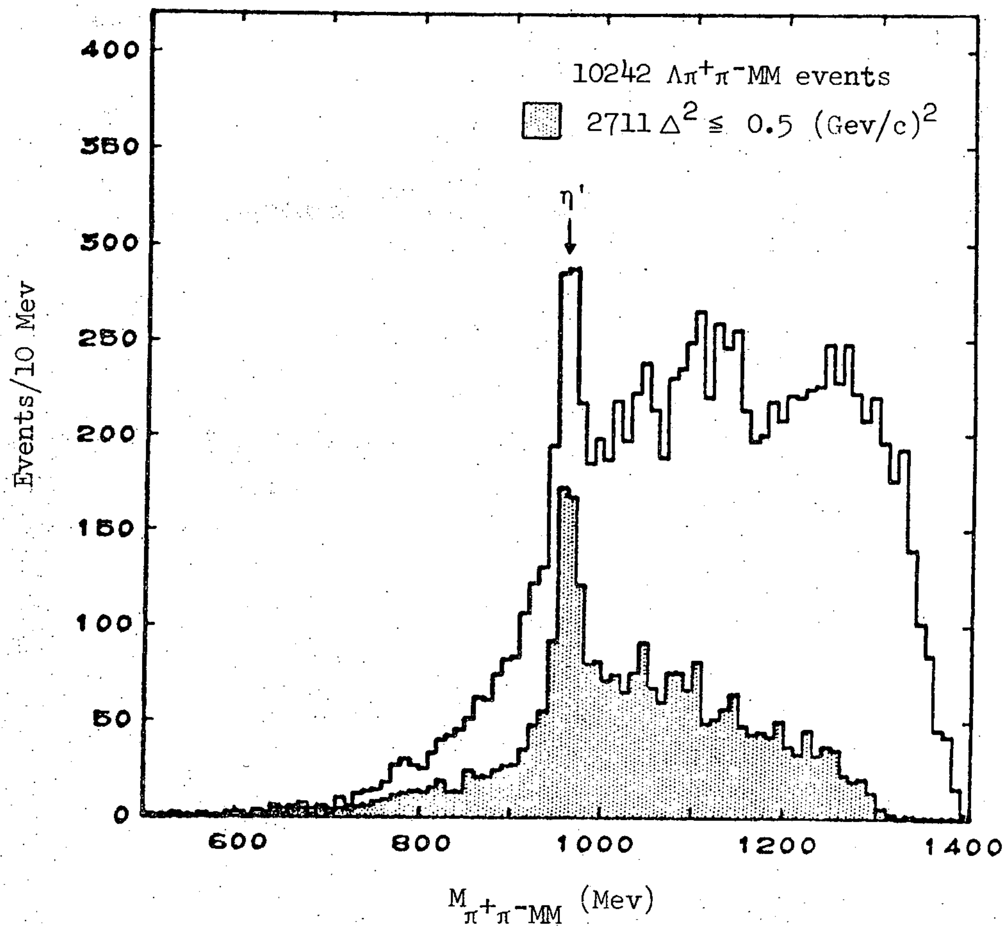

Figure 7. A plot of $M_{\pi^+\pi^-MM}$ for events assigned to the $K^-p \rightarrow \Lambda\pi^+\pi^-MM$ hypothesis. Events with $\Delta^2 \leq$ 0.5 (Gev/c)^2 are shown shaded.

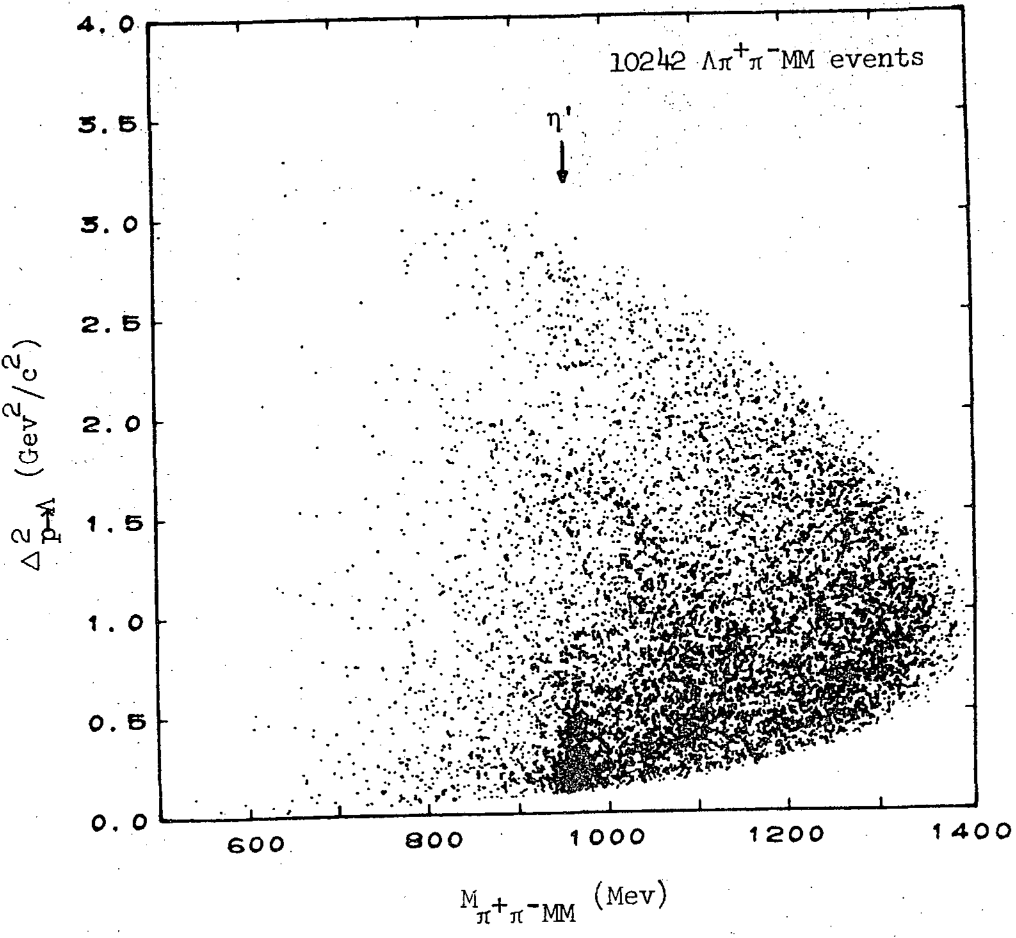

Figure 8. The Chew-Low plot for the $\Lambda\pi^+\pi^-MM$ events of Figure 7, showing Δ^2 versus $M_{\pi^+\pi^-MM}$. The sharp change in density part way up the plot results from the kinematic boundary of the 2.10 Gev/c events.

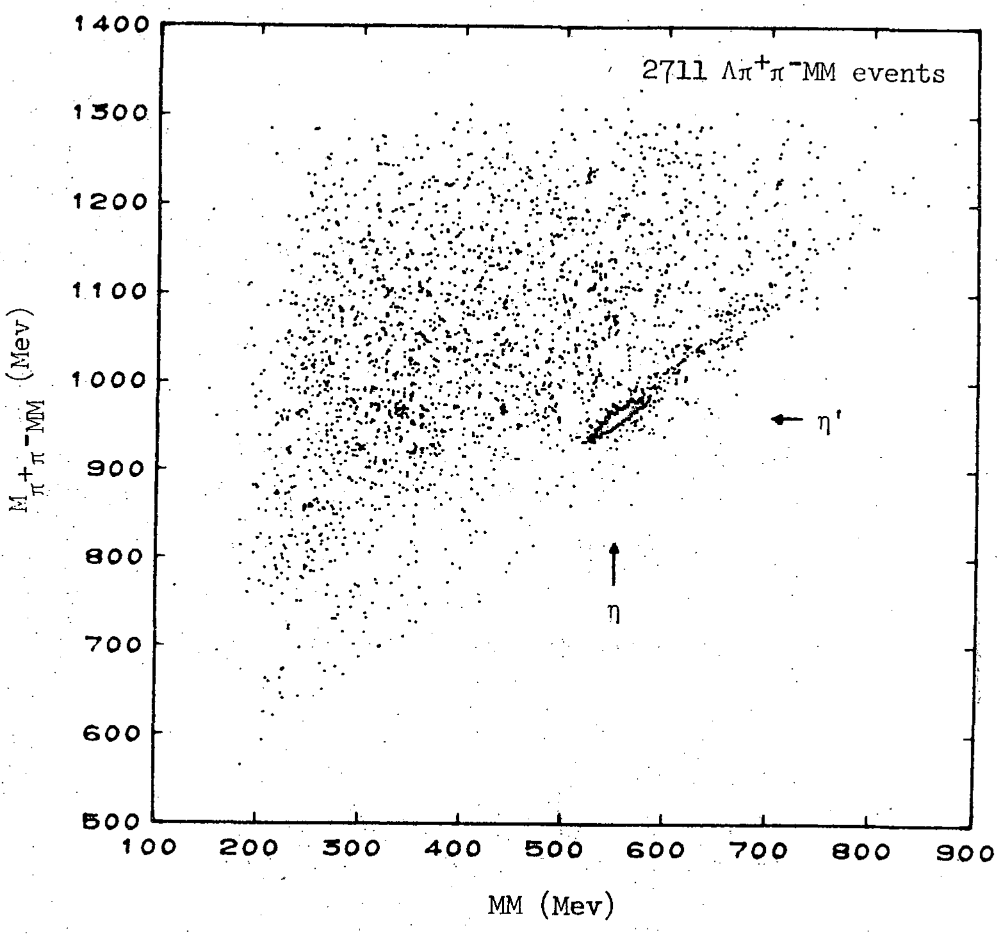

Figure 9. A scatter plot of $M_{\pi^+\pi^-MM}$ versus the missing mass MM, for $\Lambda\pi^+\pi^-$MM events with low Δ^2. The cluster at MM ≈ 550 Mev represents events where the missing mass is an η. The unusual shape and orientation of the cluster results from correlations in the errors of the two masses plotted.

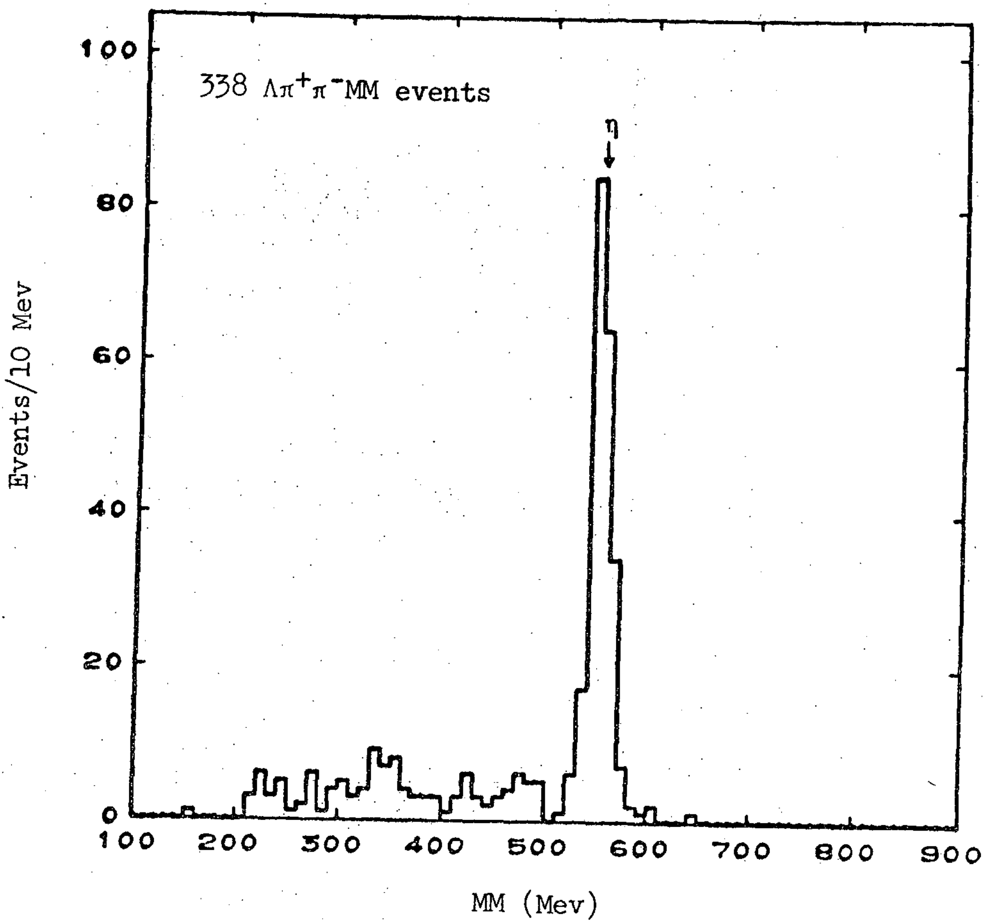

Figure 10. The projection of Figure 9 onto the MM axis for $\Lambda\pi^+\pi^-$MM events with $950 \leq M_{\pi^+\pi^-MM} \leq 970$ Mev.

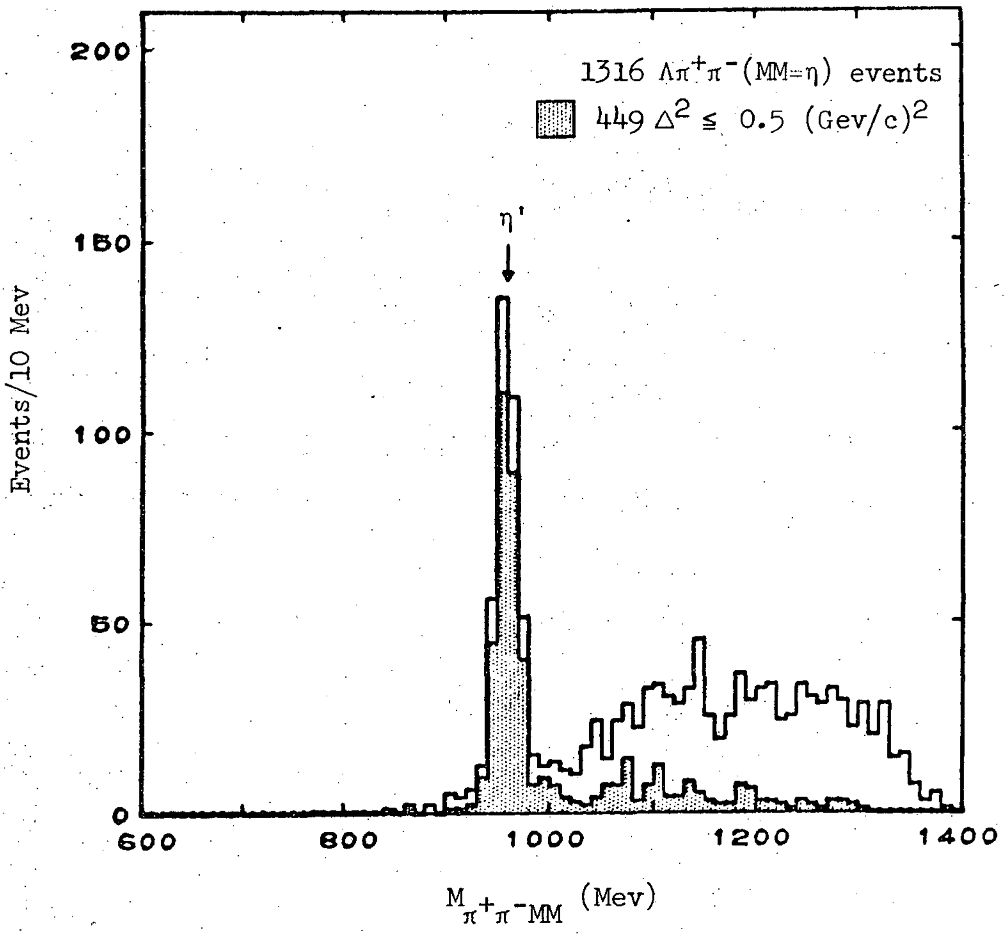

Figure 11. Plot of $M_{\pi^+\pi^-MM}$ for those $\Lambda\pi^+\pi^-$MM events having the missing mass MM in the η region: 530 ≤ MM ≤ 570 Mev. The low Δ^2 events are shown shaded.

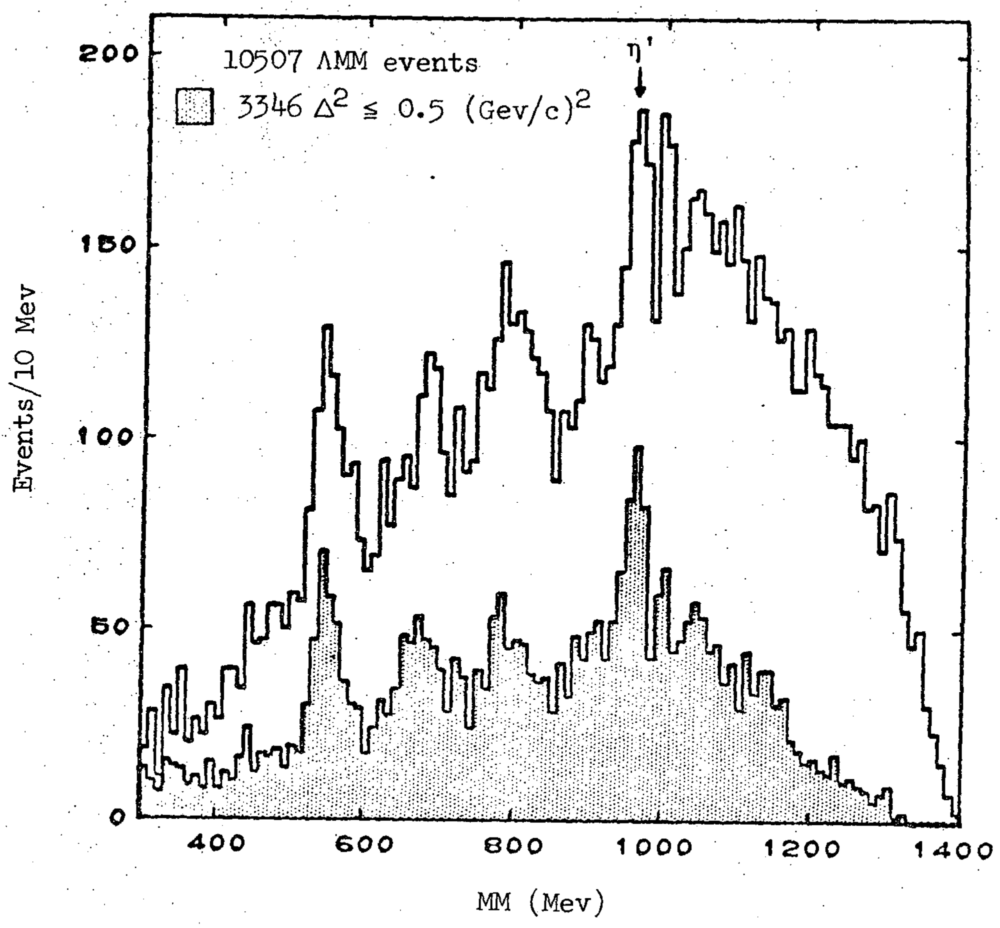

Figure 12. Plot of the missing mass MM from $K^-p \rightarrow \Lambda MM$ events; the shaded events are those with $\Delta^2 \leq 0.5$ (Gev/c)^2.

here than in the previous two cases, we see a peak once more at ~ 960 Mev, indicating an all neutral decay mode of the η':

$$\begin{tikzcd} K^- p \arrow[r] & \Lambda\, \eta' \arrow[d] \\ & \text{all neutrals .} \end{tikzcd}$$

Figure 13 shows the relevant Chew-Low plot for this channel.

D. The $\Lambda\, \pi^+\, \pi^-\, \pi^0$ Final State

Finally we turn to reaction 3): $K^- p \rightarrow \Lambda\pi^+\pi^-\pi^0$. Figure 14 shows a histogram of the $\pi^+\pi^-\pi^0$ effective mass, for all events and for those with $\Delta^2 \leq 0.5\ (\text{Gev}/c)^2$. In addition to peaks at the η, ω, and ϕ masses, there is once again a peak in the 960 Mev region, and the Chew-Low plot in Figure 15 indicates these events prefer a low Δ^2. We are thus tempted to conclude that this indicates a $\pi^+\pi^-\pi^0$ decay mode of the η'. However, as pointed out above in connection with the $\Lambda 5\pi$ events, a π^0 and a γ can easily fake each other in our experiment due to the size of our resolution. Further, since the hypothesis $K^- p \rightarrow \Lambda\pi^+\pi^-\gamma$ was not tried for our V-2 prongs, any real $\Lambda\pi^+\pi^-\gamma$ events would likely be forced into the $\Lambda\pi^+\pi^-\pi^0$ category. To investigate the possibility that the "π^0"'s in the η' region are in fact γ's, we make the following scatter plot: Consider all those events that were called $\Lambda\pi^+\pi^-\pi^0$ or $\Lambda\pi^+\pi^-$MM and which have no acceptable fit for either $\Lambda\pi^+\pi^-$ or $\Sigma^0\pi^+\pi^-$. For these events, using the fitted Λ from the decay vertex and the measured momenta of the charged tracks, we construct a missing mass momentum four-vector. We then plot the mass of the $\pi^+\pi^-$MM system versus the mass-squared of the MM

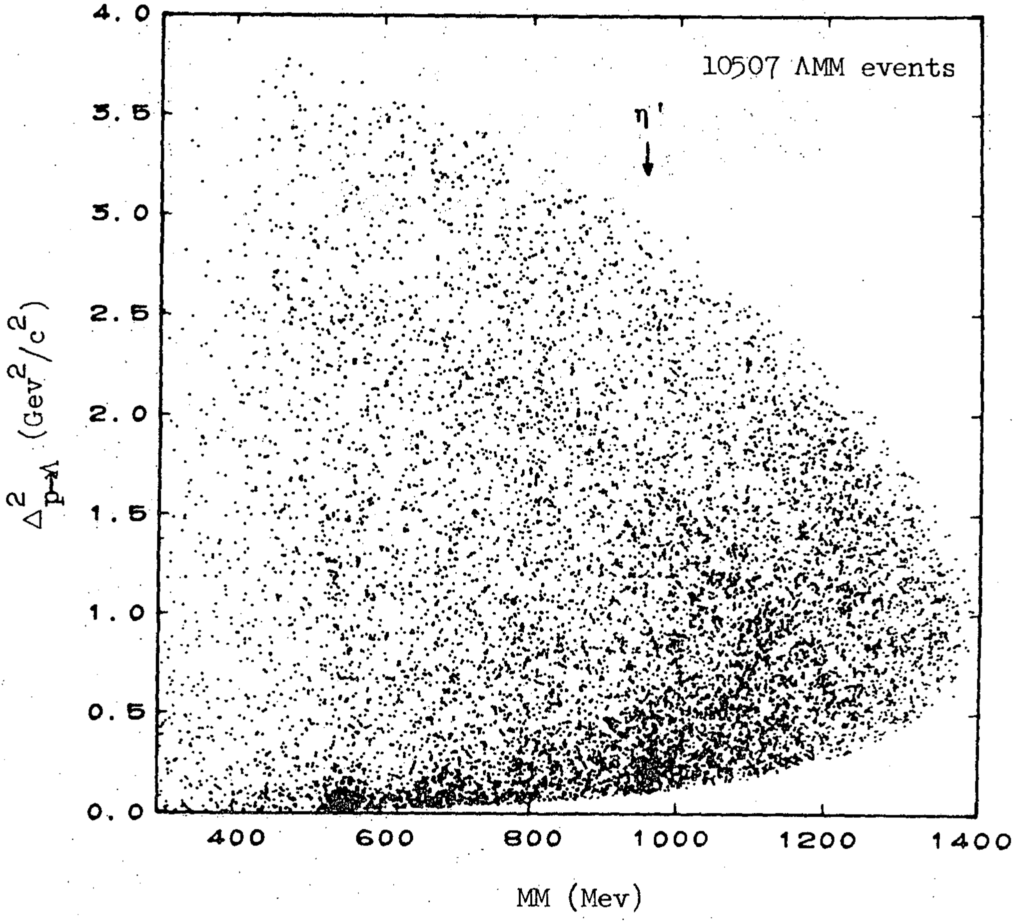

Figure 13. The Chew-Low plot for the ΛMM events of Figure 12.

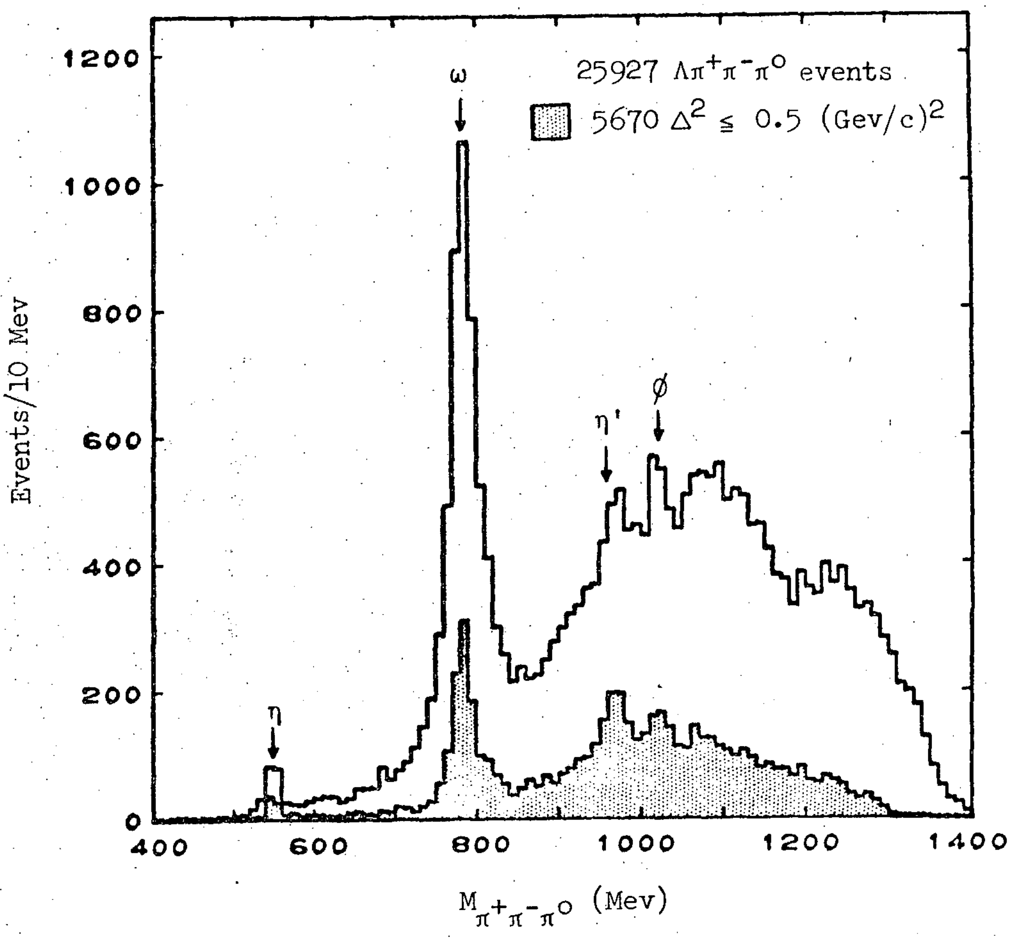

Figure 14. The $M_{\pi^+\pi^-\pi^0}$ mass spectrum for events fitting the reaction $K^-p \to \Lambda\pi^+\pi^-\pi^0$; events with $\Delta^2 \leq 0.5$ (Gev/c)^2 are shaded.

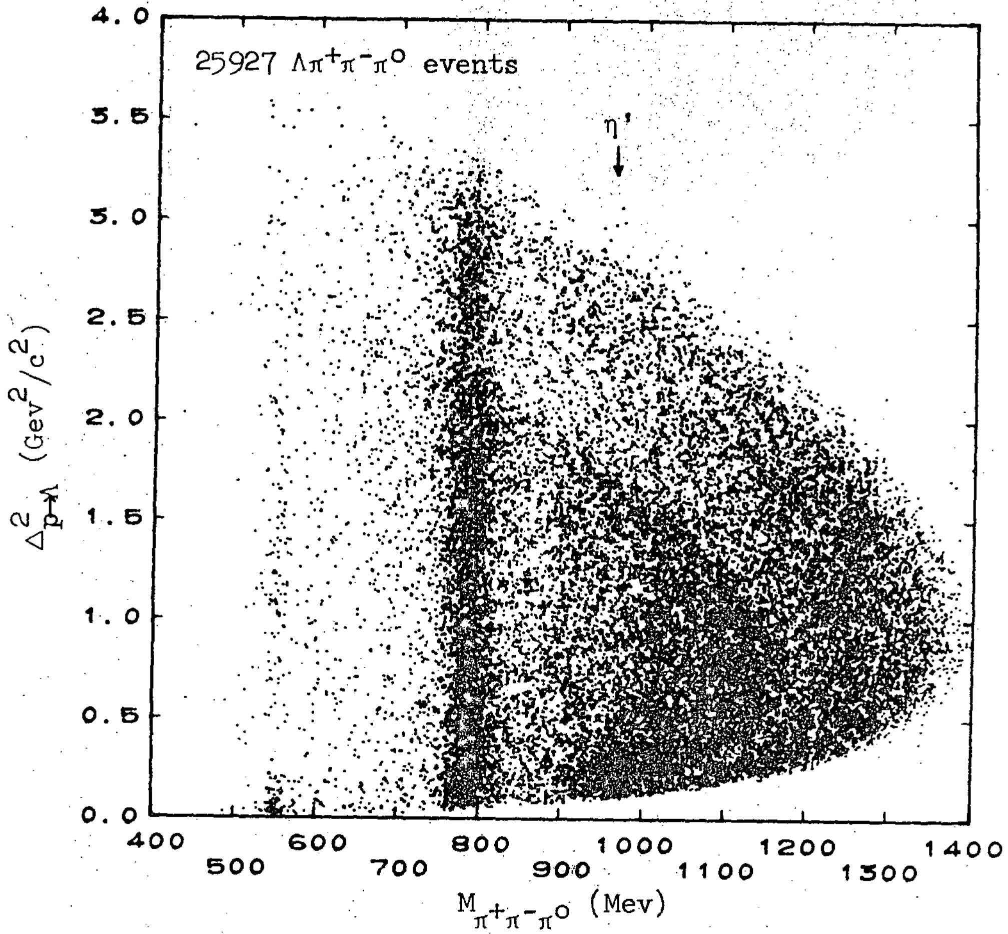

Figure 15. The Chew-Low plot for the $\Lambda\pi^+\pi^-\pi^0$events of Figure 14.

system. This plot, for events with $\Delta^2 \leq 0.5$ (Gev/c)^2 is shown in Figure 16. We use MM^2 rather than MM because the latter is very singular near MM = 0. For genuine $\Lambda\pi^+\pi^-\pi^o$ events, we expect a vertical band along $MM^2 = m_{\pi^o}{}^2 = 0.018$ Gev^2, with clusters of events at positions of $M_{\pi^+\pi^-MM}$ which correspond to $\pi^+\pi^-\pi^o$ resonances. For $MM^2 > m_{\pi^o}{}^2$ we expect a falling off of the band and the onset of events involving more than one missing neutral particle. For $MM^2 < m_{\pi^o}{}^2$, if there were no $\Lambda\pi^+\pi^-\gamma$ events and since we have specifically eliminated all events which might possibly be $\Lambda\pi^+\pi^-$ or $\Sigma^o\pi^+\pi^-$ and which would therefore have a missing mass ≈ 0, we would expect a uniform falling off of the π^o band with no structure near MM = 0. Examining Figure 16, we see the π^o band and clusters within it representing the η and the ω. However, the cluster near $M_{\pi^+\pi^-MM}$ = 960 Mev has a missing mass which is near zero rather than $m_{\pi^o}{}^2$. This effect can perhaps be seen more clearly if we project onto the missing mass-squared axis for different regions of $M_{\pi^+\pi^-MM}$. Figure 17 shows four such projections, for $M_{\pi^+\pi^-MM}$ in the ω region, in a region immediately below the η', in the η' region, and in a region immediately above the η'. We note that for all regions except that of the η', the missing mass-squared peak occurs near $m_{\pi^o}{}^2$, whereas the peak is shifted to lower missing mass for the η' region. If we assume that the number of genuine $\pi^+\pi^-\pi^o$ events is varying roughly linearly with $M_{\pi^+\pi^-\pi^o}$ when we are near the η', then we can make a subtraction using the regions below and above the η', and thus determine what the missing mass of the excess of events in the η' region looks like. The shaded portion of Figure 17c gives the results of such a subtraction. As can

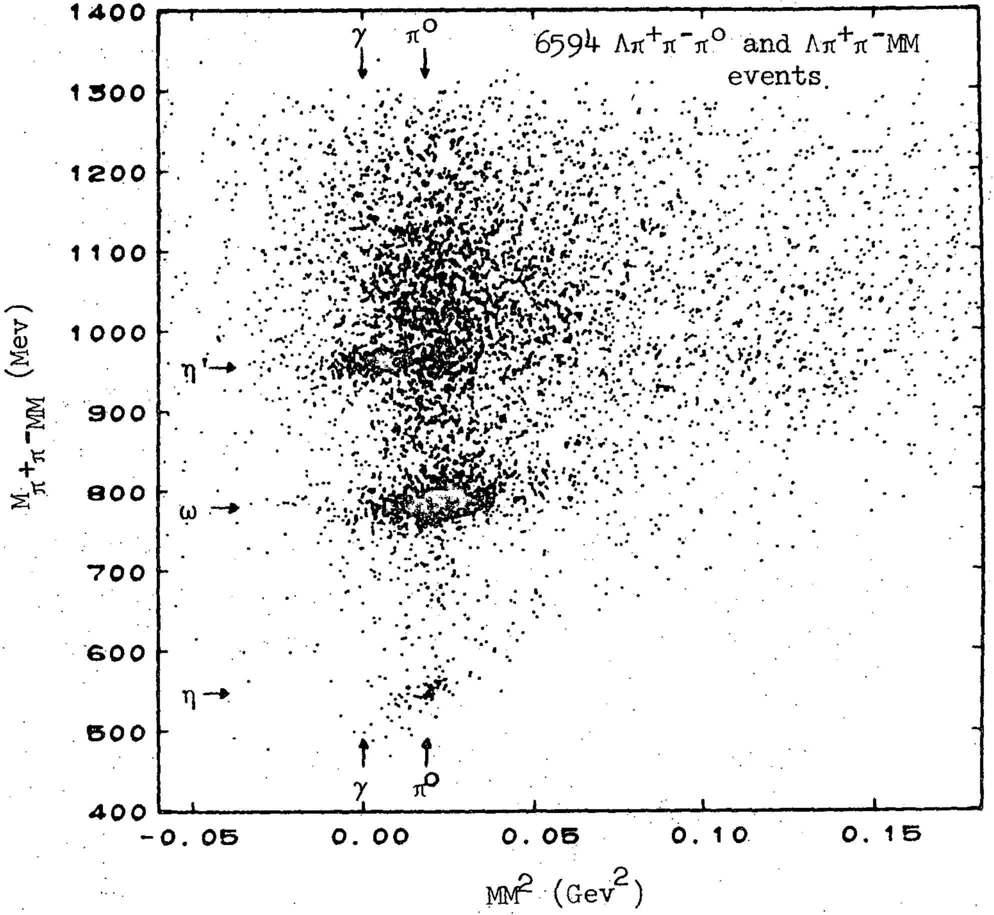

Figure 16. Plot of $M_{\pi^+\pi^-MM}$ versus MM^2 for low Δ^2 events fitting either $\Lambda\pi^+\pi^-\pi^0$ or $\Lambda\pi^+\pi^-MM$, but having no acceptable fit for $\Lambda\pi^+\pi^-$ or $\Sigma^0\pi^+\pi^-$. For the $\Lambda\pi^+\pi^-\pi^0$ events, MM represents the unfitted mass recoiling against the $\Lambda\pi^+\pi^-$ system. The arrows labeled γ and π^0 indicate the centers of the two vertical bands where $\Lambda\pi^+\pi^-\gamma$ and $\Lambda\pi^+\pi^-\pi^0$ events should appear, respectively.

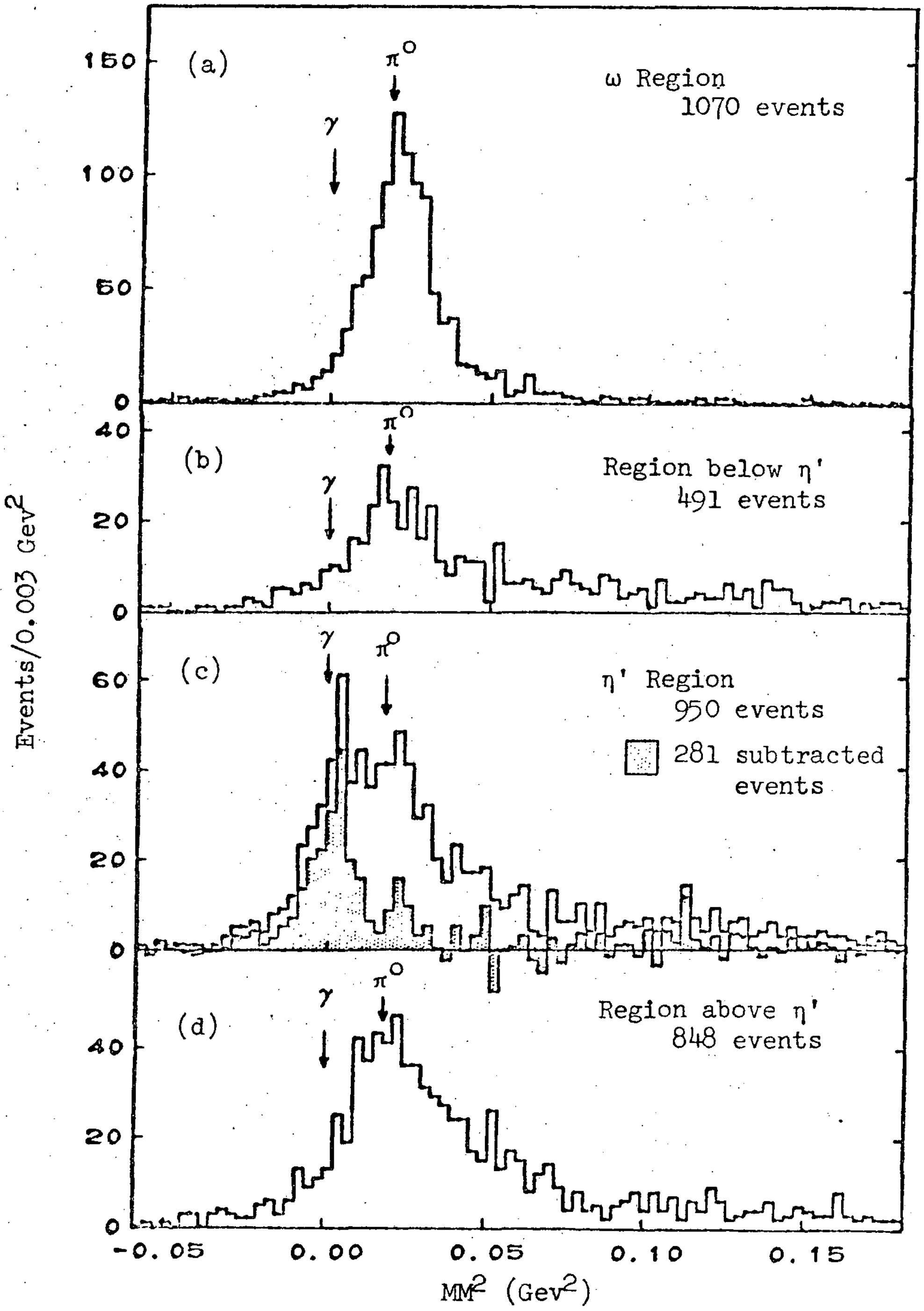

Figure 17. Projections of Figure 16 onto the MM^2 axis, for four regions of $M_{\pi^+\pi^-MM}$: (a) the ω region, 750 - 820 Mev; (b) the region below the η', 890 - 940 Mev; (c) the η' region, 940 - 990 Mev; and (d) the region above the η', 990 - 1040 Mev. The shaded portion for the η' region results when a subtraction is made using the events below and above the η'.

be seen, the remaining events peak at a missing mass ≈ 0. This then provides strong evidence that essentially all of the excess events in the η' region are in fact $\Lambda\pi^+\pi^-\gamma$ events, rather than $\Lambda\pi^+\pi^-\pi^0$.

One more set of projections of Figure 16, given in Figure 18, is worth examining, although these projections are not independent of those in Figure 17. In this case, we project onto the $\pi^+\pi^-$MM axis for the two cuts $-0.01 \leq MM^2 \leq 0.01$ Gev^2 and $0.01 \leq MM^2 \leq 0.03$ Gev^2. The first cut favors γ events, while the second one favors π^0 events. As seen in Figure 18 and as expected on the basis of the previous plots, while the η and ω show up more strongly for the π^0 cut, the peak at 960 Mev shows up more strongly for the γ cut.

We conclude that we are seeing the reaction

$$K^- p \rightarrow \Lambda\, \eta' \qquad \eta' \hookrightarrow \pi^+ \pi^- \gamma\ .$$

The identification of all three peaks we have observed, namely those for $\pi^+\pi^-\eta$, all neutrals, and $\pi^+\pi^-\gamma$, with the same resonance is based thus far only on the fact that all peaks occur at the same mass (within errors) and have widths which are roughly comparable to each other when resolution is taken into account. We shall shortly give additional evidence for the identification of all these peaks with the η'.

E. Other Final States

In Figure 19 we present plots for three remaining reactions where a strangeness zero meson with a mass less than that of two K's might

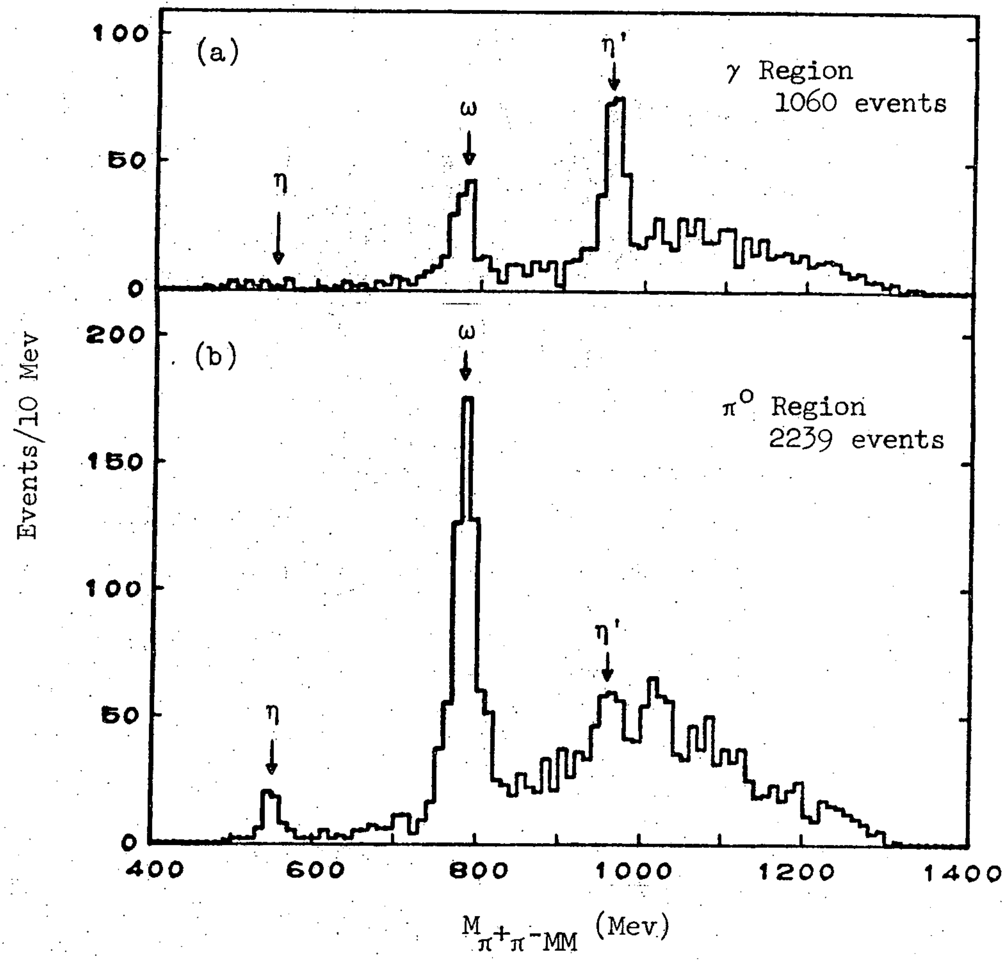

Figure 18. Two projections of Figure 16 onto the $M_{\pi^+\pi^- MM}$ axis for different MM regions: (a) the γ region, $-0.01 \leq MM^2 \leq 0.01$ Gev^2, and (b) the π^0 region, $0.01 \leq MM^2 \leq 0.03$ Gev^2.

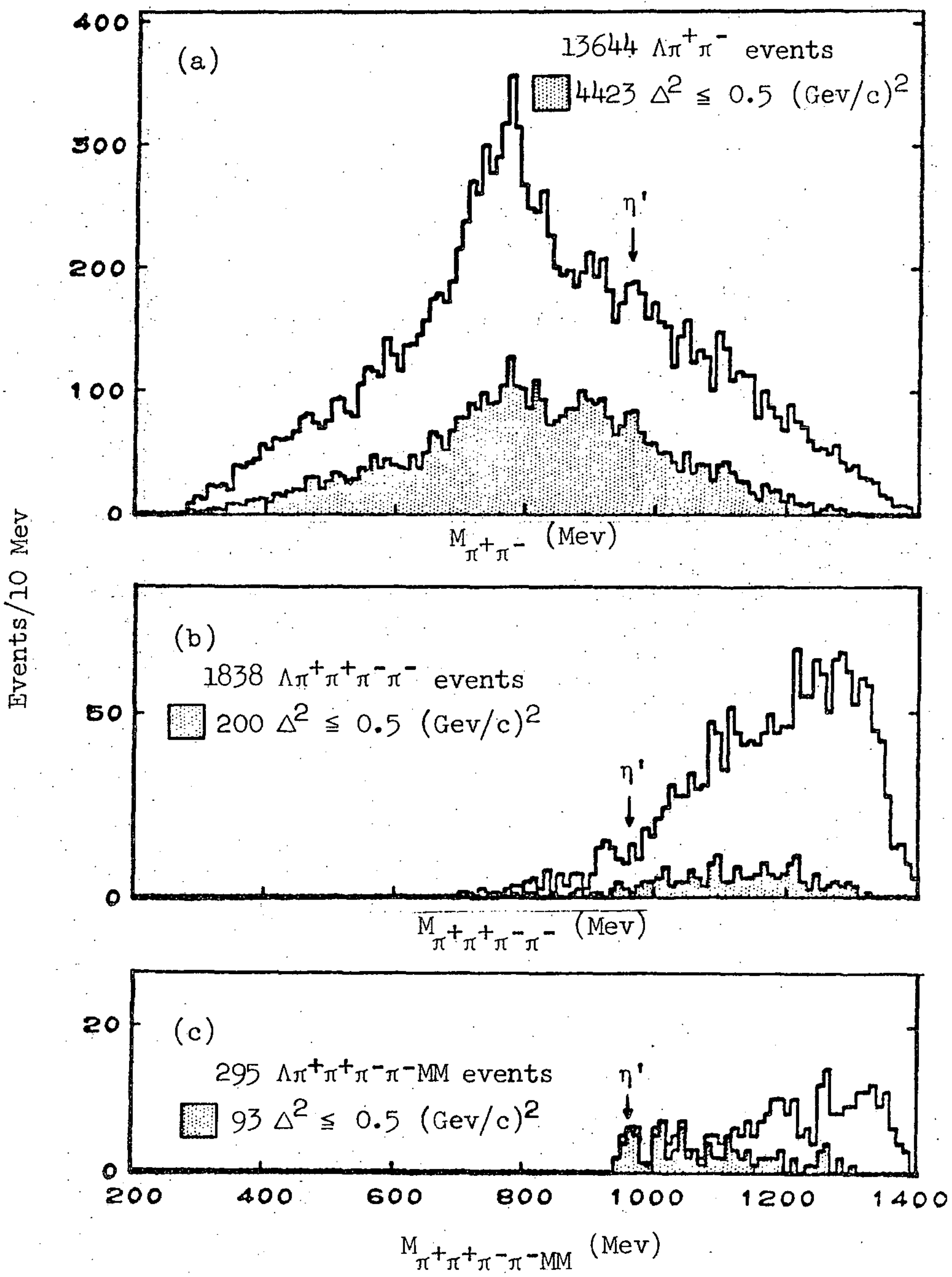

Figure 19. Plots of the mass recoiling against the Λ for (a) $\Lambda\pi^+\pi^-$ events, (b) $\Lambda\pi^+\pi^+\pi^-\pi^-$ events, and (c) $\Lambda\pi^+\pi^+\pi^-\pi^-$MM events. The shaded portions of the plots are for events with $\Delta^2 \leq 0.5$ (Gev/c)^2.

be expected to appear in conjunction with a Λ. The histograms are of the mass recoiling against the Λ in the reactions

5) $K^- p \to \Lambda \pi^+ \pi^-$

6) $\to \Lambda \pi^+ \pi^+ \pi^- \pi^-$

7) $\to \Lambda \pi^+ \pi^+ \pi^- \pi^-$ MM .

As can be seen, there is no evidence for a peak at 960 Mev in any of the mass plots.

IV. EVENT REPROCESSING AND HYPOTHESIS SEPARATION PROBLEMS

A. Reprocessing of Events

Before going on to discuss quantum number determination for the η', we give here a description of some refitting which was done in order to reduce the errors in the various effective masses of interest. As discussed in the previous section, the η' has as two of its decay modes $\pi^+\pi^-\eta$ and $\pi^+\pi^-\gamma$. In our original hypothesis fitting, done in PACKAGE, no hypotheses were tried involving either η's or γ's (except where the γ was from a Σ^0 decay). Thus in order to take advantage of the fact that demanding an η mass in the appropriate cases would further constrain the fits and thus improve the resolution, and that allowing a γ mass in addition to a π^0 mass would reduce systematic distortions in mass spectra, we have reprocessed a sample of our events through PACKAGE and subsequent programs. The events reprocessed consisted of: 1) all V-4 prongs; 2) those V-2 prongs which had as their best fit either $\Lambda\pi^+\pi^-$MM, $\Lambda\pi^+\pi^-\pi^0$, $\Lambda\pi^+\pi^-$, or $\Sigma^0\pi^+\pi^-$, and where the mass $M_{vs\Lambda}$ recoiling against the Λ satisfied $900 \leq M_{vs\Lambda} \leq 1020$ Mev; and 3) those V-2 prongs which had a successfully fit Λ decay but no successful production fit and where the mass recoiling against the Λ (as determined from the fitted Λ momentum and measured charged tracks) was again in the region 900 to 1020 Mev. Class 3) was included in case some $\Lambda\pi^+\pi^-\gamma$ events had failed to fit as $\Lambda\pi^+\pi^-\pi^0$. The fits attempted in this reprocessing were as follows:

For V-4 prongs: $K^- p \rightarrow \Lambda \pi^+ \pi^+ \pi^- \pi^-$

$\Sigma^0 \pi^+ \pi^+ \pi^- \pi^-$

$\Lambda \pi^+ \pi^+ \pi^- \pi^- \pi^0$

$\Lambda \pi^+ \pi^+ \pi^- \pi^- \gamma$

$\Lambda \pi^+ \pi^- \eta_C$

$\qquad \llcorner\!\!\rightarrow \pi^+ \pi^- \pi^0$

$\Lambda \pi^+ \pi^- \eta_C$

$\qquad \llcorner\!\!\rightarrow \pi^+ \pi^- \gamma$

$\Lambda \pi^+ \pi^+ \pi^- \pi^- MM$;

For V-2 prongs: $K^- p \rightarrow \Lambda \pi^+ \pi^-$

$\Sigma^0 \pi^+ \pi^-$

$\Lambda \pi^+ \pi^- \pi^0$

$\Lambda \pi^+ \pi^- \gamma$

$\Lambda \pi^+ \pi^- \eta_N$

$\Lambda \pi^+ \pi^- MM$.

The subscripts C and N denote the charged and neutral decay modes of the η, respectively.

B. Hypothesis Separation

The decision making procedures of DSTEXAM, as described earlier, were modified somewhat for these reprocessed events in the hopes of making a more accurate separation of hypotheses. Some of the problems connected with these modifications will be discussed here as illustrative of the problems encountered in determining the correct hypothesis.

The first modification made was that any event which successfully fit a four-constraint hypothesis ($\Lambda\pi^+\pi^-$ or $\Lambda\pi^+\pi^+\pi^-\pi^-$) was assigned to that hypothesis. In general, a four-constraint fit, such as $\Lambda 2\pi$, is ambiguous only with those hypotheses involving an additional γ, namely $\Lambda 2\pi\gamma$ and $\Sigma^0 2\pi$. For genuine $\Lambda 2\pi$ events, the one-constraint $\Lambda 2\pi\gamma$ fit can always give the unmeasured assumed γ zero momentum in the lab and thus allow such events to pass as $\Lambda 2\pi\gamma$. The two-constraint $\Sigma^0 2\pi$ fit can also set the assumed γ at rest in the lab and, as it turns out in our particular experiment, in many instances the $\Lambda\gamma$ effective mass will be near that of a Σ^0, allowing a successful fit. Figures 20a and b show scatter plots of the confidence level (C.L.) for the $\Lambda 2\pi$ fit versus that for the $\Lambda 2\pi\gamma$ and $\Sigma^0 2\pi$ fits, respectively. Only those events are shown in each plot which have as their best fit one or the other of the two hypotheses plotted, and which have $\Delta^2_{p\to\Lambda} \leqq 0.5$ $(\mathrm{Gev}/c)^2$. The ambiguities are obvious. In each case, however, there is a class of events having essentially zero C.L. for the $\Lambda 2\pi$ hypothesis; these lie on the vertical lines near the left of the plots, and are clearly separated from the remainder of the events. We have assumed that only these events are non-$\Lambda 2\pi$ events. That is, any event having a $\Lambda 2\pi$ C.L. > 0.005 has been assigned to the $\Lambda 2\pi$ hypothesis.

Another problem is encountered in separating $\Sigma^0 2\pi$ from $\Lambda 2\pi\gamma$ (or $\Sigma^0 4\pi$ from $\Lambda 4\pi\gamma$), since events of the former category will always fit the latter. A confidence level scatter plot for these two fits is shown in Figure 20c. Although the separation is not definite, it is seen that the uncertain area of the plot, where the population is relatively flat, can be divided roughly evenly by a line defined by

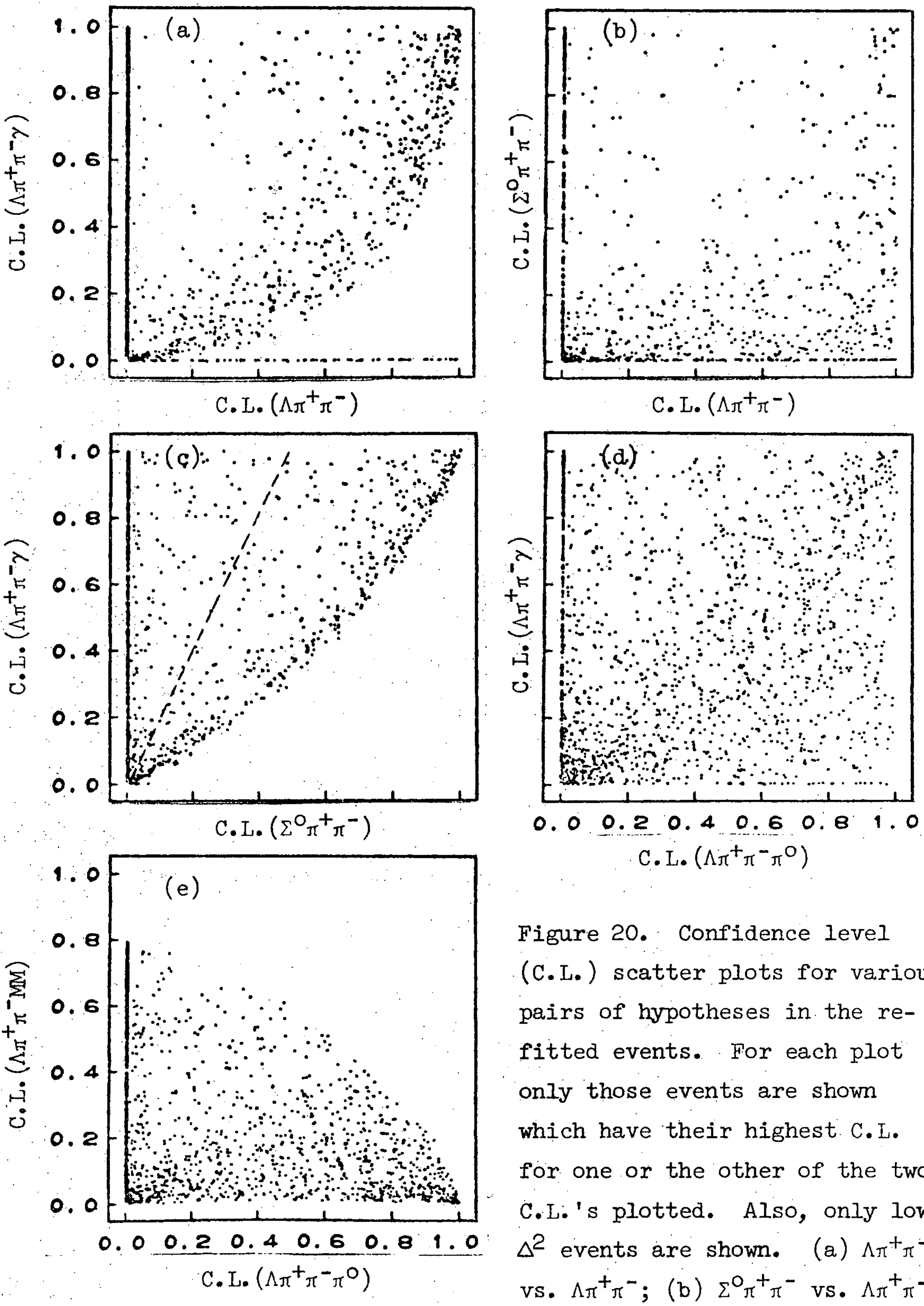

Figure 20. Confidence level (C.L.) scatter plots for various pairs of hypotheses in the refitted events. For each plot only those events are shown which have their highest C.L. for one or the other of the two C.L.'s plotted. Also, only low Δ^2 events are shown. (a) $\Lambda\pi^+\pi^-\gamma$ vs. $\Lambda\pi^+\pi^-$; (b) $\Sigma^0\pi^+\pi^-$ vs. $\Lambda\pi^+\pi^-$; (c) $\Lambda\pi^+\pi^-\gamma$ vs. $\Sigma^0\pi^+\pi^-$; (d) $\Lambda\pi^+\pi^-\gamma$ vs. $\Lambda\pi^+\pi^-\pi^0$; (e) $\Lambda\pi^+\pi^-$MM vs. $\Lambda\pi^+\pi^-\pi^0$. The dashed line on (c) represents C.L.($\Lambda\pi^+\pi^-\gamma$) = 2C.L.($\Sigma^0\pi^+\pi^-$).

$\text{C.L.}_{\Lambda 2\pi\gamma} = 2\text{C.L.}_{\Sigma^0 2\pi}$. Thus events having $\text{C.L.}_{\Lambda 2\pi\gamma} > 2\text{C.L.}_{\Sigma^0 2\pi}$ were assigned to $\Lambda 2\pi\gamma$, with the remainder being assigned to $\Sigma^0 2\pi$. With this assignment and those of the previous paragraph, Figures 21a, b, and c show histograms of the effective mass recoiling against the $\pi^+\pi^-$ system for the $\Lambda\pi^+\pi^-$, $\Sigma^0\pi^+\pi^-$, and $\Lambda\pi^+\pi^-\gamma$ events, respectively. This effective mass was calculated using the measured momenta. The Λ and Σ^0 peaks in 21a and b are seen to be centered quite well at their proper positions, and the number of $\Lambda 2\pi\gamma$ events is seen to rise smoothly as the $\Lambda\gamma$ effective mass rises above the Σ^0 mass. The Σ^0 peak does show some depletion on the high side, suggesting that we have not favored $\Sigma^0 2\pi$ over $\Lambda 2\pi\gamma$ quite strongly enough. The regions of overlap are, of course, the ambiguous areas. Changing the above criteria by small amounts has some effect on the $\pi^+\pi^-$ mass distribution of the $\Lambda\pi^+\pi^-\gamma$ events, but the effect is small and limited to $M_{\pi^+\pi^-} \gtrsim 800$ Mev. This will not be a serious problem when we discuss this $\pi^+\pi^-$ distribution.

The $\Lambda\pi^+\pi^-\pi^0$ and $\Lambda\pi^+\pi^-\gamma$ events are hopelessly entangled as shown in Figure 20d and as expected. We have left the standard criterion remain here: the hypothesis with the higher C.L. has been chosen. This turns out to be almost equivalent to choosing the $\Lambda\pi^+\pi^-\gamma$ hypothesis when the missing mass-squared $MM^2 \lesssim \frac{1}{2}m_{\pi^0}{}^2$, and the $\Lambda\pi^+\pi^-\pi^0$ hypothesis when $MM^2 \gtrsim \frac{1}{2}m_{\pi^0}{}^2$. Since the separation is poor, we will have to correct all distributions of the $\Lambda 2\pi\gamma$ events by a subtraction method, making use of the $\Lambda 3\pi$ events. We already know from the subtraction shown in Figure 17 that essentially all of the excess events in the η' region are $\Lambda 2\pi\gamma$; thus any η' signal seen in the so-called $\Lambda 3\pi$

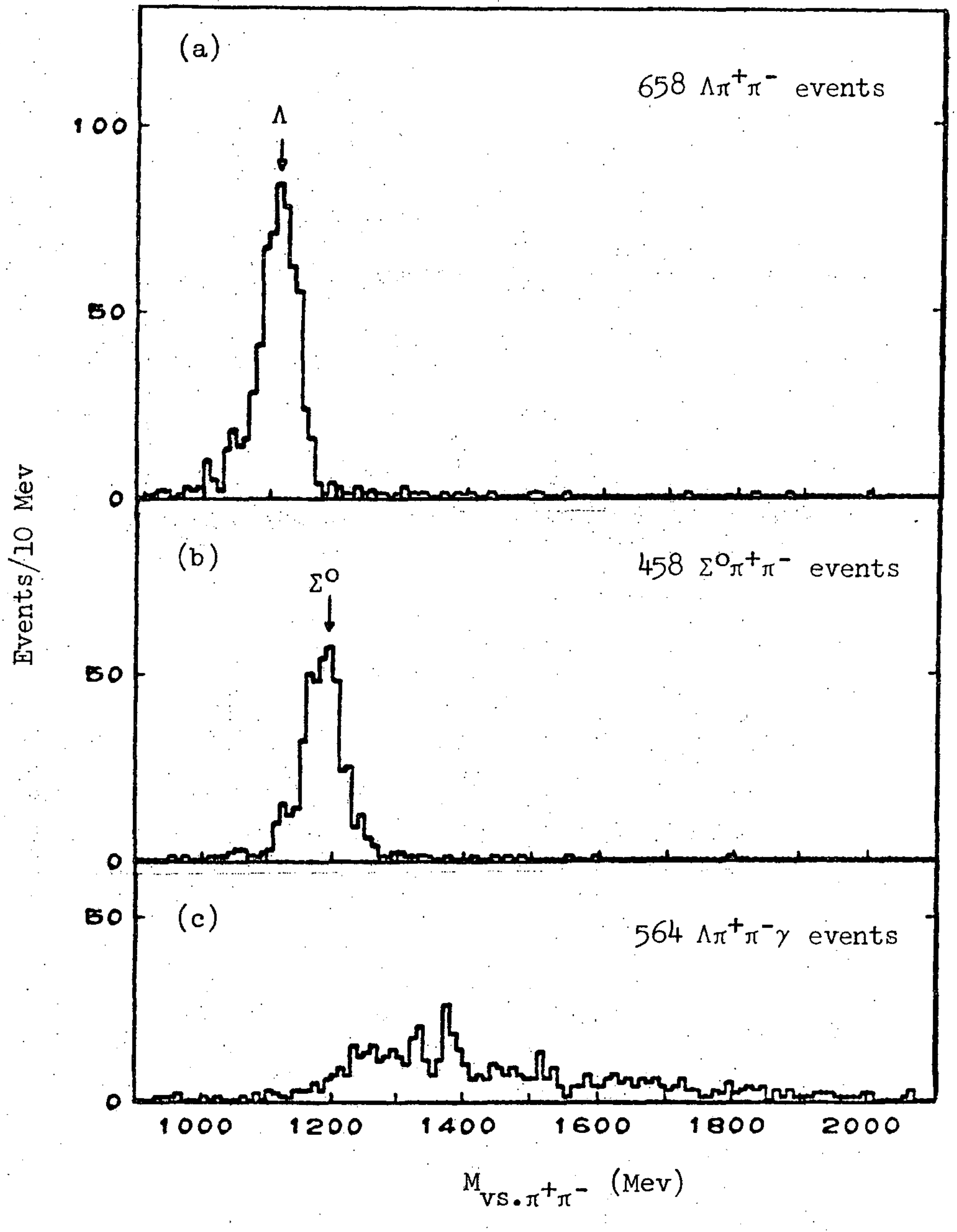

Figure 21. Plots of the unfitted mass $M_{vs.\pi^+\pi^-}$ recoiling against the $\pi^+\pi^-$ system in the reprocessed events assigned to the hypotheses: (a) $\Lambda\pi^+\pi^-$; (b) $\Sigma^0\pi^+\pi^-$; and (c) $\Lambda\pi^+\pi^-\gamma$.

events results from misidentified $\Lambda 2\pi\gamma$ events.

The $\Lambda\pi^+\pi^-\eta_C$ $(\eta_C \to \pi^+\pi^-\pi^o)$ and $\Lambda\pi^+\pi^-\eta_C$ $(\eta_C \to \pi^+\pi^-\gamma)$ events are afflicted with similar, although less severe, π^o vs. γ difficulties. However, since we are not attempting to determine η branching ratios, this does not pose any serious problems. Suffice it to say that choosing the hypothesis with the higher confidence level results in the branching ratio $(\eta \to \pi^+\pi^-\gamma)/(\eta \to \pi^+\pi^-\pi^o) = 28/120 = 0.23 \pm 0.05$, in excellent agreement with the value of 0.235 ± 0.021 given in the Particle Data Group compilation.[16]

The $\Lambda\pi^+\pi^-\eta_C$ $(\eta_C \to \pi^+\pi^-\pi^o$ or $\pi^+\pi^-\gamma)$ events present two other difficulties. All such events will also fit $\Lambda\pi^+\pi^+\pi^-\pi^-\pi^o$ and/or $\Lambda\pi^+\pi^+\pi^-\pi^-\gamma$. We have chosen the η fit over the non-η fit whenever the former passed with a C.L. > 0.005. On the basis of Figure 6, where one-quarter of the four possible $\pi^+\pi^-\pi^o$ (or $\pi^+\pi^-\gamma$) event-combinations plotted for the η' region were seen to be in the η peak, we are confident that there is no significant $\eta' \to 5\pi$ decay. Further, since there are few background events in the η' region, we cannot introduce a serious contamination by over-favoring the η fit. The other difficulty is also evident from Figure 6; namely that each event has on the average two $\pi^+\pi^-\pi^o$ (or $\pi^+\pi^-\gamma$) combinations near the η mass. This difficulty cannot be resolved, and so we will not use the $\pi^+\pi^-\eta_C$ events in any distributions dependent upon knowing which combination is the η.

The $\Lambda\pi^+\pi^-\pi^o$ and $\Lambda\pi^+\pi^-$MM events have a large region of overlap on the C.L. scatter plot as shown in Figure 20e. However, if we plot the unfitted mass recoiling against the $\Lambda\pi^+\pi^-$ system for the $\Lambda\pi^+\pi^-\pi^o$

and $\Lambda\pi^+\pi^-\gamma$ events combined, staying outside the η' region so that we are sure we have no real γ's, the π^0 peak is seen, in Figure 22, to be fairly well centered at its correct value of 0.018 Gev^2. Thus on the average, at least, we have chosen the correct hypothesis by using the standard criteria.

The final difficulty has to do with separating $\Lambda\pi^+\pi^-$MM from $\Lambda\pi^+\pi^-\eta_N$. The choice between these two hypotheses has been adjusted so as to make the confidence level for the $\Lambda\pi^+\pi^-\eta_N$ events, as shown in Figure 23a, as flat as possible. Figures 23b and c are histograms of the unfitted effective mass recoiling against the $\Lambda\pi^+\pi^-$ system for the $\Lambda\pi^+\pi^-\eta_N$ and $\Lambda\pi^+\pi^-$MM events, respectively; only events in the broad η' region ($940 \leq M_{vs\Lambda} \leq 980$ Mev) with $\Delta^2 \leq 0.5\ (\text{Gev/c})^2$ have been plotted. We see that the $\Lambda\pi^+\pi^-\eta_N$ events are centered correctly and that the number of $\Lambda\pi^+\pi^-$MM events falls off smoothly as the missing mass approaches the η mass. However, there is seemingly an excess of $\Lambda\pi^+\pi^-$MM events in the region immediately above the η mass. These probably are poorly measured $\Lambda\pi^+\pi^-\eta_N$ events, judging from the fact that they are clumped together so closely. Also, the flatness of the η peak in the $\Lambda\pi^+\pi^-\eta_N$ events and the hole at the η mass in the $\Lambda\pi^+\pi^-$MM events suggest that some genuine MM events have been lost to the η_N fit. We will discuss this problem further in the next section when the $\pi^+\pi^-\eta_N$ Dalitz plot is examined.

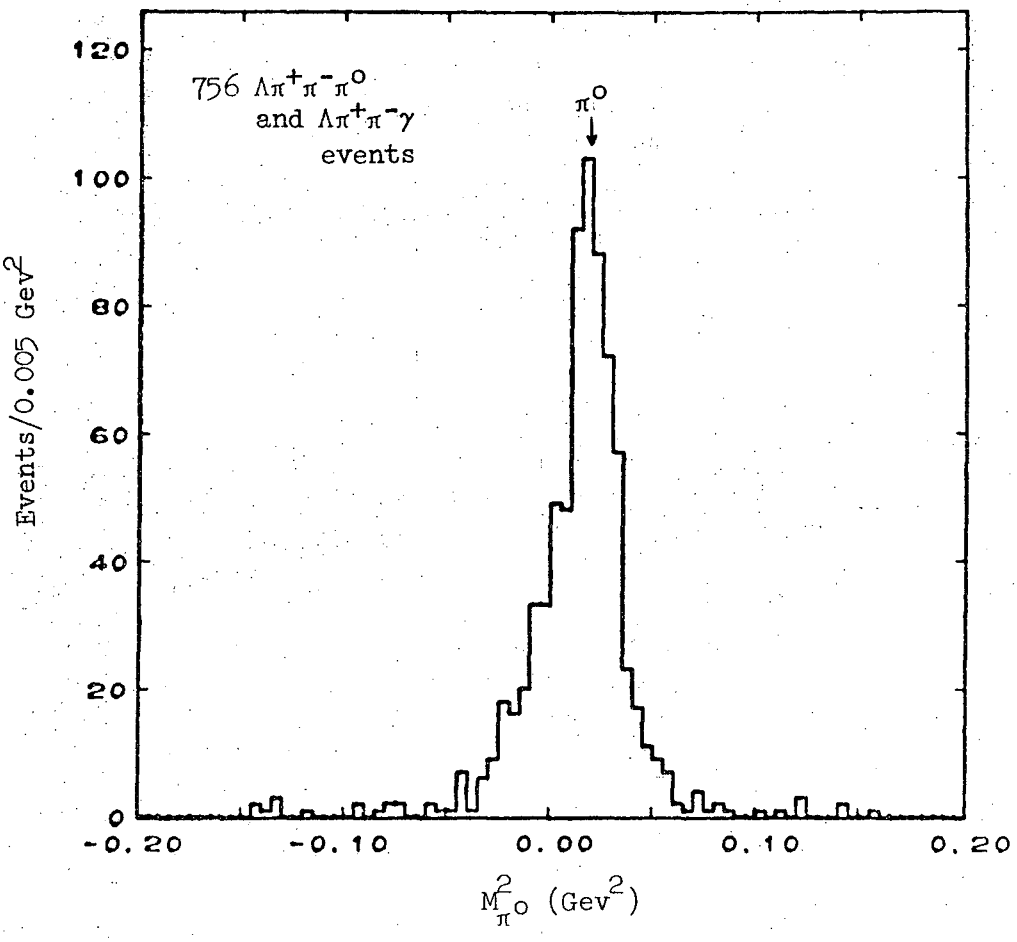

Figure 22. Histogram of the unfitted π^0 mass squared for low Δ^2, reprocessed events assigned to either the $\Lambda\pi^+\pi^-\pi^0$ or $\Lambda\pi^+\pi^-\gamma$ hypothesis. Only events with the unfitted $\pi^+\pi^-\pi^0$ or $\pi^+\pi^-\gamma$ mass outside the region 940 to 980 Mev are plotted, so as to avoid genuine γ events.

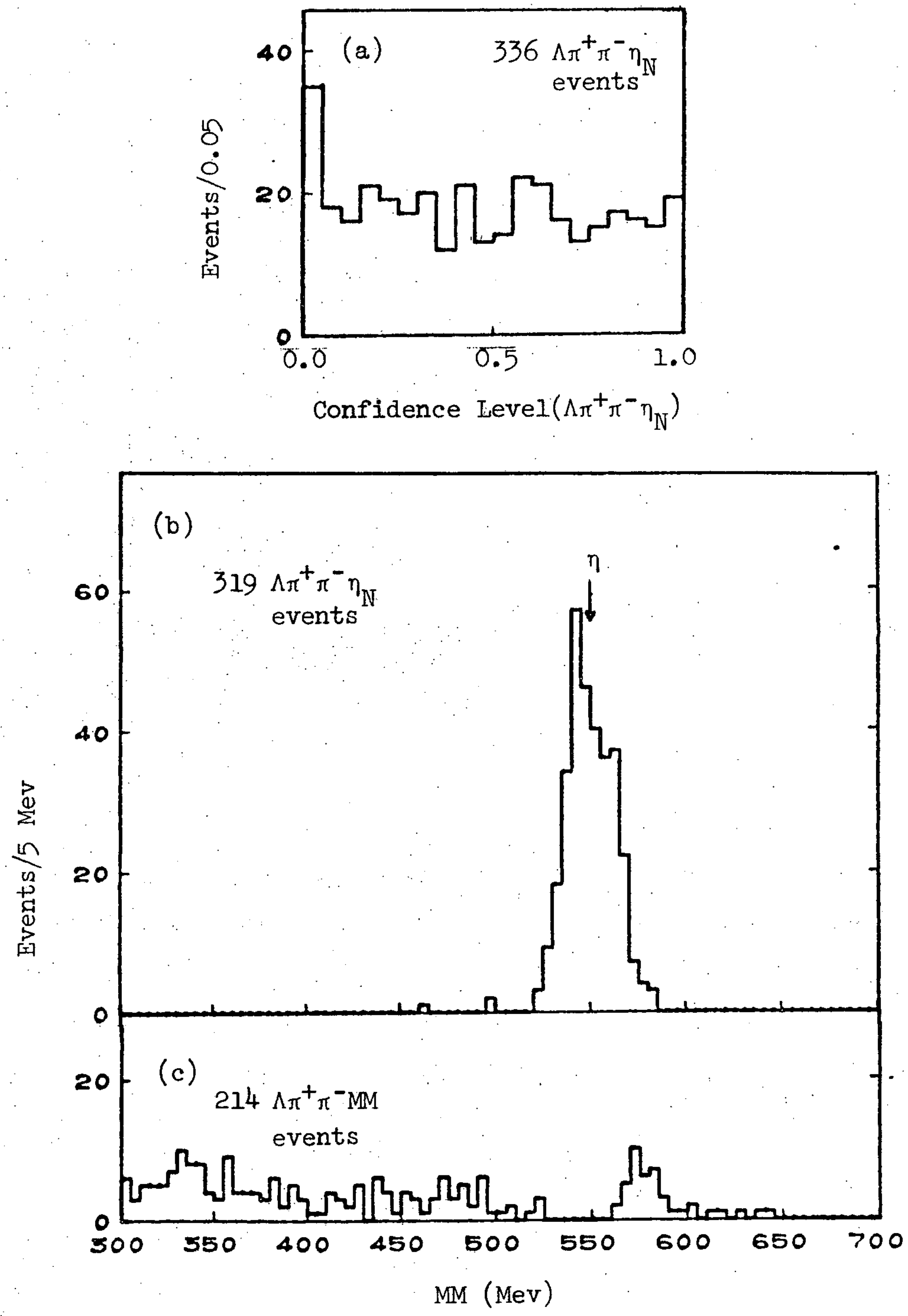

Figure 23. (a) Plot of the confidence level of low Δ^2, reprocessed events assigned to the $\Lambda\pi^+\pi^-\eta_N$ hypothesis. The unfitted mass MM recoiling against the $\Lambda\pi^+\pi^-$ system, for events assigned to $\Lambda\pi^+\pi^-\eta_N$ and $\Lambda\pi^+\pi^-$MM, is shown in (b) and (c), respectively.

V. QUANTUM NUMBER DETERMINATION -- THE η' DECAY DISTRIBUTIONS

A. The $\pi^+\pi^-\eta$ Dalitz Plot

Figure 24 shows a plot of the effective mass of the $\pi^+\pi^-\eta_N$ system for $\Lambda\pi^+\pi^-\eta_N$ events with $\Delta^2 \leq 0.5$ (Gev/c)^2. The η' peak is seen to stand out clearly, having at most 5% non-η' background. The curve drawn over the events is a Gaussian which has been fitted to the data, yielding a central mass of 957 Mev. In Figure 25 we show the analogous plot for the $\Lambda\pi^+\pi^-\eta_C$ events. Here there is no background at all, and the fitted central mass is again 957 Mev.

The Dalitz plot for low Δ^2 $\pi^+\pi^-\eta_N$ events with $950 \leq M_{\pi^+\pi^-\eta_N} \leq$ 970 Mev is shown in Figure 26. The events plotted have been normalized to a $\pi^+\pi^-\eta_N$ mass of 957 Mev. That is, if for a given event we let T_i^f be the fitted kinetic energy of particle i (π^+, π^-, or η) in the η' rest frame and we let Q^f be the fitted Q-value for the event, and if Q is the Q-value for an η' of mass 957 Mev, then the normalized kinetic energies, T_i, are given by

$$T_i = \frac{Q}{Q^f} T_i^f \; .$$

In terms of effective masses, this becomes

$$M_{ij}^2 = (M - m_k)^2 + \frac{QM}{Q^f M^f}\left[M_{ij}^{f\,2} - (M^f - m_k)^2\right]$$

where M^f is the fitted $\pi^+\pi^-\eta$ effective mass, M is the central mass of the η', M_{ij}^f is the fitted effective mass of particles i and j, m_k is the mass of the third particle, and M_{ij} is the normalized effective mass of particles i and j.

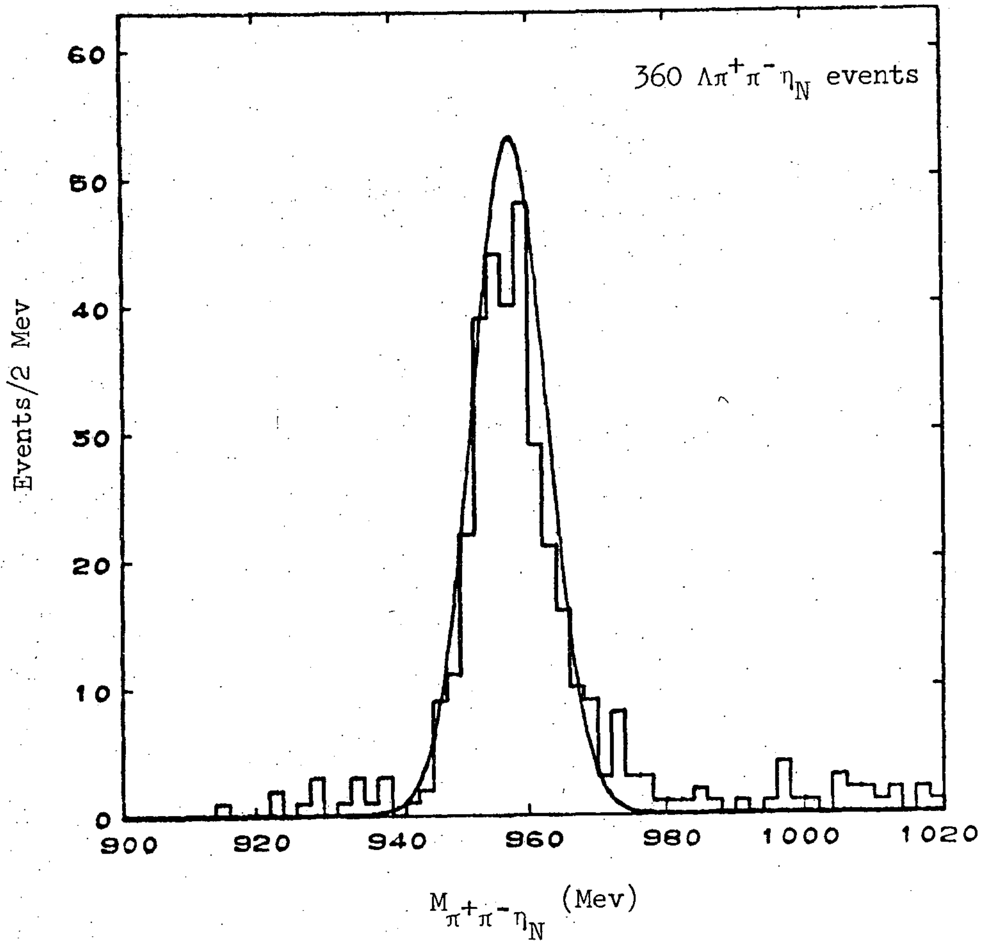

Figure 24. The $\pi^+\pi^-\eta_N$ mass spectrum for low Δ^2 $\Lambda\pi^+\pi^-\eta_N$ events. The curve is a Gaussian fit to the data.

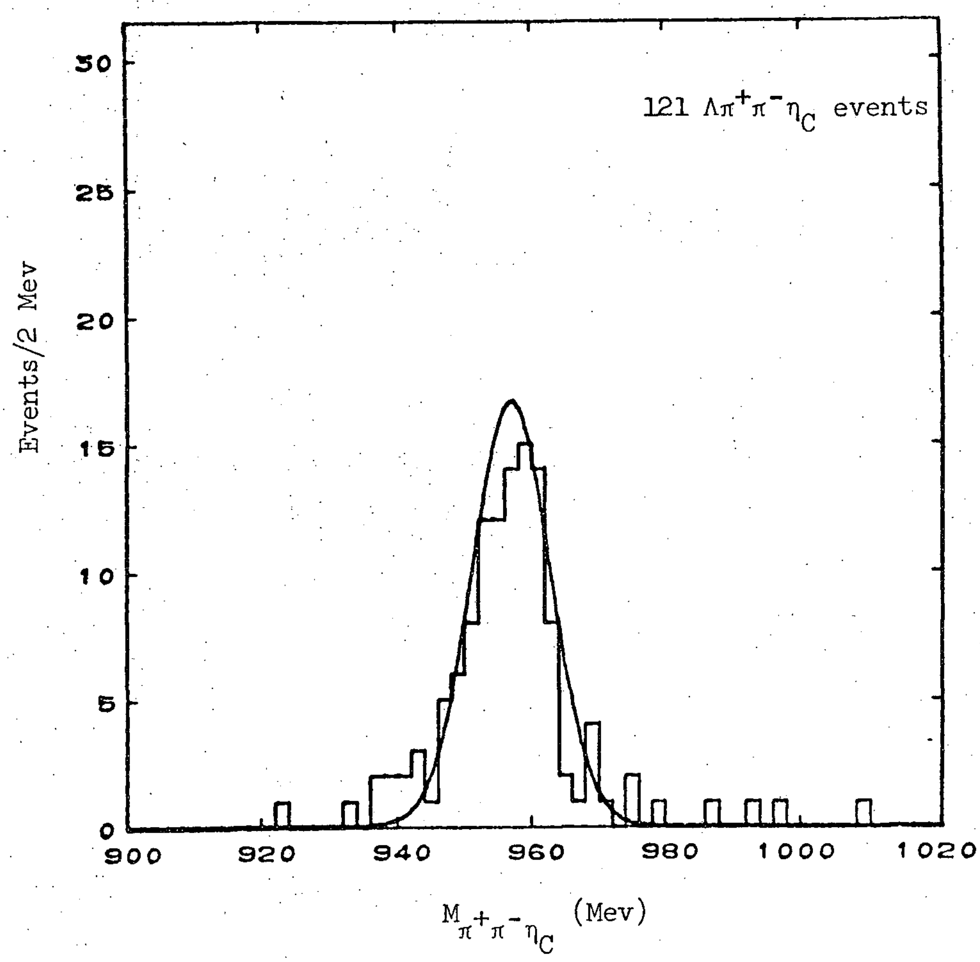

Figure 25. The $\pi^+\pi^-\eta_C$ mass spectrum for low Δ^2 $\Lambda\pi^+\pi^-\eta_C$ events. The curve is a Gaussian fit to the data.

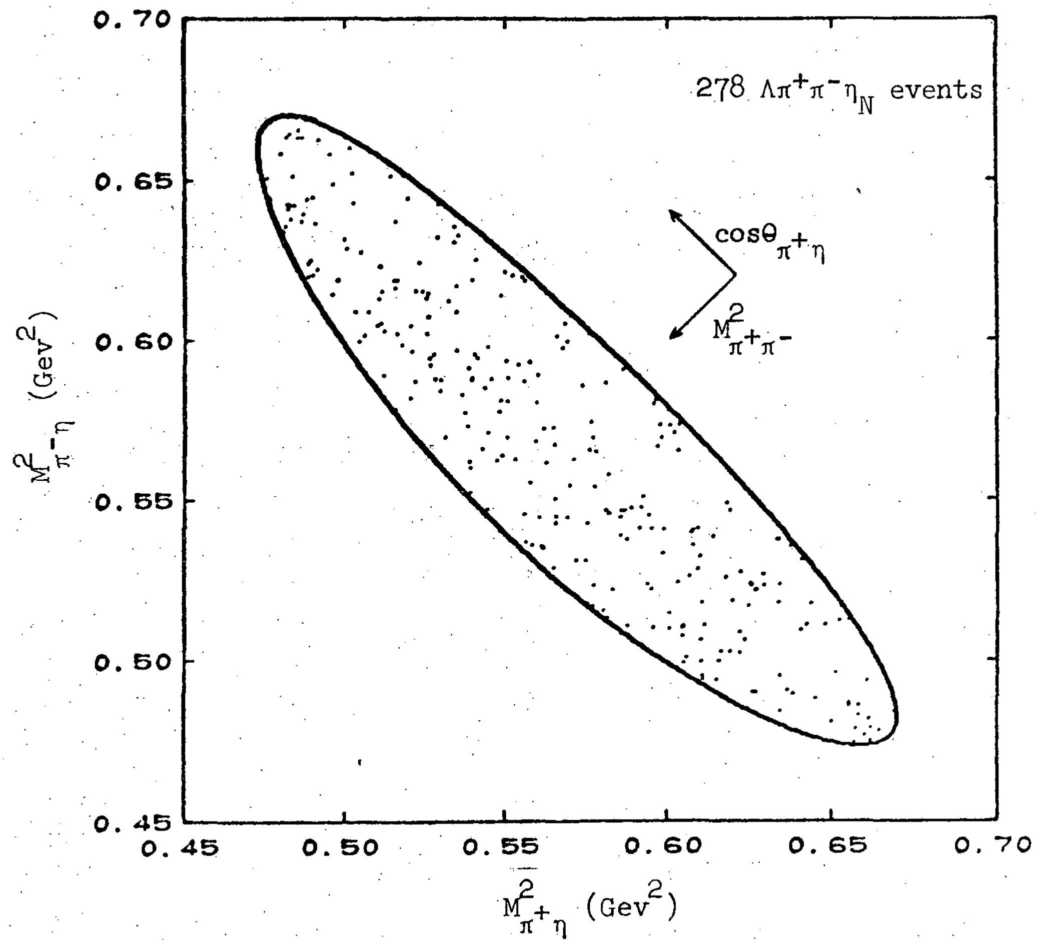

Figure 26. The normalized Dalitz plot for low Δ^2 $\pi^+\pi^-\eta_N$ events with 950 ≤ $M_{\pi^+\pi^-\eta_N}$ ≤ 970 Mev. The curve represents the kinematic boundary for the events.

Figure 27 gives four projections of the $\pi^+\pi^-\eta_N$ Dalitz plot. These projections, which are not completely independent of each other, are of the three effective masses $M_{\pi^+\eta}$, $M_{\pi^-\eta}$, and $M_{\pi^+\pi^-}$, and of the cosine of the angle $\Theta_{\pi^+\eta}$ between the π^+ and the η in the dipion rest frame. The curves drawn over the histograms represent phase space. Note that charge conjugation invariance requires the $M_{\pi^+\eta}$ and $M_{\pi^-\eta}$ distributions to be the same and the $\cos\Theta_{\pi^+\eta}$ distribution to be symmetric.

The normalized Dalitz plot for the $\pi^+\pi^-\eta_C$ events with $\Delta^2 \leqq 0.5$ $(\text{Gev/c})^2$ and $950 \leqq M_{\pi^+\pi^-\eta_C} \leqq 970$ Mev is given in Figure 28, together with its projections in Figure 29. Although these events are free of non-η' contamination, as we have previously pointed out there is a reasonably high chance that in many events the wrong $\pi^+\pi^-\pi^0$ or $\pi^+\pi^-\gamma$ combination has been picked as the η. Thus we will not use these events for the subsequent Dalitz plot analysis. We return, therefore, to the $\pi^+\pi^-\eta_N$ Dalitz plot, dropping the subscript N in what follows.

In order to study the $\eta' \rightarrow \pi^+\pi^-\eta$ decay, we need to construct decay matrix elements for each of the spin, parity, and isospin assignments under consideration. We limit ourselves to the cases of spin $J \leqq 2$, with both odd and even parities P. (Note that $J^P = 0^+$ is forbidden to decay into three pseudoscalars such as $\pi\pi\eta$.) Since the η' is produced in the reaction $K^-p \rightarrow \Lambda\eta'$, where the K^-p system has isospin $I = 0$ or 1 and the Λ has $I = 0$, the isospin of the η' must be 0 or 1. As we do not yet want to rule out the possibility that the decay $\eta' \rightarrow \pi^+\pi^-\eta$ is electromagnetic, in which case isospin

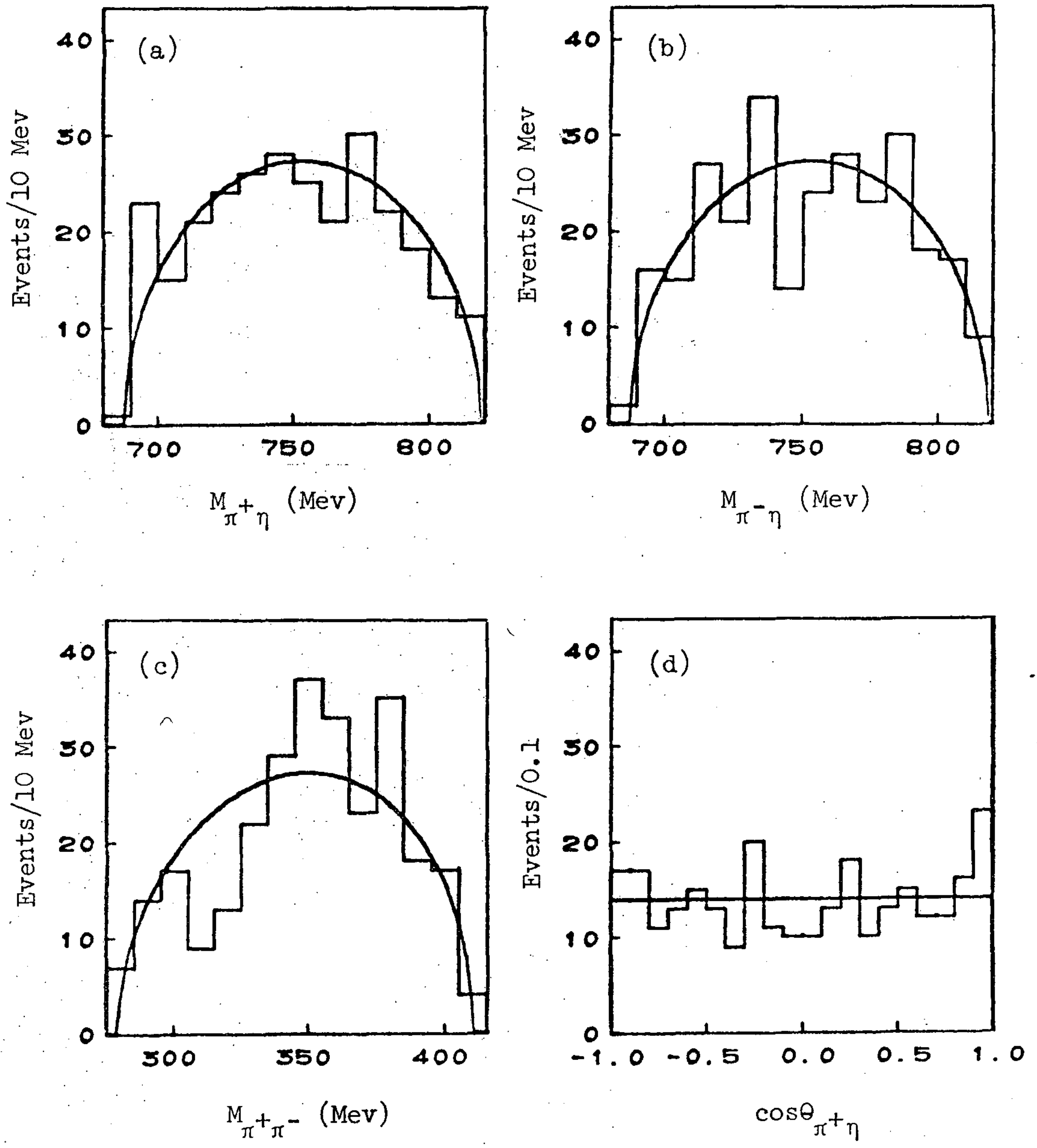

Figure 27. Four projections of the Dalitz plot for the 278 $\pi^+\pi^-\eta_N$ events of Figure 26. The projections are (a) $M_{\pi^+\eta}$, (b) $M_{\pi^-\eta}$, (c) $M_{\pi^+\pi^-}$, and (d) $\cos\theta_{\pi^+\eta}$. The angle $\theta_{\pi^+\eta}$ is measured in the dipion rest frame. The curves represent phase space.

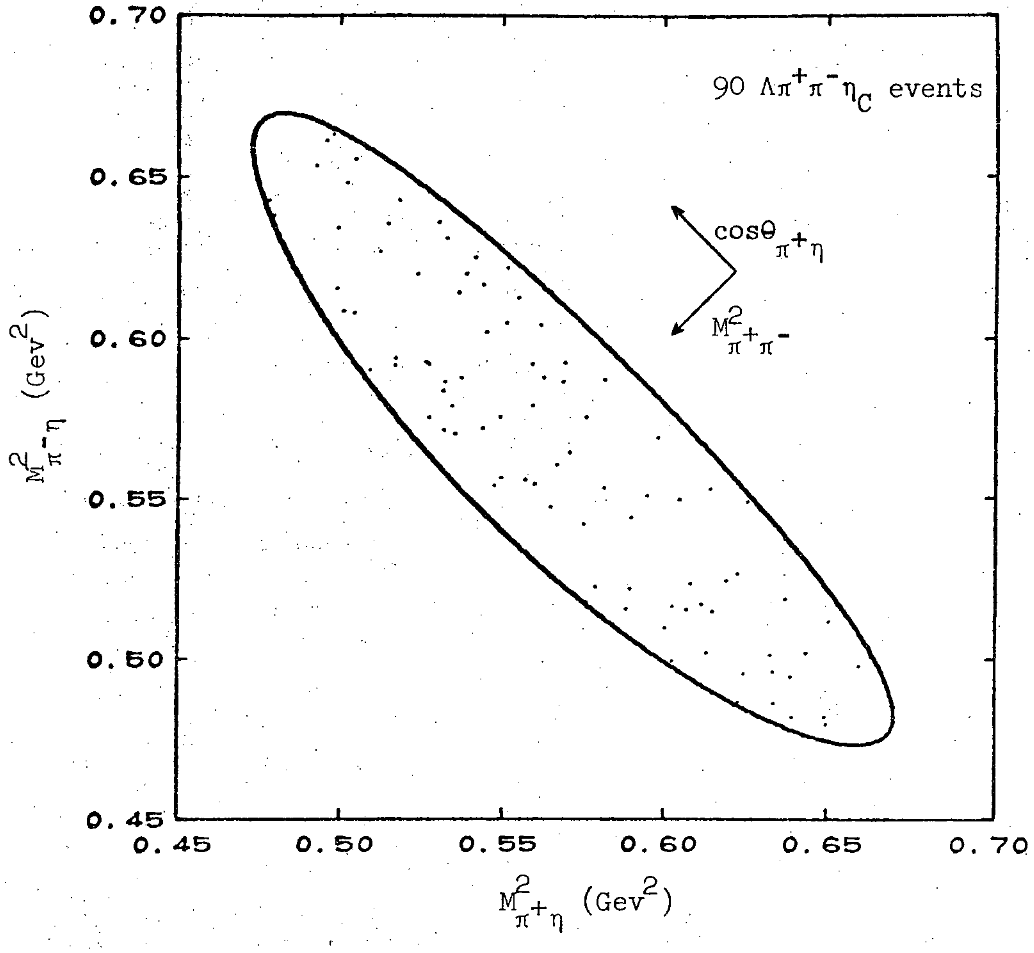

Figure 28. The normalized Dalitz plot for low Δ^2 $\pi^+\pi^-\eta_C$ events with $950 \leq M_{\pi^+\pi^-\eta_C} \leq 970$ Mev. The curve represents the kinematic boundary for the events.

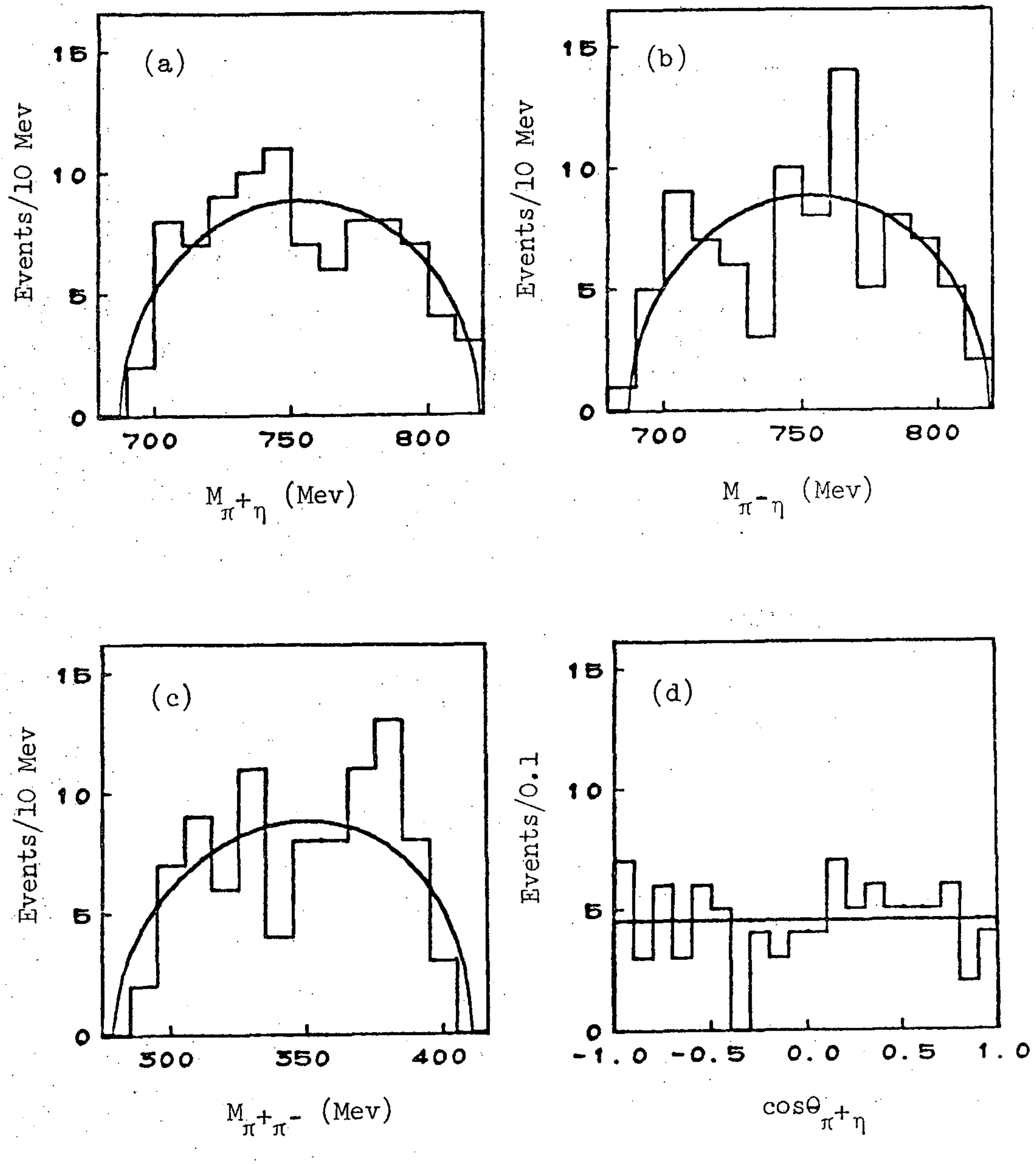

Figure 29. Four projections of the Dalitz plot for the 90 $\pi^+\pi^-\eta_C$ events of Figure 28. The projections are (a) $M_{\pi^+\eta}$, (b) $M_{\pi^-\eta}$, (c) $M_{\pi^+\pi^-}$, and (d) $\cos\Theta_{\pi^+\eta}$. The angle $\Theta_{\pi^+\eta}$ is measured in the dipion rest frame. The curves represent phase space.

would not be a good quantum number, we choose to categorize the η' state by its charge conjugation number C, which is conserved in both strong and electromagnetic decays. Thus J, P, and C of the η' are equal, respectively, to J, P, and C of the $\pi^+\pi^-\eta$ state.

We will use the linear momentum representation of the matrix elements, as discussed by Zemach.[17] Because the Q-value for $\eta' \to \pi\pi\eta$ is low (130 Mev), it is sufficient to use a non-relativistic form involving only three-vectors. For our vectors we choose

$$\vec{q} = \tfrac{1}{2}(\vec{p}_{\pi^+} - \vec{p}_{\pi^-}) \text{ in the dipion rest frame}$$

$$\text{and} \quad \vec{k} = \vec{p}_{\eta} \text{ in the } \eta' \text{ rest frame .}$$

These vectors are to be combined with the polarization tensor of the η' to make a scalar. These tensors are

for $J^P_{\eta'} = 0^-$: 1, a pseudoscalar

$= 1^\pm$: V_i, a pseudovector or vector

$= 2^\pm$: T_{ij}, a tensor or pseudotensor of second rank, symmetric and traceless.

The requirement that T_{ij} be symmetric and traceless reduces it to 5 independent components, as is proper for a spin 2 particle.

Since the $\pi\pi\eta$ intrinsic spin-parity is 0^- and thus "abnormal", for $J^P_{\eta'}$ in the normal series (1^-, 2^+) our vectors must be combined using a cross-product in order that the matrix element be a true scalar. For $J^P_{\eta'}$ in the abnormal series (0^-, 1^+, 2^-) there must be no cross-product (or an even number of them). Further, conservation of C introduces an additional restriction: we note that

$$C_{\eta'} = C(\pi\pi\eta) = C(\pi\pi)C_{\eta} = C(\pi\pi) .$$

But for a boson-antiboson pair such as $\pi\pi$,

$$C(\pi\pi)P(\pi\pi) = +1 .$$

Thus $C_{\eta'} = P(\pi\pi)$; i.e., if $C_{\eta'}$ is even (odd), then our matrix element must be even (odd) under spatial interchange of the two pions, and thus must contain an even (odd) number of powers of $\vec{q}$.

We give in Table IV, marked with an asterisk, the"simplest" matrix elements which can be constructed satisfying the conditions outlined above. By "simplest" we mean those involving the least powers of momenta. Only for $J^{PC} = 2^{-+}$ is there more than one such simplest matrix element. In this case, we list also a general linear combination of the two possibilities. The arbitrary coefficient introduced may be real (if there are no final state interactions) or complex. We have allowed for both possibilities.

Table IV also indicates the orbital angular momentum $\ell_{\pi\pi}$ of the two pions in the dipion rest frame, and the orbital angular momentum ℓ_{η} of the η in the η' rest frame, for each of the matrix elements. We note that $\ell_{\pi\pi}$ equals the power of $\vec{q}$, while ℓ_{η} equals the power of $\vec{k}$. These quantities are depicted in Figure 30.

The Dalitz plot distribution is obtained by squaring the matrix elements and summing over the spin states λ of the η'. For the purposes of this summation, we use the relationships

$$\sum_{\lambda} V_i^{\lambda} V_j^{\lambda} = \delta_{ij}$$

and $$\sum_{\lambda} T_{ij}^{\lambda} T_{mn}^{\lambda} = \tfrac{1}{2}(\delta_{im}\delta_{jn} + \delta_{in}\delta_{jm} - \tfrac{2}{3}\,\delta_{ij}\delta_{mn}) .$$

The results, apart from overall constants, are given in Table IV. In

Table IV. Matrix elements for $\eta' \rightarrow \pi^+\pi^-\eta$. The quantities $\vec{k}$, $\vec{q}$, ℓ_η, $\ell_{\pi\pi}$, and y are defined in the text; Θ represents the angle $\Theta_{\pi^+\eta}$. a is a free parameter to be fit to the data, and BW indicates a resonance in the $\pi\pi$ system with a Breit-Wigner line shape. Asterisks mark the simplest matrix elements.

Fit No.	C	J^P	$\ell_\eta, \ell_{\pi\pi}$	$\pi\pi$ Resonance or Linear Matrix Element	Matrix Element	Matrix Element Squared and Summed over Spin
* 1	+1	0^-	0,0	-	1	1
2			0,0	σ (M_σ=380, Γ_σ=100 Mev)	BW_σ	$\lvert BW_\sigma \rvert^2$
3			0,0	σ (M_σ, Γ_σ fit to data)	BW_σ	$\lvert BW_\sigma \rvert^2$
4			0,0	linear matrix element: real	$1 + ay$	$1+2ay+a^2y^2$
5			0,0	complex	$1 + ay$	$1+2\mathrm{Re}(a)y+\lvert a \rvert^2 y^2$
* 6		1^+	1,0	-	$\vec{k}\cdot\vec{V}$	k^2
7			1,0	σ (M_σ=380, Γ_σ=100 Mev)	$\vec{k}\cdot\vec{V}\ BW_\sigma$	$k^2 \lvert BW_\sigma \rvert^2$
* 8		1^-	2,2	-	$(\vec{q}\cdot\vec{k})\vec{q}x\vec{k}\cdot\vec{V}$	$q^4k^4\cos^2\Theta\sin^2\Theta$
* 9		2^+	1,2	-	$\vec{q}\cdot\overset{\rightrightarrows}{T}\cdot\vec{q}x\vec{k}$	$q^4k^2\sin^2\Theta$
* 10		2^-	0,2	-	$\vec{q}\cdot\overset{\rightrightarrows}{T}\cdot\vec{q}$	q^4
* 11			2,0	-	$\vec{k}\cdot\overset{\rightrightarrows}{T}\cdot\vec{k}$	k^4
12			2,0	σ (M_σ=380, Γ_σ=100 Mev)	$\vec{k}\cdot\overset{\rightrightarrows}{T}\cdot\vec{k}\ BW_\sigma$	$k^4 \lvert BW_\sigma \rvert^2$
* 13			mixture of 0,2 and 2,0: real	-	$\vec{q}\cdot\overset{\rightrightarrows}{T}\cdot\vec{q} + a\vec{k}\cdot\overset{\rightrightarrows}{T}\cdot\vec{k}$	$q^4+aq^2k^2(3\cos^2\Theta-1)+a^2k^4$
* 14			complex	-	$\vec{q}\cdot\overset{\rightrightarrows}{T}\cdot\vec{q} + a\vec{k}\cdot\overset{\rightrightarrows}{T}\cdot\vec{k}$	$q^4+\mathrm{Re}(a)q^2k^2(3\cos^2\Theta-1)+\lvert a \rvert^2k^4$
* 15	-1	0^-	1,1	-	$\vec{q}\cdot\vec{k}$	$q^2k^2\cos^2\Theta$
* 16		1^+	0,1	-	$\vec{q}\cdot\vec{V}$	q^2
* 17		1^-	1,1	-	$\vec{q}x\vec{k}\cdot\vec{V}$	$q^2k^2\sin^2\Theta$
* 18		2^+	2,1	-	$\vec{k}\cdot\overset{\rightrightarrows}{T}\cdot\vec{q}x\vec{k}$	$q^2k^4\sin^2\Theta$
* 19		2^-	1,1	-	$\vec{k}\cdot\overset{\rightrightarrows}{T}\cdot\vec{q}$	$q^2k^2(3+\cos^2\Theta)$

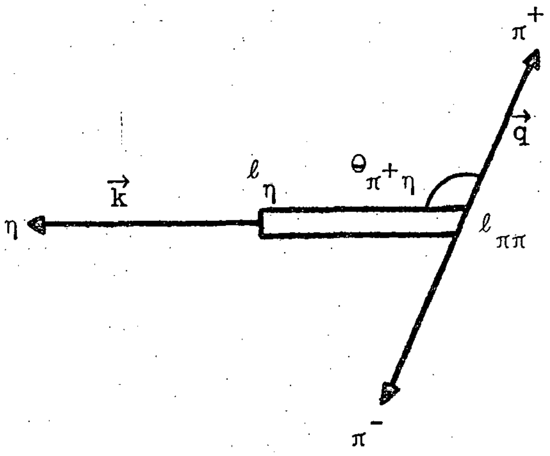

Figure 30. Diagram relevant to the $\pi^+\pi^-\eta$ Dalitz plot analysis. The definitions of the variables shown are given in the text.

Figure 31 we show the $M_{\pi^+\pi^-}$ and $\cos\theta_{\pi^+\eta}$ distributions predicted by each of the J^{PC} assignments under consideration, together with the data. Table V gives the chi-square between the prediction and the data, as well as the overall confidence level for the fits to the two distributions. For $J^{PC} = 2^{-+}$ we have done a simultaneous fit to the two distributions, using the program MINFUN,[18] in order to determine the best value of the arbitrary coefficient.

An examination of Table V, where again the results for the simplest matrix elements we have been discussing are marked with an asterisk, indicates that the C = -1 states are all ruled out, as are the $J^P = 1^+$, 1^-, and 2^+ states for C = +1. The only remaining possibilities are $J^P = 0^-$ and 2^- for C = +1. For the 2^- case we see that neither of the two separate possibilities alone is acceptable, but instead we are required to use a specific mixture of ($\ell_{\pi\pi} = 0$, $\ell_\eta = 2$) and ($\ell_{\pi\pi} = 2$, $\ell_\eta = 0$). Although this certainly does not rule out the 2^- case, it would suggest that it is less likely than 0^-.

In either case, however, 0^- or 2^-, we are still faced with the fact that the fit to the $M_{\pi\pi}$ distribution is rather poor. The χ^2 for 0^- is 27, while that for 2^- is 35, where values of 13 and ~12 are expected. The confidence levels are 0.01 and 0.0005, respectively. Thus, we have attempted to see if matters might be improved by modifying our matrix elements.

Since the $M_{\pi^+\eta}$ and $M_{\pi^-\eta}$ distributions are seen, in Figure 27, to agree quite well with phase space (which corresponds to a C = +1, $J^P = 0^-$ assumption for the η'), we are inclined to believe that the

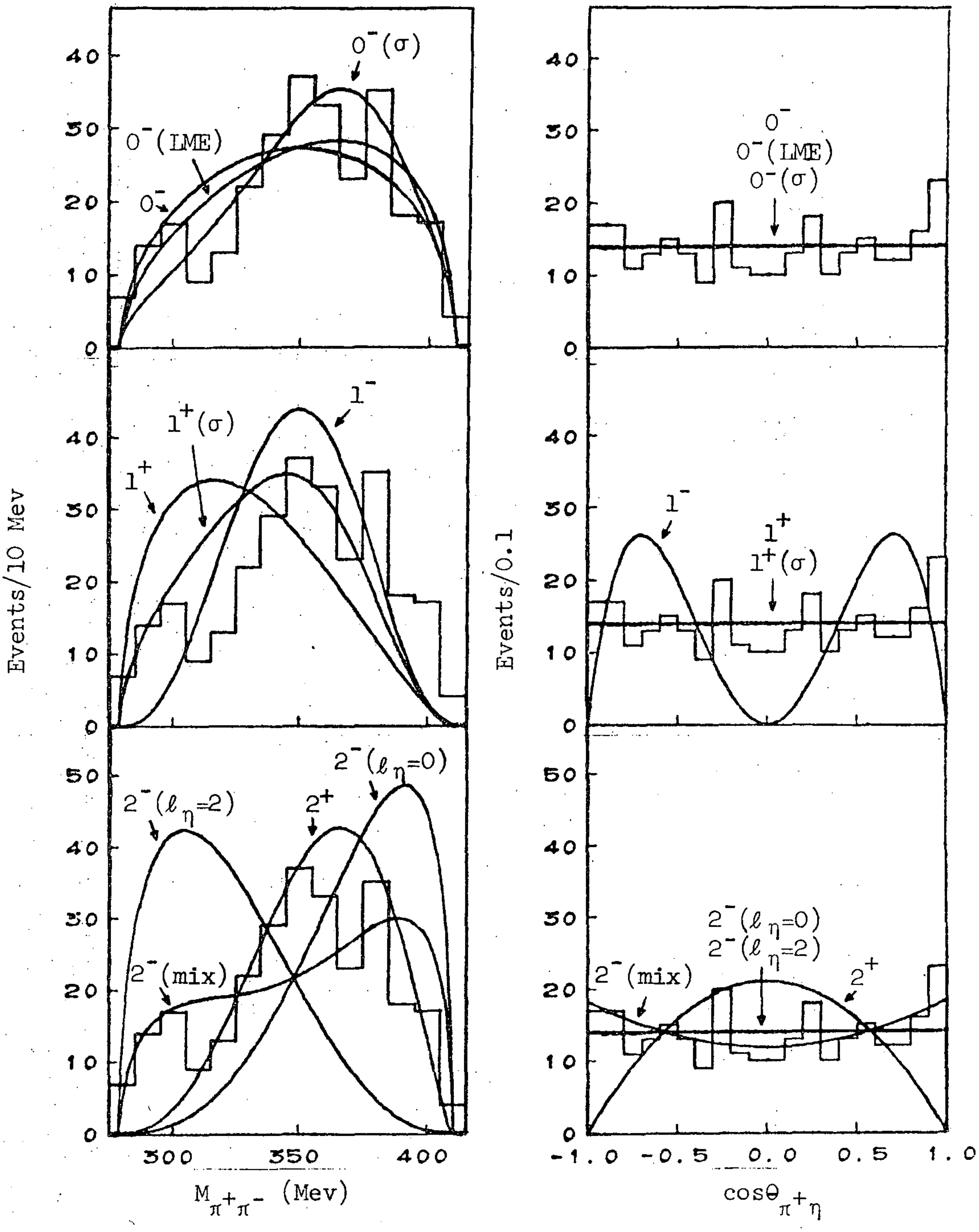

Figure 31(a). Predicted $M_{\pi^+\pi^-}$ and $\cos\theta_{\pi^+\eta}$ distributions for C=+1, $\pi^+\pi^-\eta$ matrix elements, for various values of J^P. The data (278 events) are repeated in each plot. See Tables IV and V for definitions and results of the fits. "σ" = with σ resonance (M=380,Γ=100 Mev); "LME" = linear matrix element; "mix" = complex mixture of ℓ_η=0 and ℓ_η=2 for J^P=2^-.

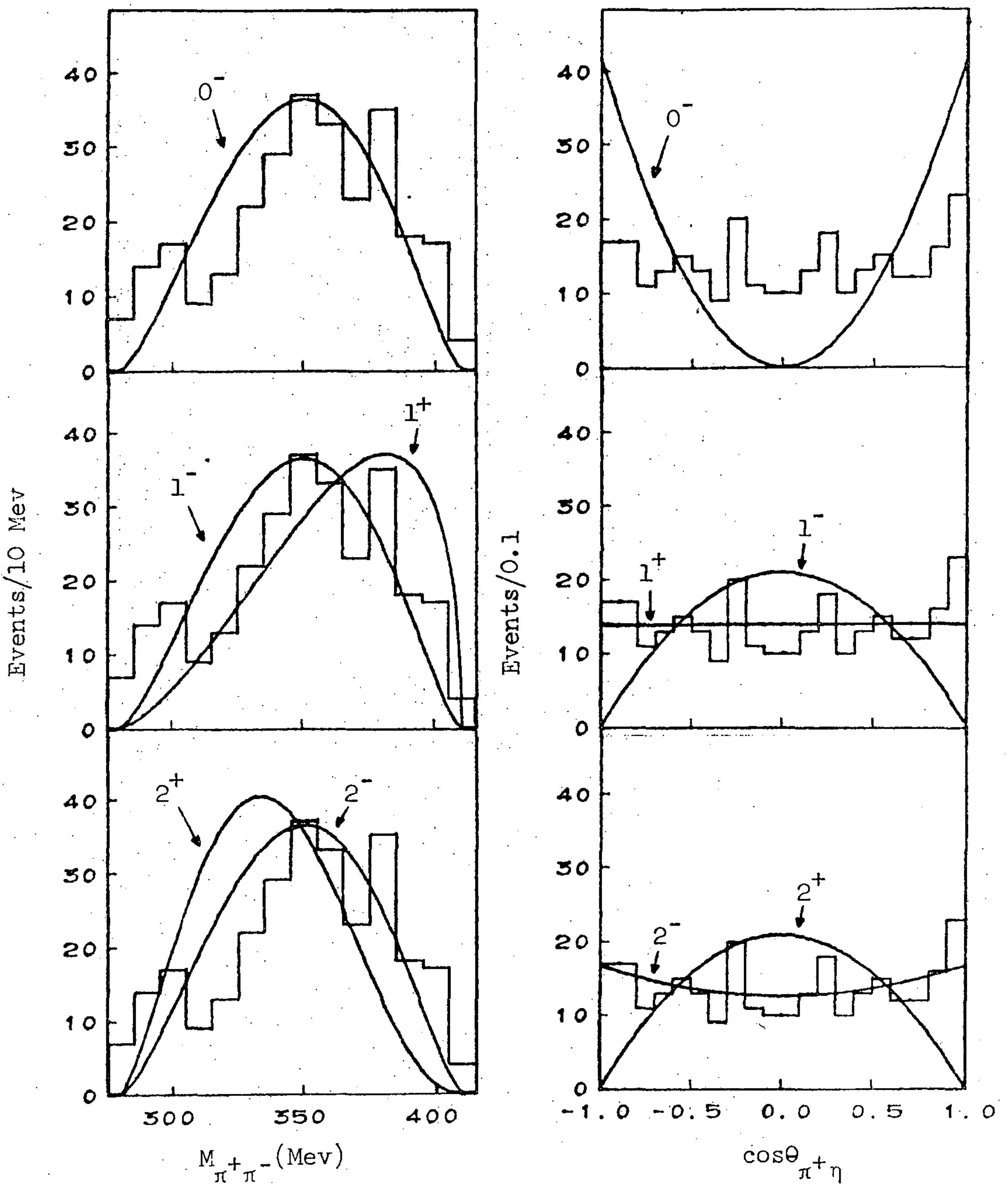

Figure 31(b). Predicted $M_{\pi^+\pi^-}$ and $\cos\theta_{\pi^+\eta}$ distributions for C=-1, $\pi^+\pi^-\eta$ matrix elements, for various values of J^P. The data (278 events) are repeated in each plot. See Tables IV and V for definitions and results of the fits.

Table V. Results of fitting the $\pi^+\pi^-\eta$ matrix elements of Table IV to the experimental $M_{\pi^+\pi^-}$ and $\cos\theta_{\pi^+\eta}$ distributions. The fit numbers correspond to those of Table IV; asterisks mark the simplest matrix elements.

Fit No.	C	J^P	$\ell_\eta, \ell_{\pi\pi}$	$\pi\pi$ Resonance or Linear Matrix Element	Value of Free Parameter(s)	$\chi^2(M_{\pi^+\pi^-})$ (14 bins)	$\chi^2(\cos\theta_{\pi^+\eta})$ (20 bins)	Combined Conf. Lev.
* 1	+1	0^-	0,0	-	-	27	18	0.07
2			0,0	σ (M_σ=380, Γ_σ=100 Mev)	-	37	18	$7\text{x}10^{-3}$
3			0,0	σ (M_σ, Γ_σ fit to data)	M_σ = 395±13 Mev Γ_σ = 155±24 Mev	23	18	0.08
4			0,0	linear matrix element: real	a = -0.11±0.05	24	18	0.10
5			0,0	linear matrix element: complex	a=(-0.11±0.05) +(0.00±0.29)i	24	18	0.08
* 6		1^+	1,0	-	-	220	18	$<10^{-10}$
7			1,0	σ (M_σ=380, Γ_σ=100 Mev)	-	132	18	$<10^{-10}$
* 8		1^-	2,2	-	-	283	384	$<10^{-10}$
* 9		2^+	1,2	-	-	301	401	$<10^{-10}$
* 10		2^-	0,2	-	-	543	18	$<10^{-10}$
* 11			2,0	-	-	788	18	$<10^{-10}$
12			2,0	σ (M_σ=380, Γ_σ=100 Mev)	-	547	18	$<10^{-10}$
* 13			mixture of 0,2 and 2,0: real	-	a = 0.31±0.03	35	19	$6\text{x}10^{-3}$
* 14			mixture of 0,2 and 2,0: complex	-	a=(0.17±0.08) +(0.27±0.06)i	35	14	0.02
* 15	-1	0^-	1,1	-	-	111	690	$<10^{-10}$
* 16		1^+	0,1	-	-	167	18	$<10^{-10}$
* 17		1^-	1,1	-	-	111	401	$<10^{-10}$
* 18		2^+	2,1	-	-	387	401	$<10^{-10}$
* 19		2^-	1,1	-	-	111	14	$<10^{-10}$

modifications we make to the matrix elements should reflect some $\pi\pi$ final state interaction rather than a $\pi\eta$ interaction. Thus as our first attempt, we have tried a spin 0 resonance between the two pions as suggested by Brown and Singer.[19] For the three cases with $\ell_{\pi\pi} = 0$, namely 0^-, 1^+, and one of the 2^- cases, we have assumed that the η' decay goes via a spin 0, isospin 0 resonance, the hypothesized σ, of mass $M_\sigma = 380$ Mev and width $\Gamma_\sigma = 100$ Mev. We have thus multiplied the matrix elements under consideration by a Breit-Wigner, which when squared has the form

$$BW(M_\sigma,\Gamma_\sigma)^2 = \left[(M_{\pi\pi}^2 - M_\sigma^2)^2 + \frac{M_\sigma^4\Gamma_\sigma^2}{M_{\pi\pi}^2} \left(\frac{q}{q_\sigma}\right)^{4J_\sigma + 2} \right]^{-1} .$$

Here q is the relative momentum of the two pions in the dipion rest frame, and q_σ is the value of q when $M_{\pi\pi} = M_\sigma$. As indicated in Table V, this assumption does not improve matters for the 0^- case, and leaves the 1^+ and 2^- ($\ell_{\pi\pi} = 0$, $\ell_\eta = 2$) fits still highly unacceptable. Even if we fit the 0^- case with a variable M_σ and Γ_σ, the result, with $M_\sigma = 395$ Mev and $\Gamma_\sigma = 155$ Mev, is a reduction in χ^2 from 27 down to 23, hardly significant.

Our one additional attempt, applied to the 0^- case is purely a phenomenological one. Namely, we have tried a matrix element of the form 1 + ay, where a is a free parameter (real or complex) and y is defined to be

$$y = \left(\frac{m_\eta + 2m_\pi}{m_\pi}\right) \frac{T_\eta}{Q} - 1 ;$$

here T_η is the kinetic energy of the η in the η' rest frame. This linear matrix element form is suggested by an analogous form[20] applied to the $\eta \rightarrow \pi^+\pi^-\pi^0$ decay, where the $M_{\pi^+\pi^-}$ distribution favors high values of $M_{\pi^+\pi^-}$ as ours is seen to do. We note that the linear matrix element used in η decay is of the form $1 + ay_\eta$, where y_η is defined as

$$y_\eta = 3\left(\frac{T_{\pi^0}}{Q}\right) - 1 .$$

As can be verified, both our y and also y_η have the value -1 when $M_{\pi^+\pi^-}$ is at its maximum and (in the non-relativistic limit) the value +1 when $M_{\pi^+\pi^-}$ is at its minimum. Further, in both $\eta' \rightarrow \pi^+\pi^-\eta$ and $\eta \rightarrow \pi^+\pi^-\pi^0$ decays, $M_{\pi^+\pi^-}$ ranges over the same values, 280 to 410 Mev, resulting from the fact that both decays have the same Q-value. Thus if the peaking of the $M_{\pi^+\pi^-}$ distribution to higher masses were due <u>solely</u> to a $\pi^+\pi^-$ effect, we might expect the same value of the parameter <u>a</u>. Our fit for the decay of the η' yields the value $a = (-0.11 \pm 0.05) + (0.00 \pm 0.29)i$, whereas for η decay[20] $a = (-0.478 \pm 0.038) + \left(0.0025 \begin{matrix} +0.1467 \\ -0.1136 \end{matrix}\right)^{\frac{1}{2}} i$, in considerable disagreement for the real part of <u>a</u>. Furthermore, the $M_{\pi^+\pi^-}$ distribution fit obtained for the η' still has a χ^2 of 24.

So we are left with a somewhat unsatisfactory situation with respect to the $\pi^+\pi^-$ mass distribution, namely that our best fit, which corresponds to a $C = +1$, $J^P = 0^-$ η', has a confidence level of 0.01, which cannot be significantly improved by the use of any simple models. Several possibilities suggest themselves: Almost half of the χ^2 contribution (13 out of 27) comes from two bins, those surrounding $M_{\pi\pi} = 315$ Mev. It is possible that we are simply the victims of a $3\frac{1}{2}$ standard deviation statistical fluctuation in these two bins. This would likely be a vertical fluctuation rather than a horizontal one since our $M_{\pi\pi}$ resolution is ~ 6 Mev (FWHM), while our bins are 10 Mev. On the chance that the dip in these two bins might be the result of scanning or measuring biases, we have checked for such biases, but have found none which could produce the observed effect. Further, while it is true that the two pions are nearly parallel in the lab at the values of $M_{\pi\pi}$ we are concerned with, and thus might be difficult to scan and/or measure, we would expect the situation to be even worse in the lowest three bins. We have also checked that rebinning the histogram, or using the unnormalized values of $M_{\pi\pi}$, does not remove the effect.

If we assume that the high χ^2 is resulting primarily from an excess of events at the higher values of $M_{\pi\pi}$, rather than from a depletion at some of the lower values, there is another bias which might be at work here. Assuming the η' has $I = 0$ and decays into $\pi\pi\eta$ via a strong interaction, as we shall shortly argue, then we expect a decay into $\pi^0\pi^0\eta_C$ as well as $\pi^+\pi^-\eta_N$. Using the Clebsch-Gordan coefficients for the η' decay and the known branching ratios for the η,[16] we expect the ratio

$$\frac{\eta' \to \pi^0\pi^0\eta_C}{\eta' \to \pi^+\pi^-\eta_N} = \frac{1}{2} \times \frac{1}{2.5} = 0.20 \quad .$$

What is then the chance that in the $\pi^0\pi^0\eta_C$ decay the two π^0's from the η' and the π^0 (or γ) from η_C would have a mass near enough that of an η so that a genuine $\pi^0\pi^0\eta_C$ event could fake a $\pi^+\pi^-\eta_N$ event? Under the assumption that the true $\eta' \to \pi\pi\eta$ decay is flat and that the small amount of $\eta_C \rightarrow \pi^+\pi^-\gamma$ can be treated like $\eta_C \rightarrow \pi^+\pi^-\pi^o$, and using the known decay distribution of $\eta_C \rightarrow \pi^+\pi^-\pi^o$,[20] we show in Figure 32a the expected $\pi^o\pi^o\pi^o$ distribution for $\pi^o\pi^o\eta_C$ events. We have folded in our missing mass resolution of ~ 25 Mev. Figure 23b indicates that essentially all $\Lambda\pi^+\pi^-$MM events having a missing mass between 530 and 570 Mev have been assigned to the $\Lambda\pi^+\pi^-\eta_N$ hypothesis. Thus from Figure 32a we conclude that $\sim 30\%$ of all $\pi^o\pi^o\eta_C$ events would be misassigned to $\pi^+\pi^-\eta_N$. Combining this with the above ratio of 20% for $(\eta' \rightarrow \pi^o\pi^o\eta_C)/(\eta' \rightarrow \pi^+\pi^-\eta_N)$, we find that about a 6% $\pi^o\pi^o\eta_C$ contamination may have been added to our genuine $\pi^+\pi^-\eta_N$ events. This would amount to ~15 events. We show in Figure 32b the expected $\pi^+\pi^-$ mass distribution for this $\pi^o\pi^o\eta_C$ contamination; note that this is not simply the $\pi^+\pi^-$ distribution from η_C because our requirement that the three π^o's have a mass near that of an η introduces some distortion. The distribution is seen to favor high $M_{\pi^+\pi^-}$ events, but given the broadness of the peak and with only 15 such contaminating events expected, the effect is far too small to contribute significantly to our high χ^2.

Finally, it is of course possible that we are seeing a combination of the spurious effects discussed above, together with a genuine $I = 0$, $\ell = 0$ $\pi^+\pi^-$ final state interaction.

On the basis of the results shown in Table V, we conclude that the most likely J^{PC} assignment for the η' is 0^{-+}. $J^{PC} = 2^{-+}$ cannot be ruled out, but it requires a particular admixture of $(\ell_{\pi\pi} = 0, \ell_\eta = 2)$ and $(\ell_{\pi\pi} = 2, \ell_\eta = 0)$ and even then has a confidence level considerably lower than that for 0^{-+}.

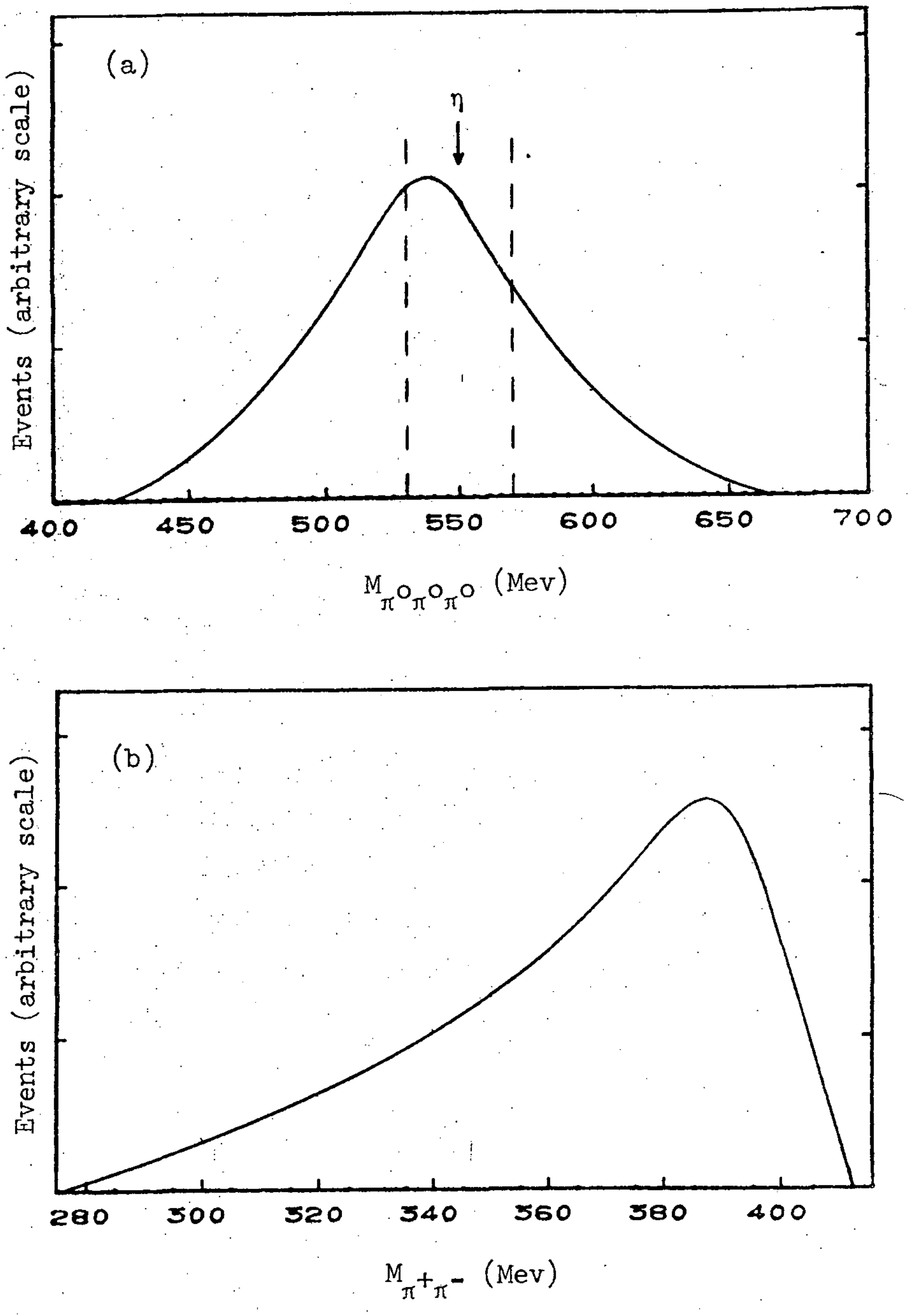

Figure 32. The calculated distribution of $M_{\pi^0\pi^0\pi^0}$ for $\eta' \to \pi^0\pi^0\eta_C$ events, where η_C decays to $\pi^+\pi^-\pi^0$, is shown in (a). Events between the two dashed lines at 530 and 570 Mev would be misidentified as $\pi^+\pi^-\eta_N$ events. The η' decay has been assumed to be flat. (b) The calculated $M_{\pi^+\pi^-}$ distribution for those events in (a) between the dashed lines.

We turn to the question of the G parity of the η', from which we will deduce its isospin. If $G_{\eta'}$ were -1, then a strong decay into $\pi^+\pi^-\pi^0$ would be allowed, while the decay into $\pi^+\pi^-\eta$ would have to be doubly electromagnetic; that is, a photon would have to be emitted and reabsorbed. In that case, we should expect the 3π decay to dominate over the $\pi\pi\eta$ decay by a factor of $(1/\alpha)^2 \sim 10^4$. Phase space considerations would further enhance the 3π decay, regardless of whether the spin of the η' were 0 or 2. Thus, barring any unforeseen quantum number which would very strongly inhibit 3π, we should expect to see many more 3π than $\pi\pi\eta$ decays. But we do not. As shown earlier, essentially all of those events which might conceivably be $\pi^+\pi^-\pi^0$ are in fact $\pi^+\pi^-\gamma$. We therefore conclude that $G_{\eta'} = +1$. Using the relation $G = C(-1)^I$, where we know $C_{\eta'}$ to be +1, it follows that $I_{\eta'}$ must be even. But as previously mentioned our production reaction limits $I_{\eta'}$ to 0 or 1. Thus we have $I_{\eta'} = 0$.

In summary then, the $\pi^+\pi^-\eta$ Dalitz plot leads us to the probable quantum numbers $I^GJ^P = 0^+0^-$, with 0^+2^- being a less preferred assignment.

B. The $\pi^+\pi^-\gamma$ Dalitz Plot

We begin this section, by showing in Figure 33 a plot of the $\pi^+\pi^-\gamma$ mass spectrum, for $\Lambda\pi^+\pi^-\gamma$ events with $\Delta^2 \leq 0.5$ (Gev/c)^2. There is a significant background contamination under the η' peak, which arises from misidentified $\pi^+\pi^-\pi^0$ events. In Figure 34 we present an analogous plot of the $\pi^+\pi^-\pi^0$ effective mass for those events assigned to the $\Lambda\pi^+\pi^-\pi^0$ hypothesis. There is, as expected,

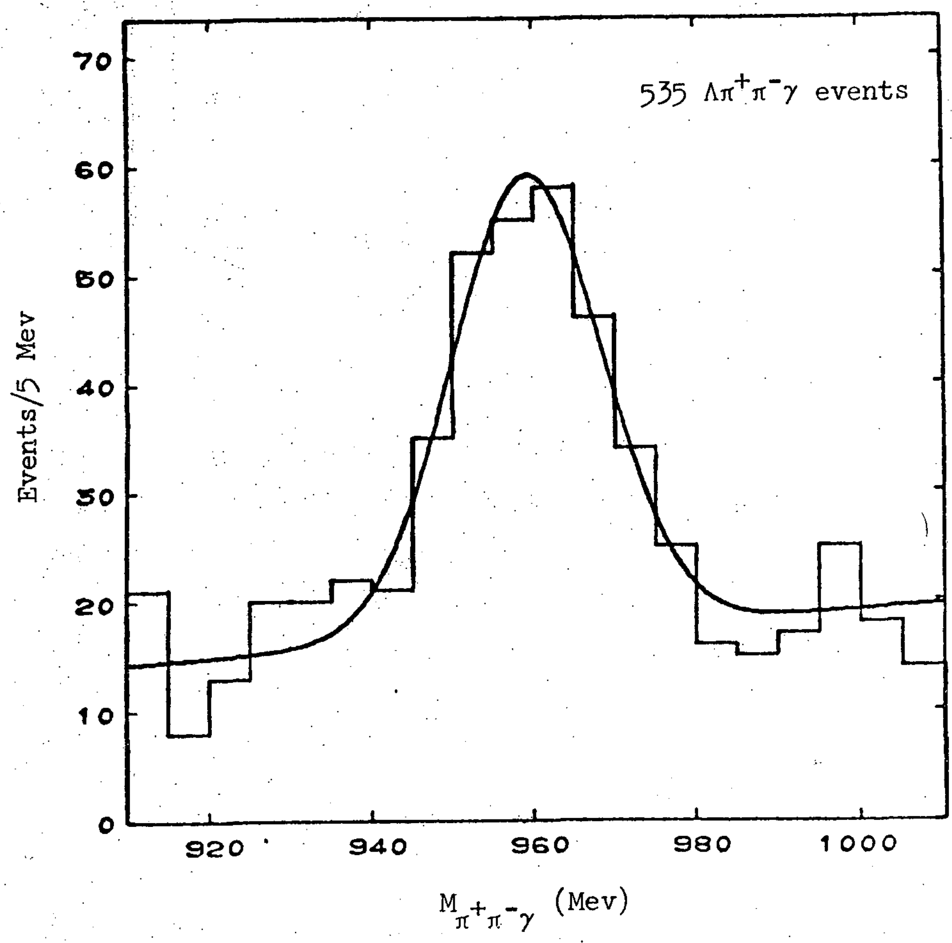

Figure 33. The $\pi^+\pi^-\gamma$ mass spectrum for low Δ^2 $\Lambda\pi^+\pi^-\gamma$ events. The curve is a fit to the data of a Gaussian plus a linear background.

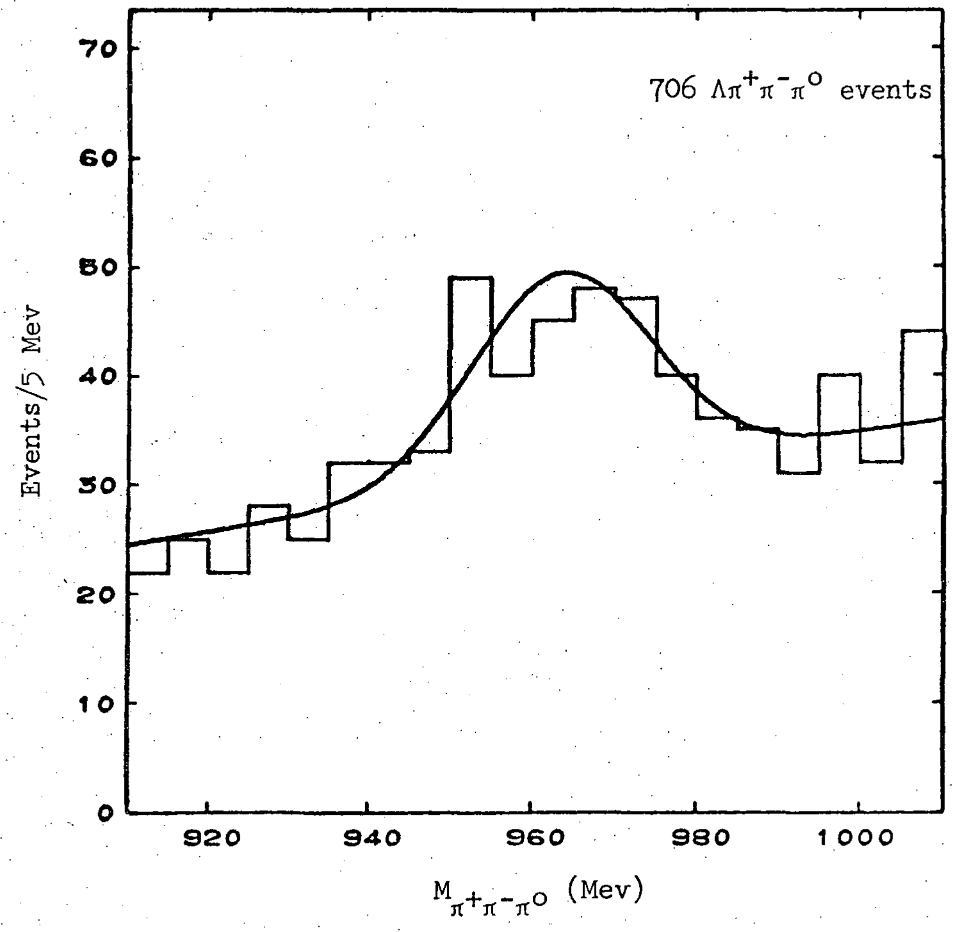

Figure 34. The $\pi^+\pi^-\pi^0$ mass spectrum for low Δ^2 $\Lambda\pi^+\pi^-\pi^0$ events. The curve is a fit to the data of a Gaussian plus a linear background.

some signal in the η' region, resulting from misidentified $\pi^+\pi^-\gamma$ events. The curves over the events for these two plots represent fits to a variable linear background plus a Gaussian of variable position and width. The width of the Gaussian required is comparable to the calculated resolution of $\sim$ 20 Mev. Although we will have to perform a subtraction on our $\pi^+\pi^-\gamma$ events in order to do our analysis, for reference we present in Figures 35 and 36 the normalized Dalitz plot and four projections for the 280 unsubtracted $\pi^+\pi^-\gamma$ events having $\Delta^2 \leqq 0.5$ (Gev/c)^2 and $945 \leqq M_{\pi^+\pi^-\gamma} \leqq 975$ Mev. The projections shown are for $M_{\pi^+\gamma}$, $M_{\pi^-\gamma}$, $M_{\pi^+\pi^-}$, and the cosine of the angle $\Theta_{\pi^+\gamma}$ between the π^+ and the γ in the dipion rest frame. Figures 37 and 38 show the analogous set of plots for the $\pi^+\pi^-\pi^0$ events. The difference in structure can easily be seen, resulting from the fact that the first set of events is primarily $2\pi\gamma$ with $\sim 35\%$ 3π, while the latter set is primarily 3π with $\sim 30\%$ $2\pi\gamma$.

Our subtraction has been performed in the following manner. The fit to the $\pi\pi\gamma$ mass spectrum indicates that, for $M_{\pi\pi\gamma}$ in the 945 to 975 Mev region, there are 178 events in the signal and 102 events in the background. The 3π events shown in Figure 34 have been reinterpreted as $\pi\pi\gamma$ events, and in the resulting $M_{\pi\pi\gamma}$ distribution the peak contains 77 events, while the background under the peak consists of 174 events. Thus, in order to remove the background from the Dalitz plot projections of the events preferring $\pi\pi\gamma$, we have subtracted from each bin a number of events given by

$$N_{\text{subtracted from }\pi\pi\gamma} = \frac{102}{174} \times N_{3\pi} ,$$

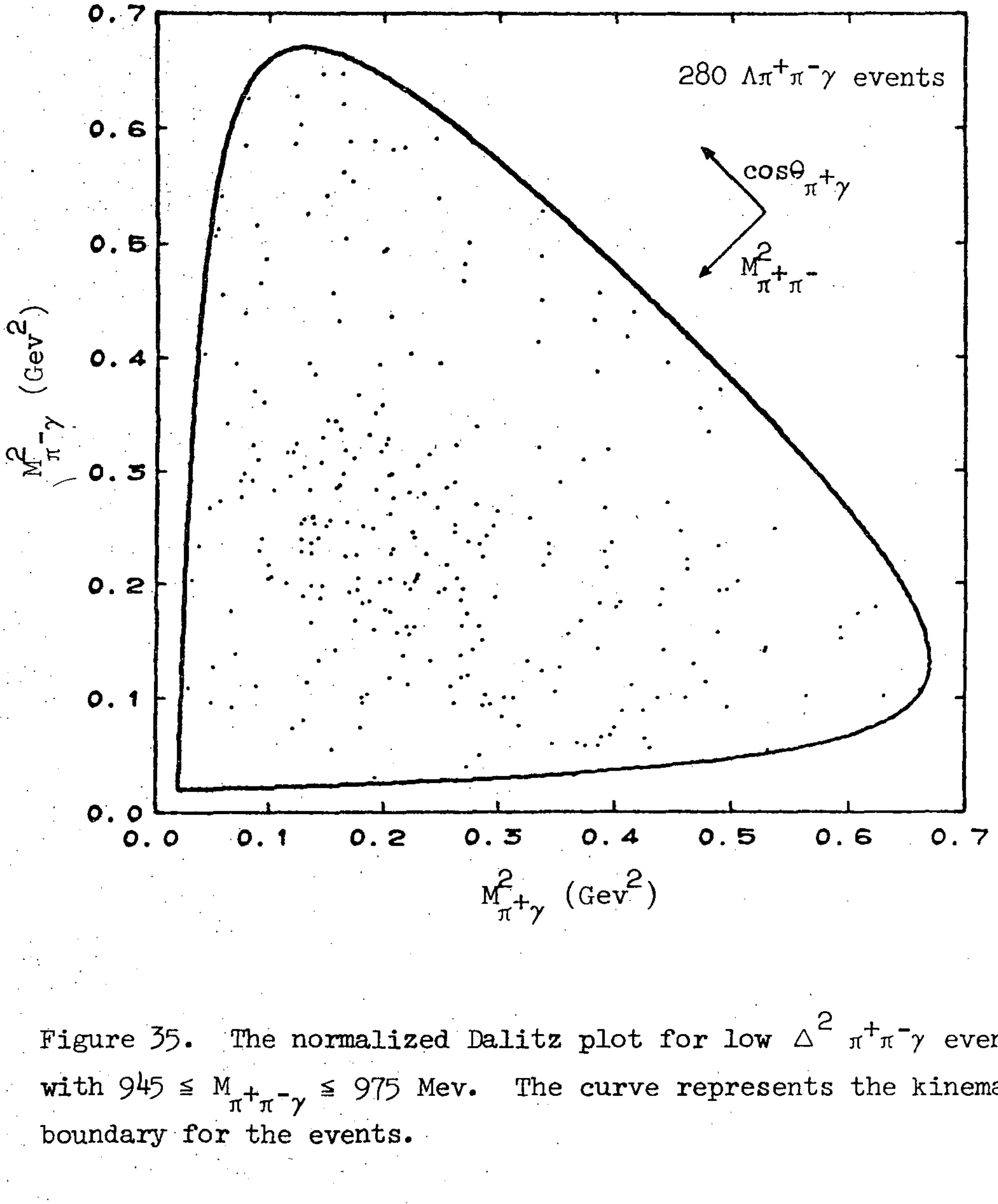

Figure 35. The normalized Dalitz plot for low Δ^2 $\pi^+\pi^-\gamma$ events with $945 \leq M_{\pi^+\pi^-\gamma} \leq 975$ Mev. The curve represents the kinematic boundary for the events.

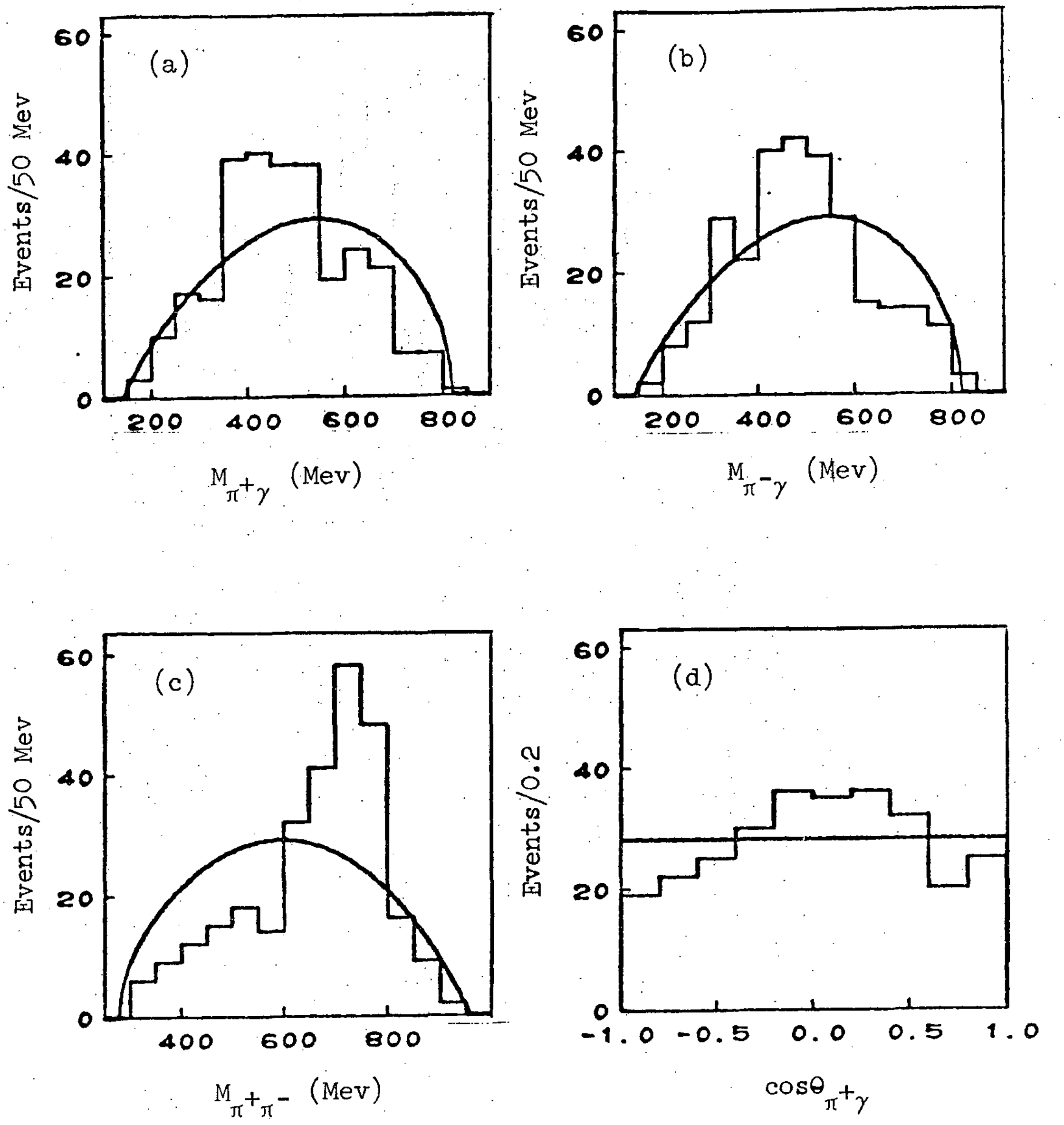

Figure 36. Four projections of the Dalitz plot for the 280 $\pi^+\pi^-\gamma$ events of Figure 35. The projections are (a) $M_{\pi^+\gamma}$, (b) $M_{\pi^-\gamma}$, (c) $M_{\pi^+\pi^-}$, and (d) $\cos\theta_{\pi^+\gamma}$. The angle $\theta_{\pi^+\gamma}$ is measured in the dipion rest frame. The curves represent phase space.

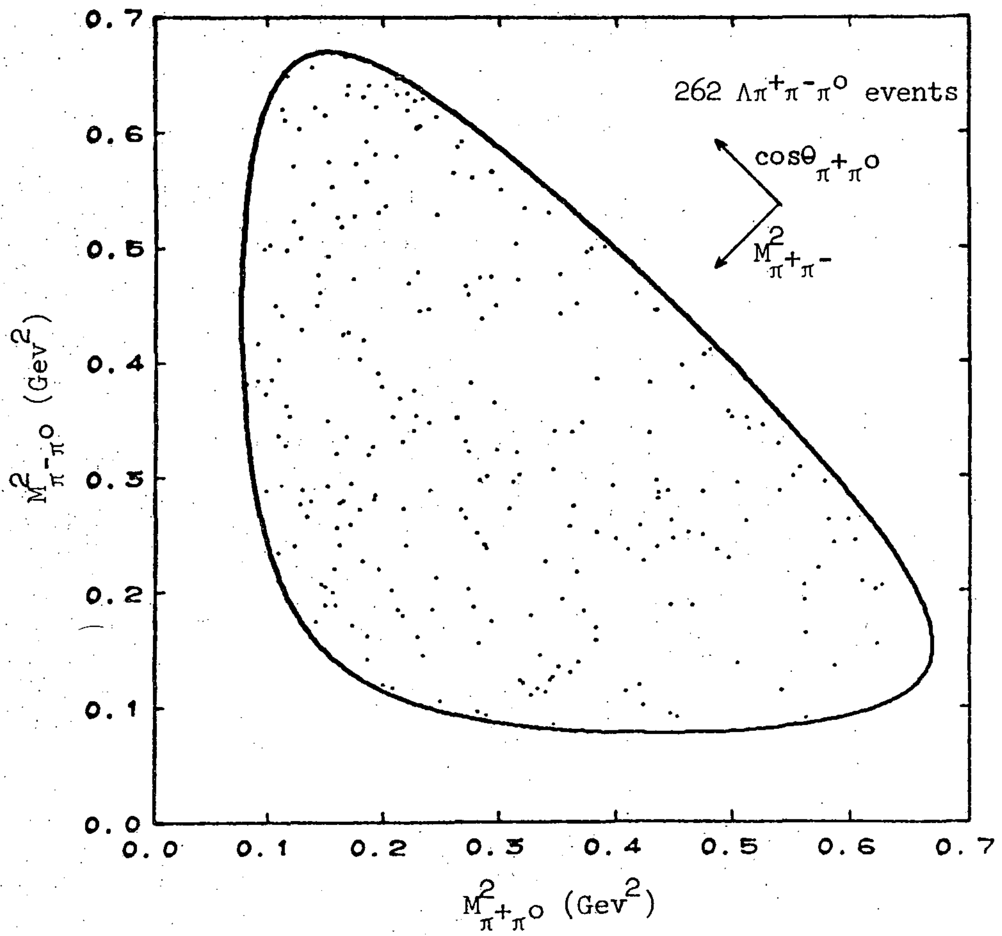

Figure 37. The normalized Dalitz plot for low Δ^2 $\pi^+\pi^-\pi^0$ events with $945 \leq M_{\pi^+\pi^-\pi^0} \leq 975$ Mev. The curve represents the kinematic boundary for the events.

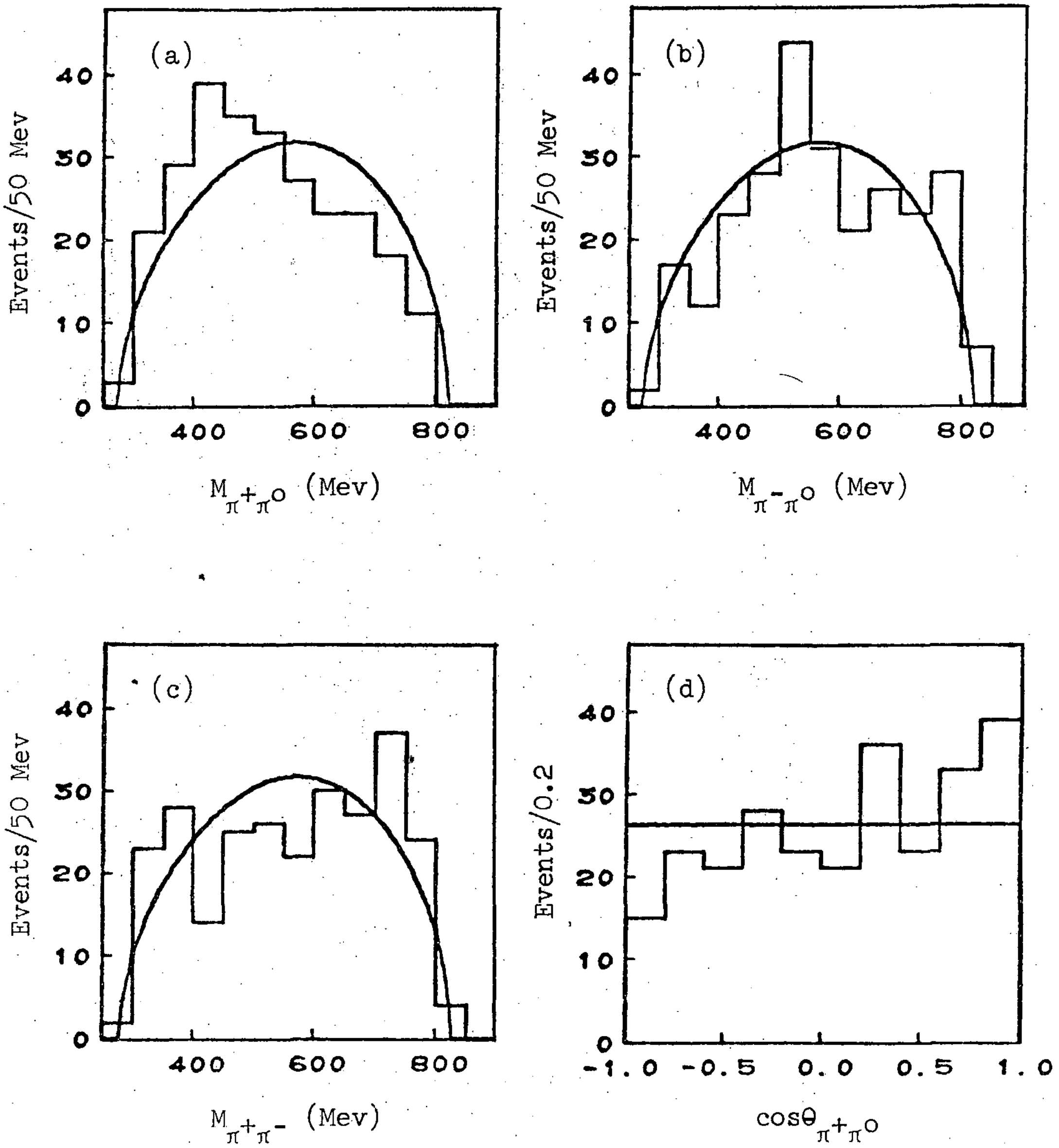

Figure 38. Four projections of the Dalitz plot for the 262 $\pi^+\pi^-\pi^0$ events of Figure 37. The projections are (a) $M_{\pi^+\pi^0}$, (b) $M_{\pi^-\pi^0}$, (c) $M_{\pi^+\pi^-}$, and (d) $\cos\theta_{\pi^+\pi^0}$. The angle $\theta_{\pi^+\pi^0}$ is measured in the $\pi^+\pi^-$ rest frame. The curves represent phase space.

where $N_{3\pi}$ is the number of events in the corresponding 3π bin. Again, we have used the 3π histograms resulting from reinterpreting the 3π events as $\pi\pi\gamma$. The resulting projections for the 132 events remaining are shown in Figure 39. We note that, due to the subtraction, the error bars shown are considerably larger than the square root of the number of events in the bin. Because of this and because the $\cos\Theta_{\pi^+\gamma}$ distribution will be important in the analysis, we have folded this distribution about $\cos\Theta_{\pi^+\gamma} = 0$ in order to reduce the relative errors. The folded distribution is shown in Figure 39e.

We now must construct the matrix elements for the various η' quantum number assignments we wish to consider. We proceed analogously to the $\pi\pi\eta$ case, with some differences. First, because the Q-value for the $\pi\pi\gamma$ decay is rather large (680 Mev) and we are dealing with a γ, we will use a relativistic formalism.[21] The four-vectors we have at our disposal consist of

P_μ = four-momentum of the η'

$q_\mu = \frac{1}{2}(p_{\pi^+} - p_{\pi^-})_\mu$ = relative four-momentum of the two pions

k_μ = four-momentum of the γ

and e_μ = polarization four-vector of the γ, satisfying the relation $k_\mu e_\mu = 0$.

As before, these vectors are to be combined with the polarization tensor of the η' to make a scalar. For the possible polarization tensors we have

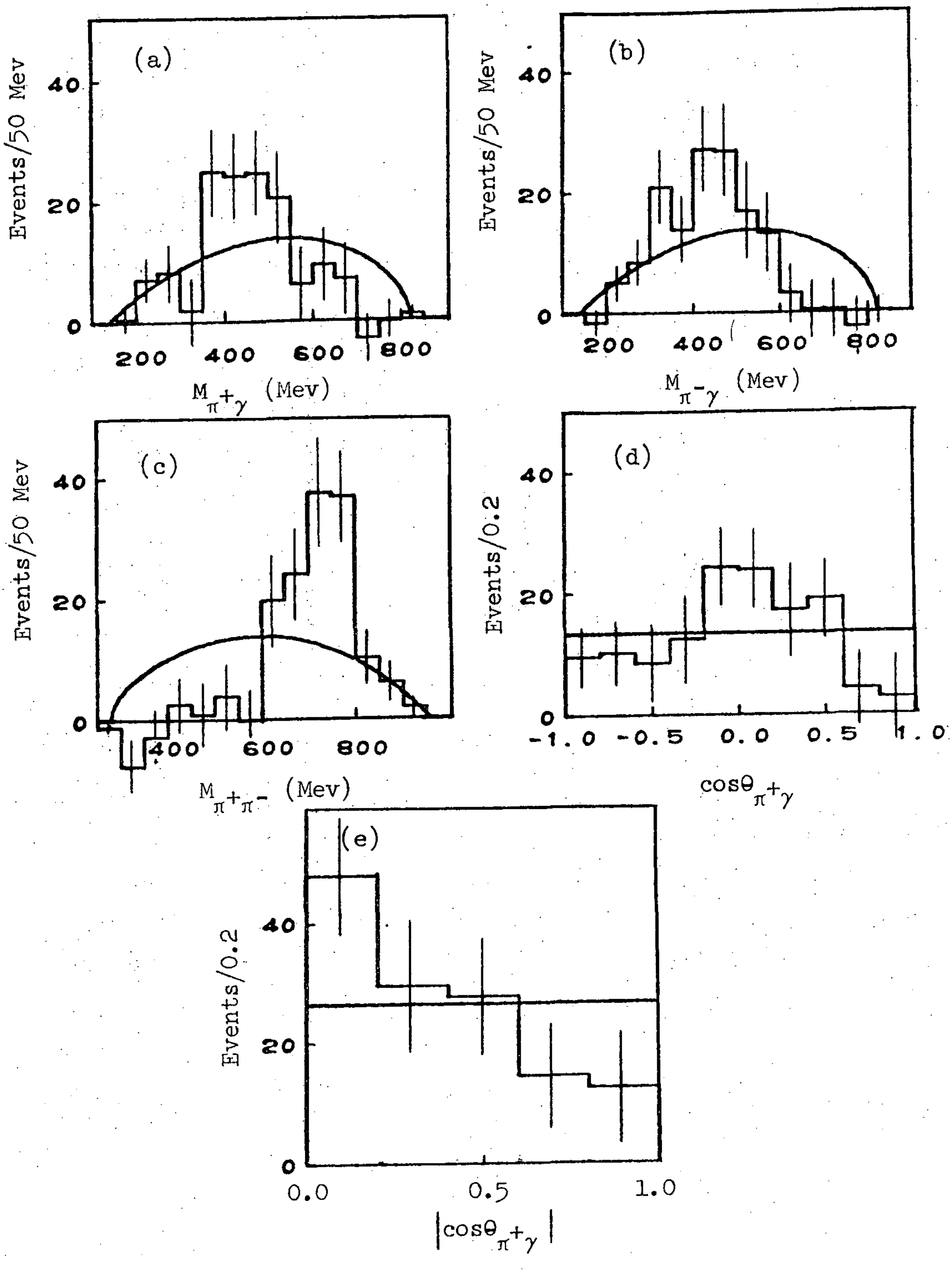

Figure 39. The Dalitz plot projections for the 132 low Δ^2 $\pi^+\pi^-\gamma$ events, having $945 \leq M_{\pi^+\pi^-\gamma} \leq 975$ Mev, which remain after the subtraction discussed in the text has been carried out. The projections are (a) $M_{\pi^+\gamma}$, (b) $M_{\pi^-\gamma}$, (c) $M_{\pi^+\pi^-}$, (d) $\cos\theta_{\pi^+\gamma}$, and (e) $|\cos\theta_{\pi^+\gamma}|$. The curves again represent phase space.

for $J^P_{\eta'} = 0^\pm$: 1, a scalar or pseudoscalar

$= 1^\pm$: V_μ, a pseudovector or vector, satisfying

$$V_\mu P_\mu = 0$$

$= 2^\pm$: $T_{\mu\upsilon}$, a tensor or pseudotensor, symmetric, traceless, and satisfying $T_{\mu\upsilon}P_\mu = 0$.

The requirements on V_μ and $T_{\mu\upsilon}$ reduce them to 3 and 5 independent components respectively, as desired for spins 1 and 2, and also guarantee that in the η' rest frame they reduce to the proper three-vector forms.

We have two invariant tensors with which to combine the various quantities above, namely the metric tensor $g_{\mu\upsilon}$ and the totally anti-symmetric tensor of fourth rank $\epsilon_{\mu\upsilon\alpha\beta}$. Since the intrinsic spin-parity of the $\pi\pi\gamma$ system is 1^-, and thus "normal", for $J^P_{\eta'}$ in the normal series (0^+, 1^-, 2^+) we must combine our tensors with an even number of $\epsilon_{\mu\upsilon\alpha\beta}$. For $J^P_{\eta'}$ in the abnormal series (0^-, 1^+, 2^-) we require an odd number of $\epsilon_{\mu\upsilon\alpha\beta}$. This insures that our matrix element is a true scalar under spatial reflections.

As for the charge conjugation quantum number C, which is conserved in electromagnetic decays, we note that

$$C_{\eta'} \quad = \quad C(\pi\pi\gamma) \quad = \quad C(\pi\pi)C_\gamma \quad = \quad -C(\pi\pi) \ .$$

But again, since CP for a boson-antiboson pair such as $\pi\pi$ is +1, we have

$$C_{\eta'} \quad = \quad -P(\pi\pi) \ .$$

Thus for $C_{\eta'}$ even (odd), our matrix element must be odd (even) under spatial interchange of the two pions, which means that q_μ must appear an odd (even) number of times.

The final requirement is that of gauge invariance, which implies that under the transformation $e_\mu \rightarrow e_\mu + k_\mu$, the matrix element must remain invariant.

In Table VI we give the simplest matrix elements, indicated by an asterisk, which can be formed subject to the above conditions. "Simplest" in this case means having the lowest number of appearances of k_μ. This is equivalent to the lowest order multipole transition allowed. We observe that, except for the C = -1, $J^P = 0^\pm$ cases, a dipole transition will suffice (one appearance of k_μ); C = -1, $J^P = 0^\pm$ requires a quadrupole transition (two appearances of k_μ). We are allowing for the possibility of $J^P_{\eta'} = 0^+$, even though this is strictly forbidden for $\pi\pi\eta$, because we want to leave open the possibility that the particle we are discussing here is not the same as that decaying into $\pi\pi\eta$ (although we have referred to both by the same name).

The Dalitz plot distribution is obtained by squaring the matrix element and summing over the polarizations of the γ and the η'. For this sum, we have the relations

$$\sum_\lambda e^\lambda_\mu e^\lambda_\nu = -g_{\mu\nu}$$

$$\sum_\lambda V^\lambda_\mu V^\lambda_\nu = \Pi_{\mu\nu}$$

and

$$\sum_\lambda T^\lambda_{\mu\nu} T^\lambda_{\alpha\beta} = \tfrac{1}{2}\left(\Pi_{\mu\alpha}\Pi_{\nu\beta} + \Pi_{\mu\beta}\Pi_{\nu\alpha} - \frac{2}{3}\Pi_{\mu\nu}\Pi_{\alpha\beta}\right)$$

where

$$\Pi_{\mu\nu} = -g_{\mu\nu} + \frac{P_\mu P_\nu}{M^2_{\eta'}} .$$

Table VI. Matrix elements for $\eta' \rightarrow \pi^+\pi^-\gamma$. The four-vectors appearing here are defined in the text; in the expressions on the right, q and k are the magnitudes of the three-vector parts of q_μ and k_μ, evaluated in the dipion rest frame. The abbreviations $A\cdot B$ and $[A,B,C,D]$ represent $g_{\mu\upsilon} A_\mu B_\upsilon$ and $\epsilon_{\mu\upsilon\alpha\beta} A_\mu B_\upsilon C_\alpha D_\beta$, respectively, while M and Θ represent $M_{\pi^+\pi^-}$ and $\Theta_{\pi^+\gamma}$. a is a free parameter to be fit to the data and BW indicates a resonance in the $\pi\pi$ system with a Breit-Wigner line shape. The mass and width of the ρ are taken as 765 and 125 Mev, respectively. Asterisks mark the simplest matrix elements.

Fit No.	C	J^P	Multipole	$\pi\pi$ Resonance	Matrix Element	Matrix Element Squared and Summed over Spins
* 1	+1	0^+	Dipole	-	$q\cdot kP\cdot e-q\cdot eP\cdot k$	$q^2k^2M^2\sin^2\theta$
		0^-	Dipole	-	$[q,k,P,e]$	
2		0^+	Dipole	ρ	$(q\cdot kP\cdot e-q\cdot eP\cdot k)BW_\rho$	$q^2k^2M^2\sin^2\theta\|BW_\rho\|^2$
		0^-	Dipole	ρ	$[q,k,P,e]BW_\rho$	
* 3		1^+	Dipole	-	$[q,k,V,e]$	$q^2k^2\{1+\cos^2\theta-(2kM/m^2_{\eta'})\sin^2\theta\}$
		1^-	Dipole	-	$q\cdot kV\cdot e-q\cdot eV\cdot k$	
4		1^+	Dipole	ρ	$[q,k,V,e]BW_\rho$	$q^2k^2\{1+\cos^2\theta-(2kM/m^2_{\eta'})\sin^2\theta\}\|BW_\rho\|^2$
		1^-	Dipole	ρ	$(q\cdot kV\cdot e-q\cdot eV\cdot k)BW_\rho$	
5		1^+	Quadrupole	ρ	$k\cdot V[q,k,P,e]BW_\rho$	$(q^2k^4M^4/m^2_{\eta'})\sin^2\theta\|BW_\rho\|^2$
		1^-	Quadrupole	ρ	$k\circ V(q\cdot kP\cdot e-q\cdot eP\cdot k)BW_\rho$	
* 6		2^+	Dipole	-	$P\cdot kq\cdot T\cdot e-P\cdot eq\cdot T\cdot k$	$q^2k^2M^2\{6+\sin^2\theta+6(k/m_{\eta'})^2\cos^2\theta\}$
		2^-	Dipole	-	$[P,k,q\cdot T,e]$	
7		2^+	Dipole	ρ	$(P\cdot kq\cdot T\cdot e-P\cdot eq\cdot T\cdot k)BW_\rho$	$q^2k^2M^2\{6+\sin^2\theta+6(k/m_{\eta'})^2\cos^2\theta\}\|BW_\rho\|^2$
		2^-	Dipole	ρ	$[P,k,q\cdot T,e]BW_\rho$	

(continued on next page)

Table VI. (continued)

Fit No.	C	J^P	Multipole		ππ Resonance	Matrix Element	Matrix Element Squared and Summed over Spins
8	+1	2^+	Octupole		ρ	$k\cdot T\cdot k(q\cdot kP\cdot e-q\cdot eP\cdot k)BW_\rho$	$(q^2k^6M^6/m_{\eta'}^4)\sin^2\theta\,\lvert BW_\rho\rvert^2$
		2^-	Octupole		ρ	$k\cdot T\cdot k[q,k,P,e]BW_\rho$	
9		2^+	mixture of dipole and quadrupole	real	ρ	$\{P\cdot kq\cdot T\cdot e-P\cdot eq\cdot T\cdot k$ $+a(q\cdot kk\cdot T\cdot e-q\cdot ek\cdot T\cdot k)\}BW_\rho$	$[q^2k^2M^2\{6+\sin^2\theta+6(k/m_{\eta'})^2\cos^2\theta\}$ $-4aq^2k^3M\{1+2\cos^2\theta-(kM/m_{\eta'}^2)(2+\cos^2\theta)\}$ $+2a^2(q^2k^4M^2/m_{\eta'}^2)\{2+\cos^2\theta$ $-4(kM/m_{\eta'}^2)\sin^2\theta\}]\,\lvert BW_\rho\rvert^2$
		2^-		real	ρ	$\{[P,k,q\cdot T,e]$ $+a[q,k,k\cdot T,e]\}BW_\rho$	
10		2^+		complex	ρ	same as above two, but <u>a</u> complex	same as above, but $a\rightarrow \mathrm{Re}(a)$, $a^2\rightarrow \lvert a\rvert^2$
		2^-		complex	ρ		
* 11	-1	0^+	Quadrupole		-	$q\cdot k(q\cdot kP\cdot e-q\cdot eP\cdot k)$	$q^4k^4M^2\sin^2\theta\cos^2\theta$
		0^-	Quadrupole		-	$q\cdot k[q,k,P,e]$	
* 12		1^+	Dipole		-	$[P,k,V,e]$	k^2M^2
		1^-	Dipole		-	$P\cdot kV\cdot e-P\cdot eV\cdot k$	
* 13		2^+	Dipole		-	$q\cdot kq\cdot T\cdot e-q\cdot eq\cdot T\cdot k$	$q^4k^2[1+\cos^2\theta+(2kM/m_{\eta'}^2)\{(2kM/3m_{\eta'}^2)\cos^2\theta$ $-\sin^2\theta\}+(2k^2/3m_{\eta'}^2)\{1+(4kM/m_{\eta'}^2)\}\cos^4\theta]$
		2^-	Dipole		-	$[q,k,q\cdot T,e]$	

Table VI gives the results, where all momenta have been evaluated in the dipion rest frame. We observe that states of opposite parity yield the same distributions, since such states differ only in the polarization of the γ, which we are not observing.

Figure 40 shows the $M_{\pi^+\pi^-}$ and $\cos\theta_{\pi^+\gamma}$ distributions predicted in Table VI, together with the data. The χ^2's and confidence levels for these fits are given in Table VII. We see from the Table that none of the fits is acceptable. We are led by an examination of the $\pi^+\pi^-$ mass spectrum to suspect that the $\pi^+\pi^-\gamma$ decay is being mediated by the two step process $\eta' \rightarrow \rho^0\gamma$, $\rho^0 \rightarrow \pi^+\pi^-$. Since the ρ has $C = -1$ (or equivalently, $P = -1$), such a decay process could take place only for $C_{\eta'} = C_\rho C_\gamma = +1$. Thus we have modified our $C = +1$ matrix elements by inserting a Breit-Wigner of the same form as that used for the σ discussion earlier. We have taken $M_\rho = 765$ Mev and $\Gamma_\rho = 125$ Mev. The resulting distributions are given in Figure 40, and as indicated in Table VII the fits to the $\pi\pi$ distribution are completely acceptable for $J^P = 0^\pm$ and $2^\pm$, and moderately acceptable for $1^\pm$. (We note that the ρ peak in the $\pi\pi$ distribution is shifted from 765 Mev to 730 Mev as a result of the k^2 factor in the matrix element squared.) The distinction between $J = 0$, 1, and 2 thus rests upon the $\cos\theta_{\pi^+\gamma}$ distribution. This distribution yields χ^2's of 2.0, 32, and 8.9, respectively, corresponding to confidence levels of 0.74, 3×10^{-6}, and 0.06. We are therefore led to the conclusion that spin 0 is the most acceptable case, with spin 2 the next most likely possibility. In order to further affirm the preference of spin 0 over spin 2, we have made a cut on the $\pi^+\pi^-$ mass, to favor ρ, of

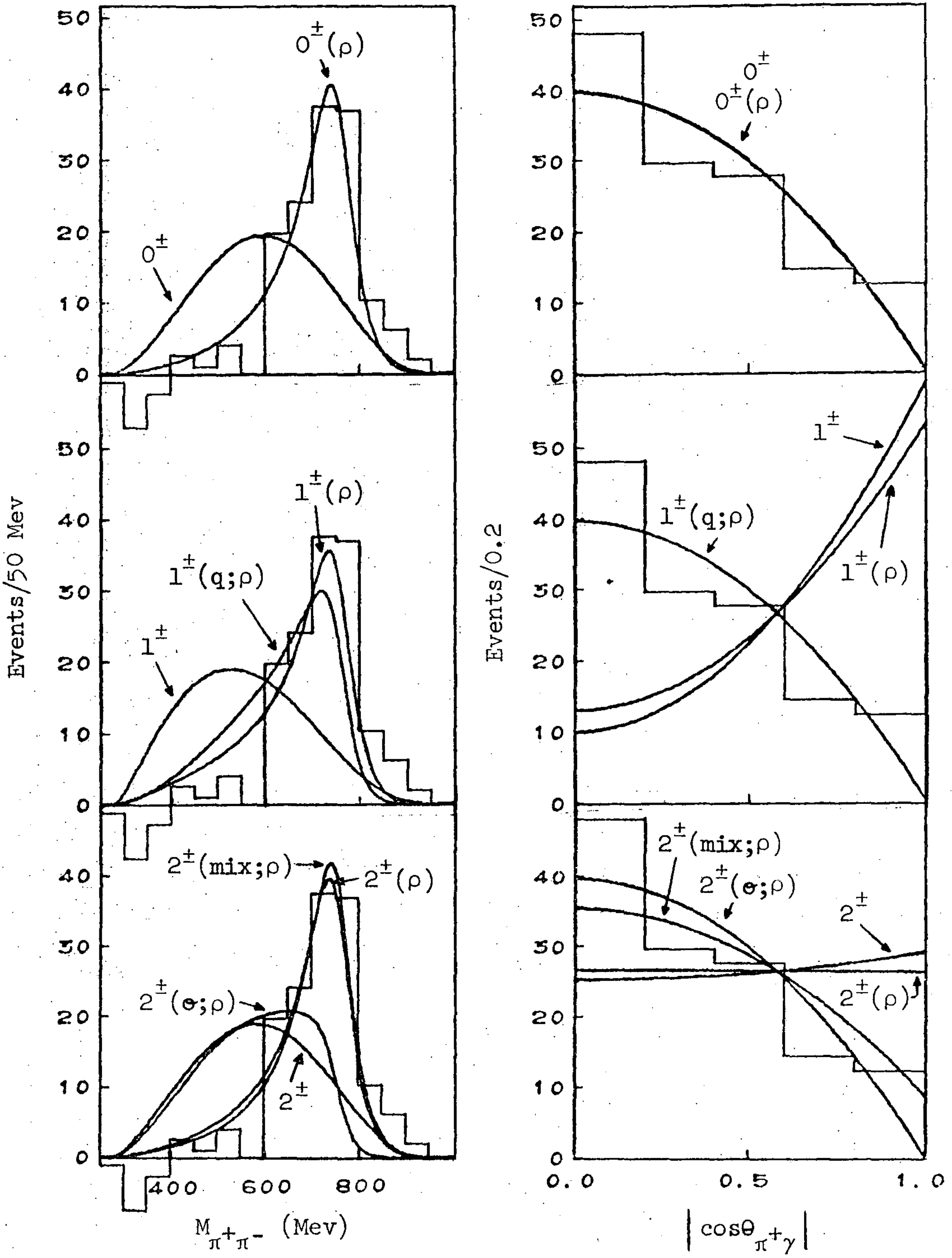

Figure 40(a). Predicted $M_{\pi^+\pi^-}$ and $\cos\theta_{\pi^+\gamma}$ distributions for C=+1, $\pi^+\pi^-\gamma$ matrix elements, for various values of J^P. The data (132 events) are repeated in each plot. See Tables VI and VII for definitions and results of the fits. "ρ" = with ρ resonance; "q" = quadrupole; "ɵ" octupole; "mix" = complex mixture of dipole and quadrupole for $J^P=2^\pm$.

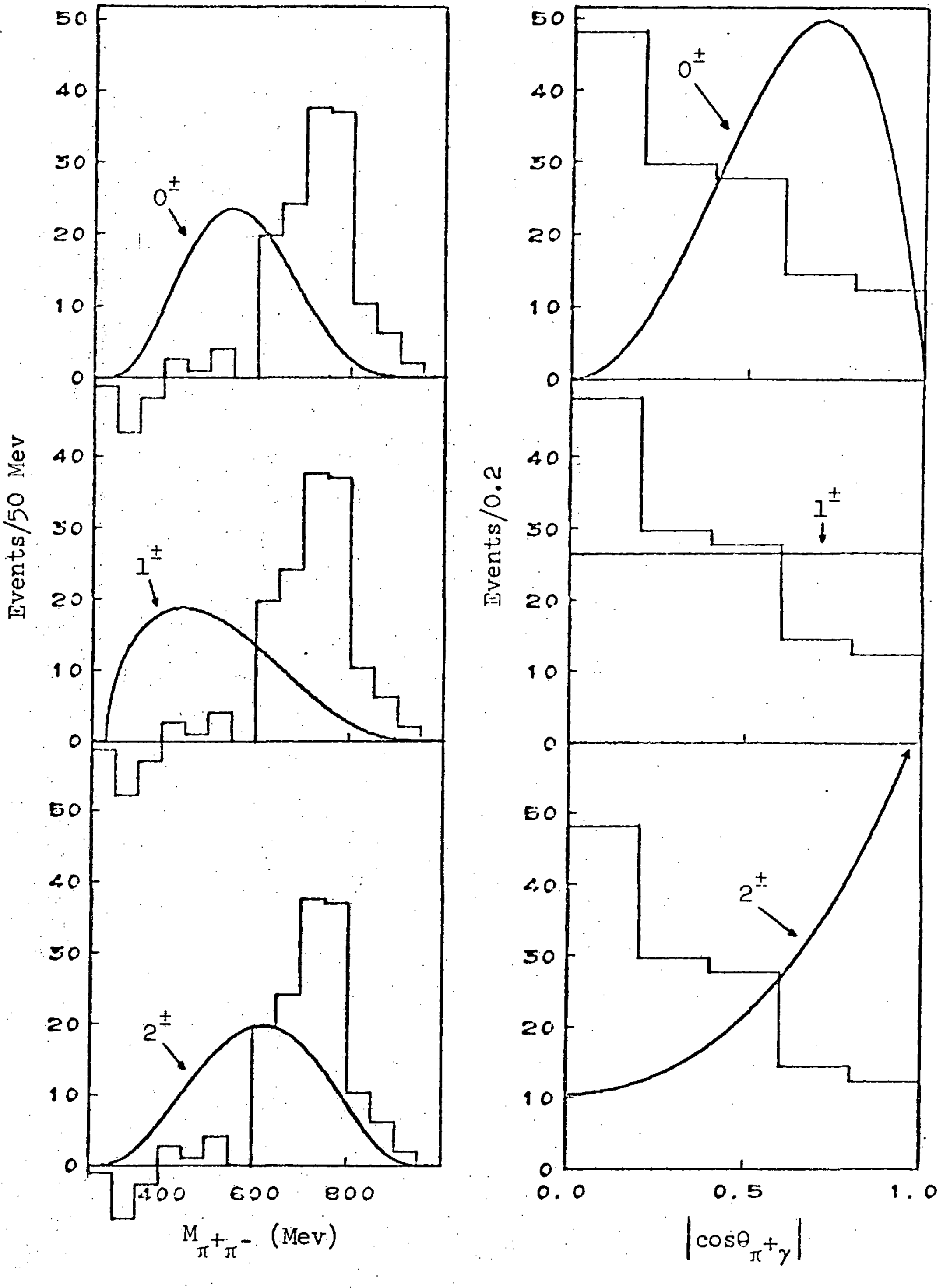

Figure 40(b). Predicted $M_{\pi^+\pi^-}$ and $\cos\theta_{\pi^+\gamma}$ distributions for C=-1, $\pi^+\pi^-\gamma$ matrix elements, for various values of J^P. The data (132 events) are repeated in each plot. See Tables VI and VII for definitions and results of the fits.

Table VII. Results of fitting the $\pi^+\pi^-\gamma$ matrix elements of Table VI to the experimental $M_{\pi^+\pi^-}$ and $\cos\theta_{\pi^+\gamma}$ distributions. The fit numbers correspond to those of Table VI; asterisks mark the simplest matrix elements.

Fit No.	C	J^P	Multipole	ππ Resonance	Value of Free Parameter	$\chi^2(M_{\pi^+\pi^-})$ (15 bins)	$\chi^2(\cos\theta_{\pi^+\gamma})$ (5 bins)	Combined Conf. Level
* 1	+1	$0^\pm$	Dipole	-	-	66	2.0	1×10^{-7}
2			Dipole	ρ	-	16	2.0	0.47
* 3		$1^\pm$	Dipole	-	-	94	39	$<10^{-10}$
4			Dipole	ρ	-	22	32	2×10^{-5}
5			Quadrupole	ρ	-	38	2.0	2×10^{-3}
* 6		$2^\pm$	Dipole	-	-	71	11	4×10^{-10}
7			Dipole	ρ	-	17	8.9	0.11
8			Octupole	ρ	-	72	2.0	7×10^{-9}
9			mixture of dipole and quadrupole real	ρ	$a = 1.8\pm0.5$	14	2.7	0.46
10			complex	ρ	$a=(1.8\pm0.5)+(0.0\pm0.6)i$	14	2.7	0.39
* 11	-1	$0^\pm$	Quadrupole	-	-	102	42	$<10^{-10}$
* 12		$1^\pm$	Dipole	-	-	140	9.0	$<10^{-10}$
* 13		$2^\pm$	Dipole	-	-	55	39	$<10^{-10}$

$640 \leq M_{\pi^+\pi^-} \leq 800$ Mev, with the expectation that such a cut would reduce our background. We find with this mass cut that the $\pi^+\pi^-\pi^0$ contamination is reduced to 15% , thus permitting us to fit the $\cos\theta_{\pi^+\gamma}$ distribution with only a relatively small subtraction. The resulting curves for $J^P = 0^\pm$ and $2^\pm$ are shown over the subtracted data in Figure 41. The confidence level for spin 0 is 0.53, while that for spin 2 is 0.003. Thus spin 2 would seem to be ruled out.

In order to determine if a more complicated matrix element might allow $J^P = 1$ or 2, we have tried three possibilities: for spin 1, a pure quadrupole matrix element, and for spin 2 a variable mixture of dipole and quadrupole and also a pure octupole. In all three cases, we have also assumed the presence of a ρ. The pure quadrupole and pure octupole were tried because they have the same $\sin^2\theta_{\pi^+\gamma}$ dependence as the spin 0 dipole. These three matrix elements are given in Table VI and the results of the fits in Table VII. The pure quadrupole and octupole are seen to be unacceptable, resulting from the fact that the $\pi\pi$ mass distributions predicted do not match the data. However, with the proper admixture of dipole and quadrupole, spin 2 produces an overall confidence level of 0.46, essentially equal to the value of 0.47 for spin 0.

Thus we conclude that $C = +1$, $J = 0$ is the favored hypothesis, while $C = +1$, $J = 2$ can be admitted only with a suitable mixing of two matrix elements.

We have not yet determined the parity and G parity of the η', based on its decay into $\pi^+\pi^-\gamma$. The four choices open to us are

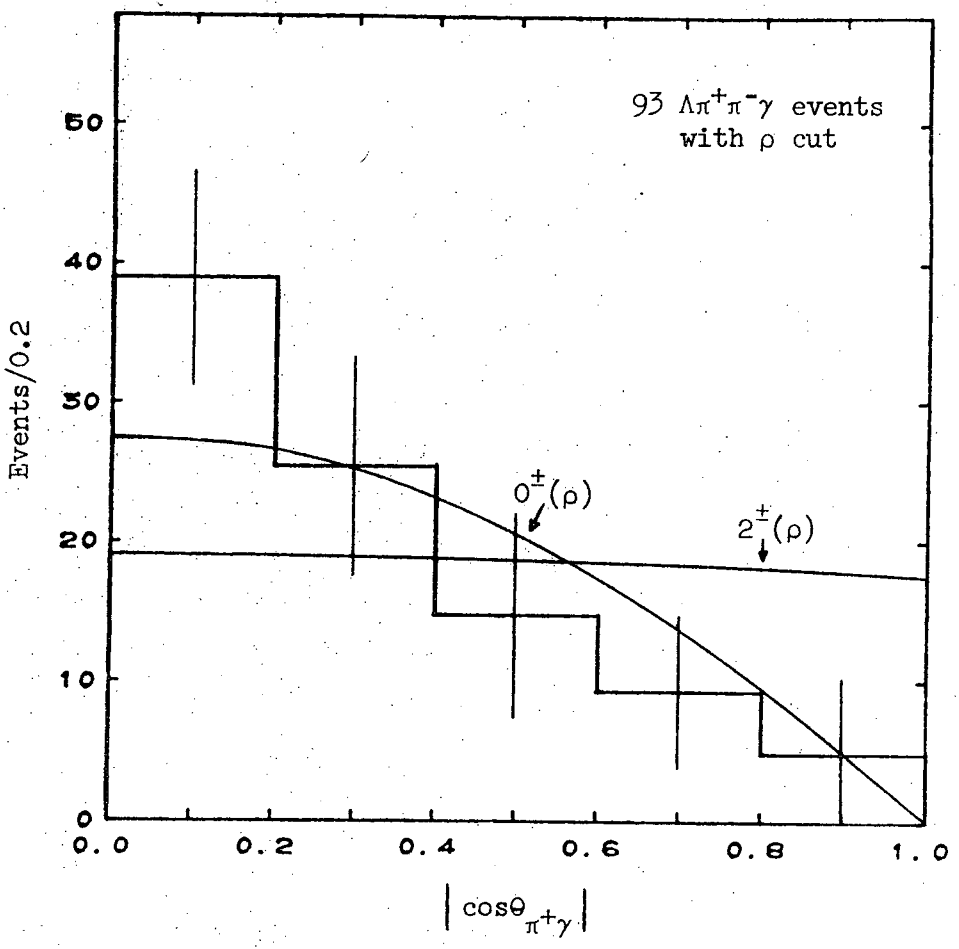

Figure 41. The folded $\cos\theta_{\pi^+\gamma}$ distribution for low Δ^2 $\pi^+\pi^-\gamma$ events having $945 \leqq M_{\pi^+\pi^-\gamma} \leqq 975$ Mev and a cut of $640 \leqq M_{\pi^+\pi^-} \leqq 800$ Mev to favor ρ events. A background subtraction has been carried out. The curves indicate the predictions for $C = +1$, $J^P = 0^{\pm}$ and $2^{\pm}$, with ρ assumed.

indicated via the box below:

G Parity \ Parity	+1	-1
+1	$\pi\pi$	$\pi\pi\eta$
-1	$\pi\eta$	$\pi\pi\pi$

The entries in the box show the least massive allowed strong decay mode for each of the four possibilities. On the basis of coupling constants, these decays would be expected to dominate over the (electromagnetic) $\rho\gamma$ mode by $1/\alpha \sim 100$. Phase space considerations would push this factor even higher for the (two-body) $\pi\pi$ and $\pi\eta$ cases; for the (three-body) $\pi\pi\pi$ case, a rough calculation suggests that the phase space factor might be ~ 1 when the $\rho\gamma$ angular momentum barrier is taken into account. Since we have ~ 300 $\rho\gamma$ events at low Δ^2, we would then expect $\sim 10^3 - 10^5$ events for one of these three strong decays, namely $\pi\pi$, $\pi\eta$, or $\pi\pi\pi$, unless P were -1 and G were +1. We have already seen that there is no significant $\pi^+\pi^-\pi^o$ decay of the η'. Figure 42a shows the $\pi^+\pi^-$ spectrum for our reprocessed $\Lambda\pi^+\pi^-$ events, while Figure 42b shows the $\pi^+\pi^-$MM distribution from the reprocessed $\Lambda\pi^+\pi^-$MM events. Approximately 30% of any $\pi\eta$ events would appear in the latter distribution. In neither case can we accommodate the expected number of events. Thus we conclude that the only acceptable case is P = -1, G = +1. The G = +1 conclusion is equivalent, when taken with the C = +1 result, to I = 0.

In connection with the above discussion, we point out that the strong decay mode allowed for P = -1, G = +1, namely $\pi\pi\eta$, although

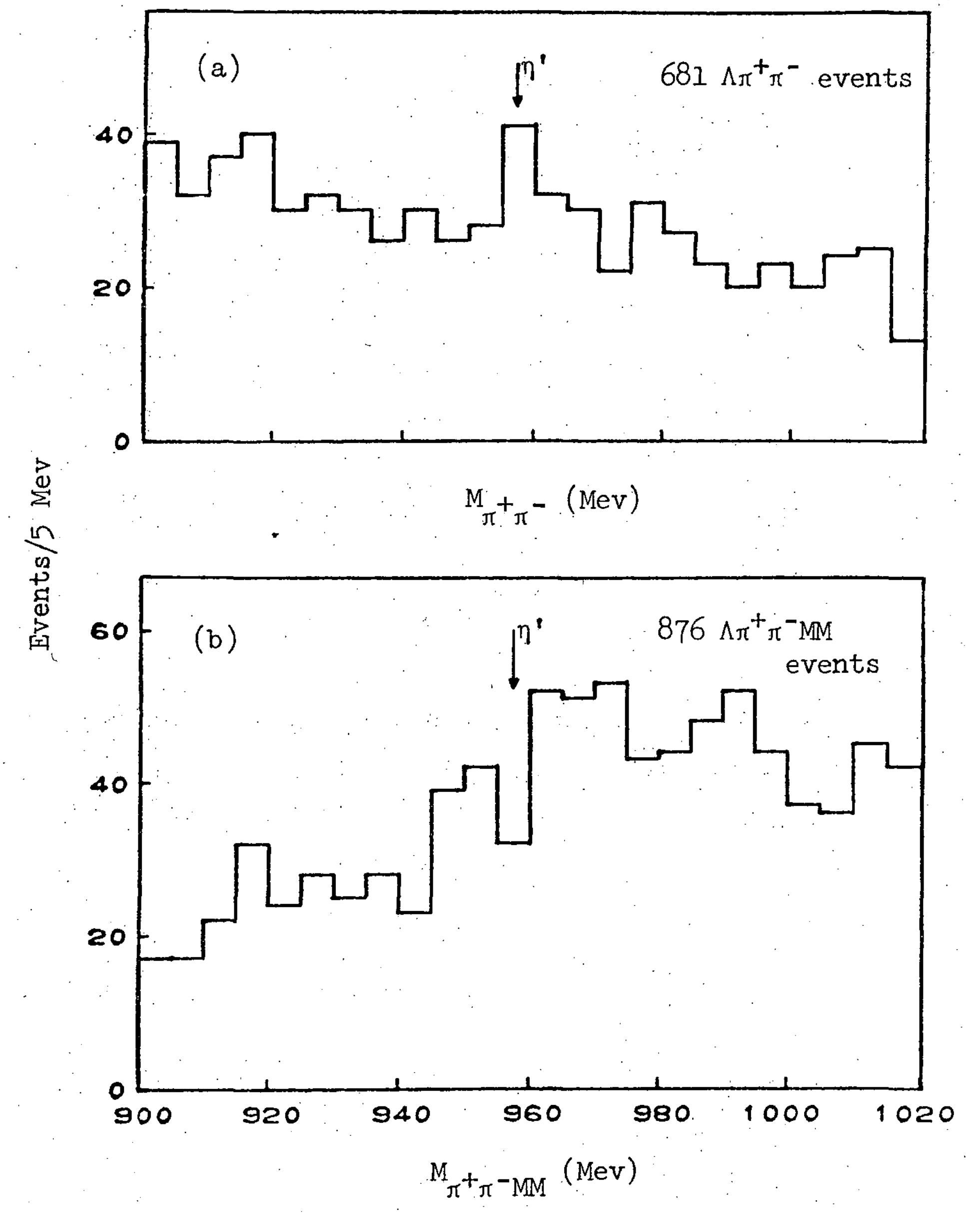

Figure 42. (a) The $\pi^+\pi^-$ mass spectrum of the low Δ^2, reprocessed $\Lambda\pi^+\pi^-$ events. (b) The $\pi^+\pi^-$MM mass spectrum of the low Δ^2, reprocessed $\Lambda\pi^+\pi^-$MM events.

enhanced over $\rho\gamma$ by a factor of $1/\alpha$, could very well have a phase space suppression factor of order 10 due to its being a three-body decay with low Q. This would then allow $\rho\gamma$ to compete favorably with the strong $\pi\pi\eta$ mode.

Since the $\pi^+\pi^-\gamma$ decay has now been shown to come from a resonance whose preferred quantum numbers are $I^GJ^P = 0^+0^-$, and since the central mass of the $\pi\pi\gamma$ peak is found to be 957 Mev, in exact agreement with the $\pi\pi\eta$ central mass, it seems reasonable to assume that both decays are from the same resonance -- the η'. There is the additional fact that the widths of the two decay modes are comparable when the expected resolutions in their respective channels are taken into account.

VI. BRANCHING FRACTIONS, MASS, AND WIDTH

A. Branching Fractions

For the purpose of calculating branching fractions for the η', we have combined the 2.10, 2.47, and 2.65 Gev/c data, and have used only those events with $\Delta^2_{p\to\Lambda} \leq 0.5$ (Gev/c)^2. Table VIII gives in the second column the number of events found within our fiducial volume for each of the five decay modes: $\pi^+\pi^-\eta_N$, $\pi^+\pi^-\eta_C$, $\pi^+\pi^-$+ neutrals, all neutrals, and $\pi^+\pi^-\gamma$. Column 3 gives the number of events after correcting for measuring efficiency (see Table III) and the loss of events where the Λ decays near the primary interaction vertex ("short" Λ's) or outside the fiducial volume ("escaping" Λ's). The measuring efficiency, as defined for Table III, already includes the scanning efficiency for those events where the Λ is neither short (i.e., decays less than 6 mm. from the primary interaction vertex, as projected onto the plane parallel to the glass window of the bubble chamber) nor escaping. The additional correction for the latter two cases is made in the following manner: Any event with a short or escaping Λ which was detected is discarded. All other events are given a weight W which is the reciprocal of the probability that the Λ in question, given its momentum and direction and the position of the event in the chamber, should have decayed neither close to the vertex nor outside the fiducial volume. Thus

$$W = \left[e^{-\ell_s/\eta c\tau} - e^{-\ell_e/\eta c\tau}\right]^{-1} ,$$

where ℓ_s is our short length cutoff; ℓ_e is the distance, along the

Table VIII. Branching fractions for the η'.

Decay Mode	Number of Events		Branching Fraction	
	Raw	Corrected[a]		
$\pi^+\pi^-\eta_N$	281 ± 18	412 ± 32	0.314 ± 0.026	0.437 ± 0.030
$\pi^+\pi^-\eta_C$	107 ± 10	161 ± 17	0.123 ± 0.014	
$\pi^+\pi^-$+neutrals	42 ± 27	60 ± 40	0.045 ± 0.029	
all neutrals	123 ± 18	248 ± 39	0.189 ± 0.026	
$\pi^+\pi^-\gamma$ $(\rho^0\gamma)$	298 ± 37	433 ± 56	0.329 ± 0.033	
$\pi^+\pi^-$		< 30	< 0.02	
$\pi^+\pi^-\pi^0$		< 60	< 0.05	
$\pi^+\pi^+\pi^-\pi^-$		< 10	< 0.01	
$\pi^+\pi^+\pi^-\pi^-\pi^0$		< 10	< 0.01	
$\pi^+\pi^+\pi^-\pi^-$+neutrals		< 10	< 0.01	

[a] The corrections are those for scanning and measuring efficiency and for short and escaping Λ's.

line of flight of the Λ, from the primary vertex to the wall of the fiducial volume; η is the momentum of the Λ divided by its mass; c is the speed of light; and τ is the lifetime of the Λ. These short and escaping Λ corrections should ideally be independent of the decay mode of the η', but because the different decay modes occur in several different topologies, scanning biases may vary.

The errors given in Table VIII are a combination of the statistical error, the estimated errors in the corrections discussed above, and our uncertainty as to how the background curve should be drawn. The latter problem is particularly acute for the $\pi^+\pi^-$ + neutrals decay mode, as can be seen from Figure 42b, and mildly problematical for the $\pi^+\pi^-\gamma$ and all-neutrals modes.

Before going on to discuss the branching fractions themselves, several brief comments are in order as to how the events were assigned to the categories listed in Table VIII. We have discussed earlier the difficulties involved in this assignment.

Events listed as $\pi^+\pi^-\eta_N$ include all those chosen as this final state by our selection criteria. As was noted in connection with Figure 23c, which shows a plot of the missing mass from $\pi^+\pi^-$MM events, there are clearly some $\pi^+\pi^-\eta_N$ events which have been misidentified as $\pi^+\pi^-$MM. But the converse is also true, and we estimate that the exchanges are roughly equal. Thus we have accepted the assignments as made, and appropriately enlarged our errors to take into account the uncertainty involved.

To measure the total $\pi^+\pi^-\gamma$ signal, we have combined those events preferring the $\pi^+\pi^-\gamma$ fit and those preferring $\pi^+\pi^-\pi^0$. This decision was based on the assumption that there are essentially no genuine $\pi^+\pi^-\pi^0$ decays of the η' and that there is not some other resonance with the same mass and width as the η' decaying into 3π. That this assumption is correct is strongly suggested by Figure 17, where the missing mass of those events in the 960 Mev signal is seen to peak very close to zero and to have at most a $\sim 10\%$ excess in the π^0 region. Also, the $\pi^+\pi^-\gamma$ (or $\pi^+\pi^-\pi^0$) signal in the combined events has a width comparable to the resolution, which makes further unlikely the possibility of another resonance being present and decaying into 3π, since such a resonance would have to be within about 5 Mev of the η' and have, like the η', a very small width ($\lesssim$ 10 Mev). The δ meson might be a candidate for such a resonance, but the most recent data[22] on the δ suggests that its mass and width are probably enough different from that of the η' so that it would not be included in our signal. Thus we have attributed the entire signal to the $\pi^+\pi^-\gamma$ decay of the η'. We have, however, allowed for the possibility of some $\pi^+\pi^-\pi^0$ decays by appropriately increasing our upper limit estimate for a possible $\pi^+\pi^-\pi^0$ decay mode.

Finally, we have observed a small signal in the η' region in the mass recoiling against the Λ in events assigned to $\Sigma^0\pi^+\pi^-$ and $\Sigma^0\pi^+\pi^+\pi^-\pi^-$. Since the γ from a genuine Σ^0 cannot combine with 2 or 4 π's to create an η' (or any resonance), we have counted these events as $\Lambda\pi^+\pi^-\gamma$ and $\Lambda\,\pi^+\pi^-\eta_C$, respectively.

The branching fractions derived from the observed events are presented in column 4 of Table VIII. At the two momenta where we have sufficient statistics, namely 2.10 and 2.65 Gev/c, we have calculated the branching fractions separately, and find some discrepancies. In particular, using the $\pi^+\pi^-\eta$ mode as our standard, we find

$$\frac{\eta' \to \text{all neutrals}}{\eta' \to \pi^+\pi^-\eta} = 0.59 \pm 0.16 \text{ at } 2.10 \text{ Gev/c}$$
$$= 0.29 \pm 0.08 \text{ at } 2.65 \text{ Gev/c}$$

and

$$\frac{\eta' \to \pi^+\pi^-\gamma}{\eta' \to \pi^+\pi^-\eta} = 0.99 \pm 0.19 \text{ at } 2.10 \text{ Gev/c}$$
$$= 0.63 \pm 0.10 \text{ at } 2.65 \text{ Gev/c} .$$

For both the all-neutrals mode and the $\pi^+\pi^-\gamma$ mode, there is an excess of events, compared to $\pi^+\pi^-\eta$, at 2.10 Gev/c; the effect is 1.7 standard deviations in both cases. Again the possibility of a second resonance suggests itself. But because the three modes are so similar in mass, width, production angular distribution, and, in the case of $\pi^+\pi^-\eta$ and $\pi^+\pi^-\gamma$, probable spin-parity assignment, we attribute these discrepancies to statistical fluctuations. Parenthetically, it should be noted that the $\pi^+\pi^-\gamma$ discrepancy remains even if a ρ cut is made.

In concluding this section on branching fractions, we note that if the isospin of the η' is 0, as our Dalitz plot analyses have indicated and as our deuterium search will further show, the η' should decay into $\pi^0\pi^0\eta$, at a rate half that for $\pi^+\pi^-\eta$. Using the branching ratios of the η, we should then have the η' branching ratios

$$\eta' \to \pi^0\pi^0\eta_C : \pi^0\pi^0\eta_N : \pi^+\pi^-\eta_C : \pi^+\pi^-\eta_N$$
$$= 0.20 : 0.50 : 0.40 : 1.00 .$$

If we assume that our $\pi^+\pi^-$ + neutrals mode is entirely due to $\pi^o\pi^o\eta_C$ and that our all-neutrals mode originates only from $\pi^o\pi^o\eta_N$, the above ratios are found experimentally to be

$$\eta' \rightarrow \quad \pi^o\pi^o\eta_C \; : \; \pi^o\pi^o\eta_N \; : \; \pi^+\pi^-\eta_C \; : \; \pi^+\pi^-\eta_N$$
$$= 0.15 \pm 0.09 : 0.60 \pm 0.11 : 0.39 \pm 0.05 : 1.00 \quad .$$

Within errors, the agreement is quite good. The excess of all-neutrals observed amounts to 0.03 ± 0.03 of the total η' decay, and while statistically insignificant, could be attributed to a 2γ decay mode. Such a mode has recently been reported[23] with the branching fraction $0.055 \begin{smallmatrix} + 0.036 \\ - 0.030 \end{smallmatrix}$ and has been predicted theoretically[24,25] to have a branching ratio to $\rho\gamma$ of ~ 0.1. The latter ratio, when combined with our $\rho\gamma$ branching fraction of 0.33, would yield a 2γ branching fraction of ~ 0.03.

B. Mass and Width

Fitting a Gaussian plus a linear background to our $\pi^+\pi^-\eta_N$, $\pi^+\pi^-\eta_C$, $\pi^+\pi^-\gamma$, and all-neutrals events yields for the mass of the η' 957.4 ± 0.4, 956.9 ± 0.7, 957 ± 1, and 963 ± 1 Mev, respectively. The errors given are purely statistical and do not reflect systematic shifts. Because the all-neutrals events are a zero-constraint fit and because both they and the $\pi\pi\gamma$ events have a significant amount of background, we feel it best to use only the $\pi^+\pi^-\eta$ events to determine the mass of the η'. Combining the $\pi^+\pi^-\eta_N$ and $\pi^+\pi^-\eta_C$ events yields the result $M_{\eta'} = 957 \pm 1$ Mev, where the error represents our estimate as to possible systematic shifts in the data.

Our experimental full widths at half-maximum are found to be 13 ± 1 for $\pi^+\pi^-\eta_N$, 15 ± 1 for $\pi^+\pi^-\eta_C$, 25 ± 3 for $\pi^+\pi^-\gamma$, and 23 ± 3 Mev for all neutrals. Our calculated resolutions (FWHM) are ≅ 10 Mev for the first two classes of events above, and ≅ 20 Mev for the latter two classes. We cannot determine an actual value for $\Gamma_{\eta'}$ because these calculated values are probably an underestimate of the actual values, but we set an upper limit of $\Gamma_{\eta'} < 10$ Mev.

VII. PRODUCTION CHARACTERISTICS

A. Cross Sections

In order to determine cross sections for η' production in the reaction $K^-p \rightarrow \Lambda\eta'$, for each of the momentum settings except 1.70 Gev/c we have combined all of the final states in which the η' is seen. For the 1.70 data, since the V-0 prong events were not measured and the background under the $\pi^+\pi^-\gamma$ and $\pi^+\pi^-$ + neutrals events is large and steeply falling, we have used only the $\pi^+\pi^-\eta$ events; we have then employed the branching fractions already determined to obtain a correction factor. Table IX gives in the second column the raw number of events observed at each momentum, with $\Delta^2_{p\to\Lambda} \leq 0.5$ (Gev/c)^2. The number of events given in column 3 then results after applying corrections for measuring efficiency, short and escaping Λ's, neutral Λ decay, and events at $\Delta^2 > 0.5$ (Gev/c)^2. The 1.70 Gev/c data are also corrected for the modes not included, as referred to above. The correction for high Δ^2 events was determined by using only the $\pi^+\pi^-\eta$ events, where the background is small and thus could be easily accounted for. Combining these results with the path lengths of Table I, we determine the cross sections as given in the final column of Table IX.

Figure 43 shows a plot of these cross sections versus beam momentum, together with those determined by several other K^-p experiments. The gross shape of the cross section plot consists of a rise from threshold (at 1.62 Gev/c) to a maximum near 2.1 Gev/c, followed by a slow tapering off. Whether the suggested wiggle in

Table IX. Production cross sections for the η' in the reaction $K^-p \to \Lambda\eta'$.

P_{beam} (Gev/c)	Number of Events Raw	 Corrected[a]	σ (μb)
1.70	31 ± 6	312 ± 81	95 ± 25
2.10	321 ± 27	968 ± 98	168 ± 17
2.47	73 ± 14	164 ± 34	93 ± 20
2.65	442 ± 27	1334 ± 112	104 ± 9

[a] The corrections are those for scanning and measuring efficiency, events with $\Delta^2 > 0.5$ $(\text{Gev/c})^2$, short and escaping Λ's, and neutral Λ decay. In addition, the 1.70 Gev/c data have been corrected for modes other than $\pi^+\pi^-\eta$.

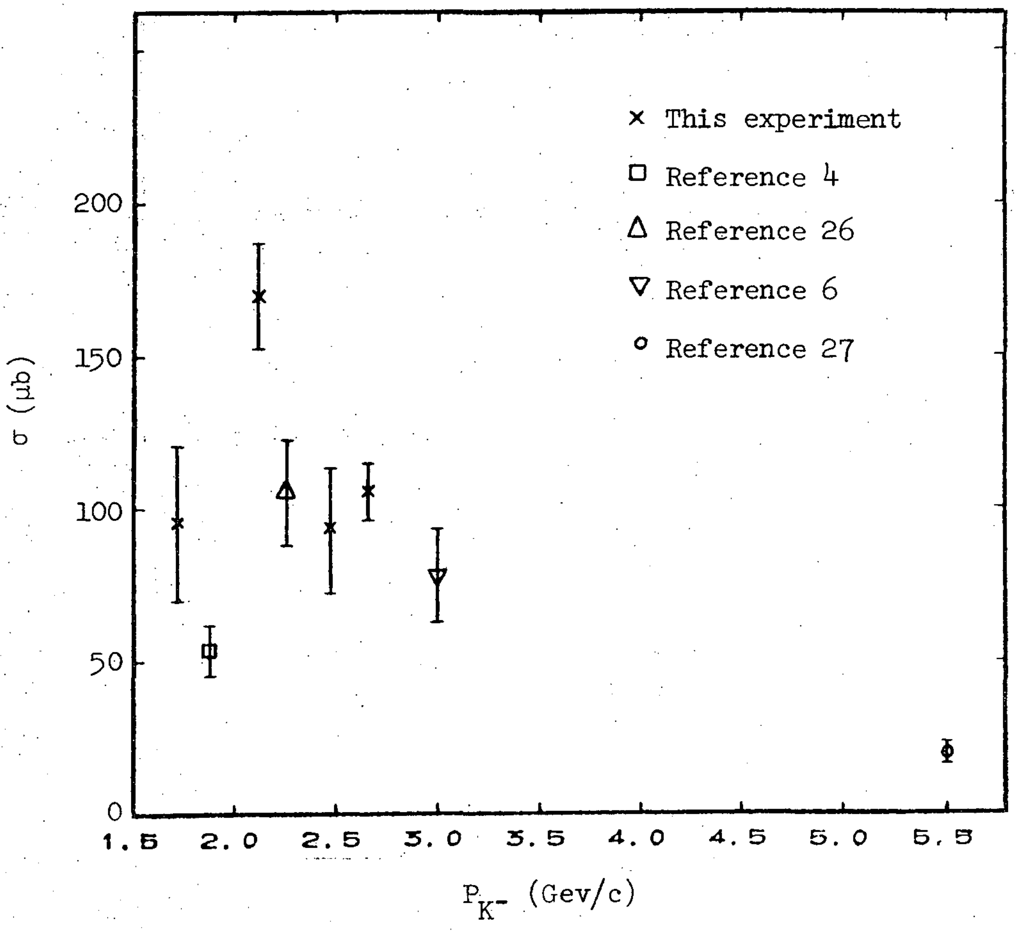

Figure 43. Plot of the total cross section for production of η' in the reaction $K^-p \rightarrow \Lambda\eta'$, as a function of the beam momentum, P_{K^-}.

the vicinity of 1.7 - 1.9 Gev/c is genuine or not we cannot say, although a smooth curve would seem to be in considerable disagreement with the data.

B. Production Angular Distributions and Λ Polarization

Figure 44 gives the production angular distributions for our $\pi^+\pi^-\eta$, all-neutrals, and $\pi^+\pi^-\gamma$ events at 2.10 and 2.65 Gev/c. Events on either side of the η' have been used to perform a background subtraction. Although this subtraction is fairly severe for the all-neutrals and $\pi^+\pi^-\gamma$ events, as is obvious from the Chew-Low plots of Figures 13 and 15, the distributions at each of the two momenta can be seen to be qualitatively the same for each of the three decay modes, as would be expected for different decay modes of the same particle. Referring to the $\pi^+\pi^-\eta$ distributions, which are the cleanest, the sharp forward peaking, which is somewhat more pronounced at 2.65 Gev/c than at 2.10 Gev/c, suggests that the reaction is proceeding predominantly via one meson exchange. The 2.65 Gev/c data also show a slight backward peak, indicating that at that momentum some other process such as an s channel effect or baryon exchange is also playing a small role.

We have attempted to see how well a simple unmodified one meson exchange process would fit the data. For a 0^- (or 2^-) η', the lightest meson which could be exchanged would be a $K^*(891)$. Figure 45 shows the diagram which we thus wish to consider. The production matrix element we have used is given by

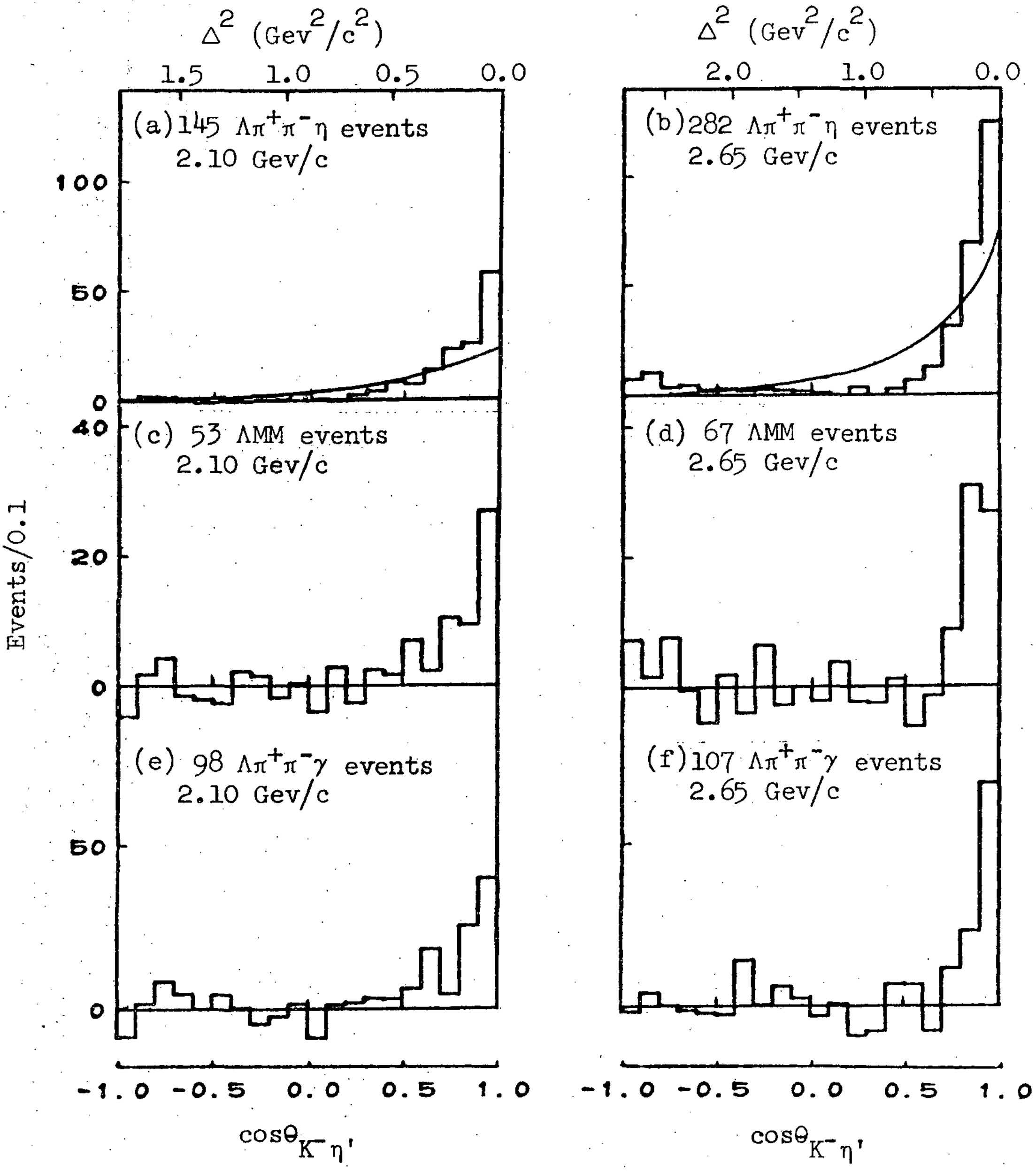

Figure 44. The production angular distribution of the η' in the reaction $K^-p \to \Lambda\eta'$, at 2.10 (a,c,e) and 2.65 (b,d,f) Gev/c, as determined from the $\pi^+\pi^-\eta$ (a-b), all-neutrals (c-d), and $\pi^+\pi^-\gamma$ (e-f) decay modes of the η'. The events plotted are weighted for short and escaping Λ's and have had a subtraction performed. The curves on the $\pi^+\pi^-\eta$ data in (a) and (b) show the predictions of the $K^*(891)$ exchange model discussed in the text. The Δ^2 scales at the top of the plots are for $\Delta^2_{p\to\Lambda}$, or equivalently, $\Delta^2_{K^-\to\eta'}$.

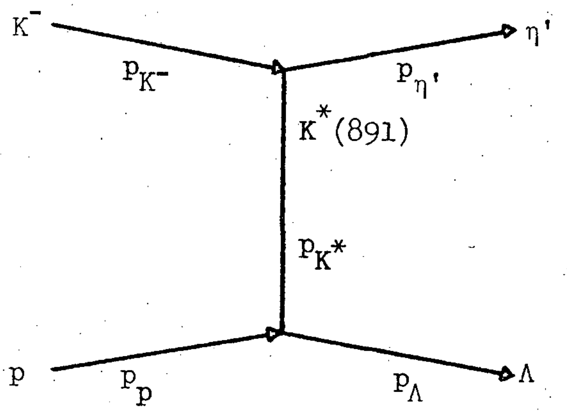

Figure 45. Diagram for the $K^*(891)$ exchange model discussed in the text.

$$M_p = \overline{u}(p_\Lambda)(p_{K^-} + p_{\eta'})_\mu \left\{ \frac{-g^{\mu\upsilon} + \dfrac{p^\mu_{K^*} p^\upsilon_{K^*}}{M^2_{K^*}}}{\Delta^2 + M^2_{K^*}} \right\} \gamma_\upsilon u(p_p) \quad ,$$

where p_{K^-}, p_p, p_Λ, $p_{\eta'}$, and p_{K^*} are the four-momenta of the particles indicated by the subscripts, $u(p_p)$ is the initial state proton spinor, $\overline{u}(p_\Lambda)$ is the final state Λ spinor, γ_υ is a Dirac matrix, and $\Delta^2 = -p^\mu_{K^*} p^\mu_{K^*}$ is the four-momentum transfer squared. The curves shown over the $\pi^+\pi^-\eta$ data in Figure 44 indicate the distributions predicted by this matrix element. As is usually the case for unmodified one meson exchange models, the data are considerably more peaked than the model would predict. Including a tensor term involving $\sigma_{\upsilon\rho}$ would only make matters worse since such a term goes to zero in the forward direction. Presumably absorption effects and/or a Regge pole treatment would sharpen up the peak, but we have not tried such modifications.

For $\pi^+\pi^-\eta$ events having $\Delta^2 \leqq 0.5$ (Gev/c)^2, we have determined the Λ polarization at 2.10 and 2.65 Gev/c to be 0.19 ± 0.25 and 0.26 ± 0.19, respectively. Although both of these values are consistent with zero, as would be expected for simple K^* exchange, the errors are sufficiently large to allow a wide range of possible values.

C. Decay Correlations of the η'

For this discussion, we define a coordinate system in the η' rest frame by letting z be along the beam direction and y along the normal to the production plane; x is then perpendicular to y and z. We let β and ϕ be the polar and azimuthal angles of the normal to the η' decay plane with respect to this coordinate system. Figure 46 shows these relationships. In Figures 47 through 50 we give, for each of our four momentum settings, the distributions in $\cos\beta$ and ϕ for $\pi^+\pi^-\eta$ events with $\Delta^2 \leq 0.5$ (Gev/c)^2. We have folded about $\cos\beta = 0$ and $\phi = 180^\circ$, as we are allowed to do by parity conservation. As can be seen, the distributions are consistent with isotropy, as would be expected for a spin 0 η'. For $J^P_{\eta'} = 2^-$, the most general form for the $\cos\beta$ distribution, after integration over ϕ, would consist of a constant term and terms in $\cos^2\beta$ and $\cos^4\beta$, with the coefficients of the three terms depending upon the spin density matrix elements and the decay matrix element. Our observed isotropy in $\cos\beta$ would require that the $\cos^2\beta$ and $\cos^4\beta$ coefficients be vanishingly small at all four of our momenta. This requirement adds further suggestive evidence against a $J^P = 2^-$ assignment for the η'.

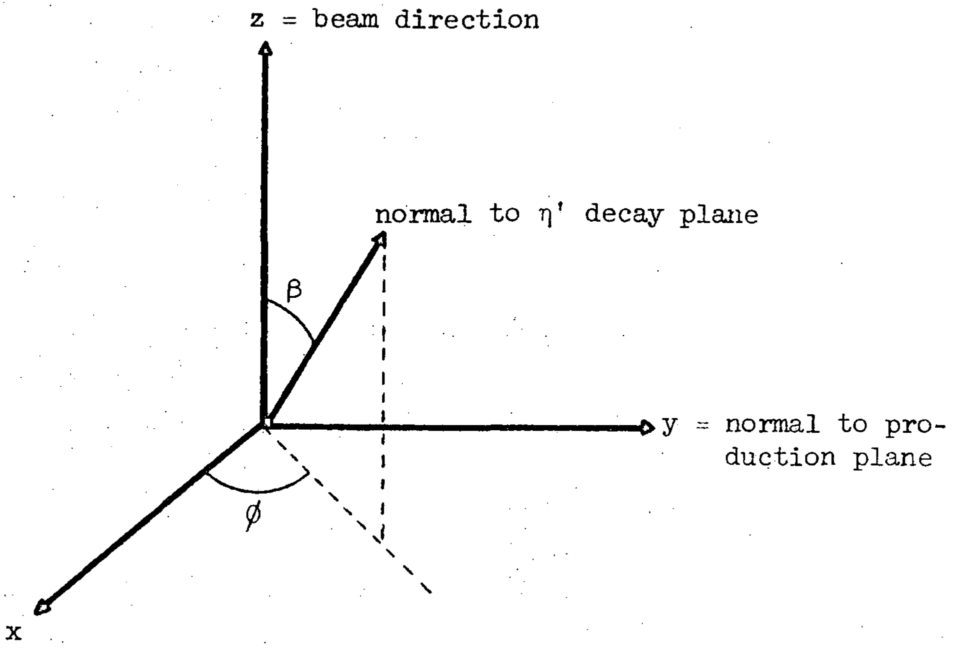

Figure 46. Diagram indicating the definitions of the angles used for the decay correlation plots of Figures 47-50. All vectors are measured in the η' rest frame.

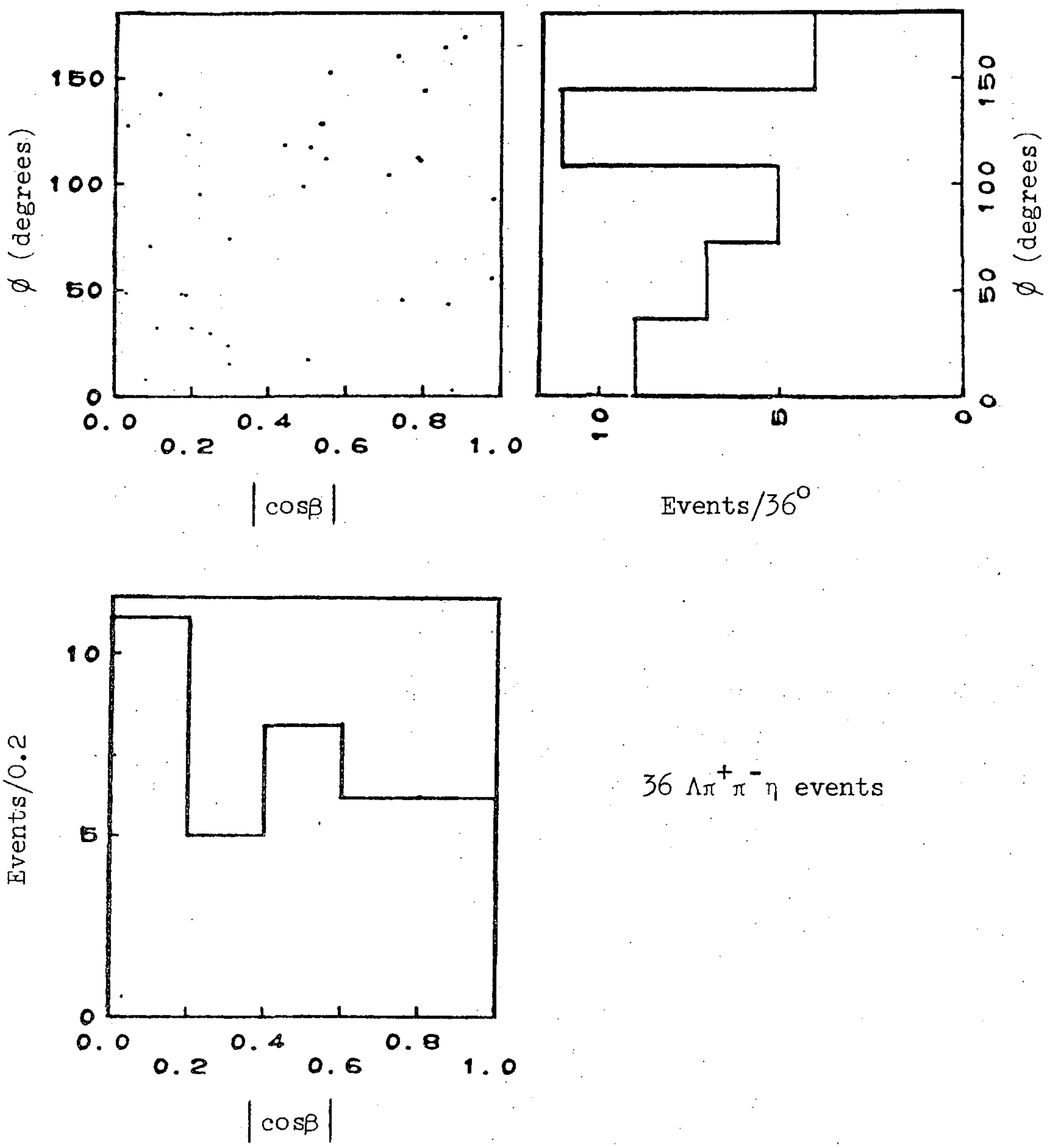

Figure 47. Decay correlations for the η' at 1.70 Gev/c. Only low Δ^2 $\pi^+\pi^-\eta$ events with $945 \leq M_{\pi\pi\eta} \leq 975$ Mev have been used. The angles β and ϕ are defined in the text and in Figure 46; the plots have been folded about $\cos\beta = 0$ and $\phi = 180°$.

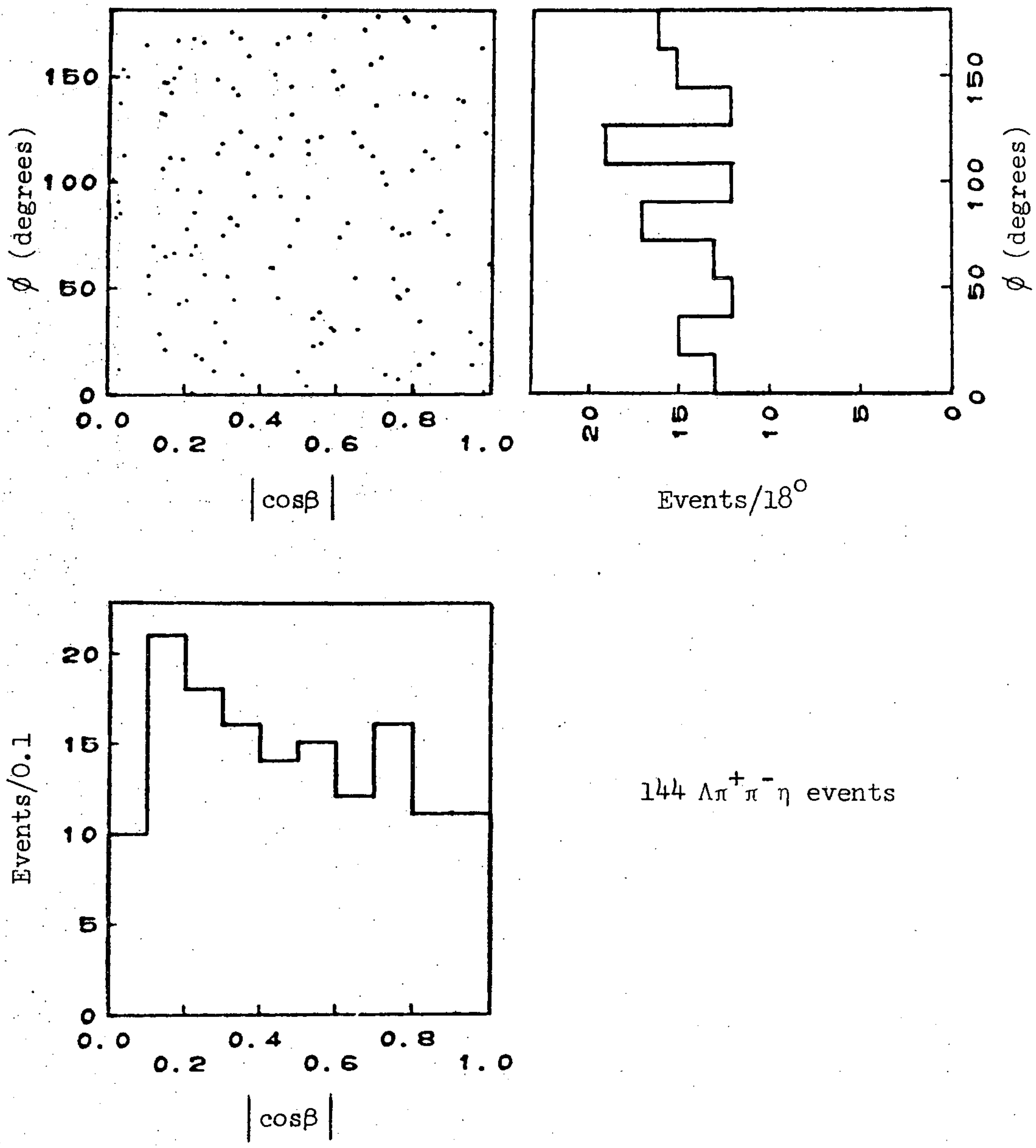

Figure 48. Decay correlations for the η' at 2.10 Gev/c. Only low Δ^2 $\pi^+\pi^-\eta$ events with $945 \leq M_{\pi\pi\eta} \leq 975$ Mev have been used. The angles β and ϕ are defined in the text and in Figure 46; the plots have been folded about $\cos\beta = 0$ and $\phi = 180^\circ$.

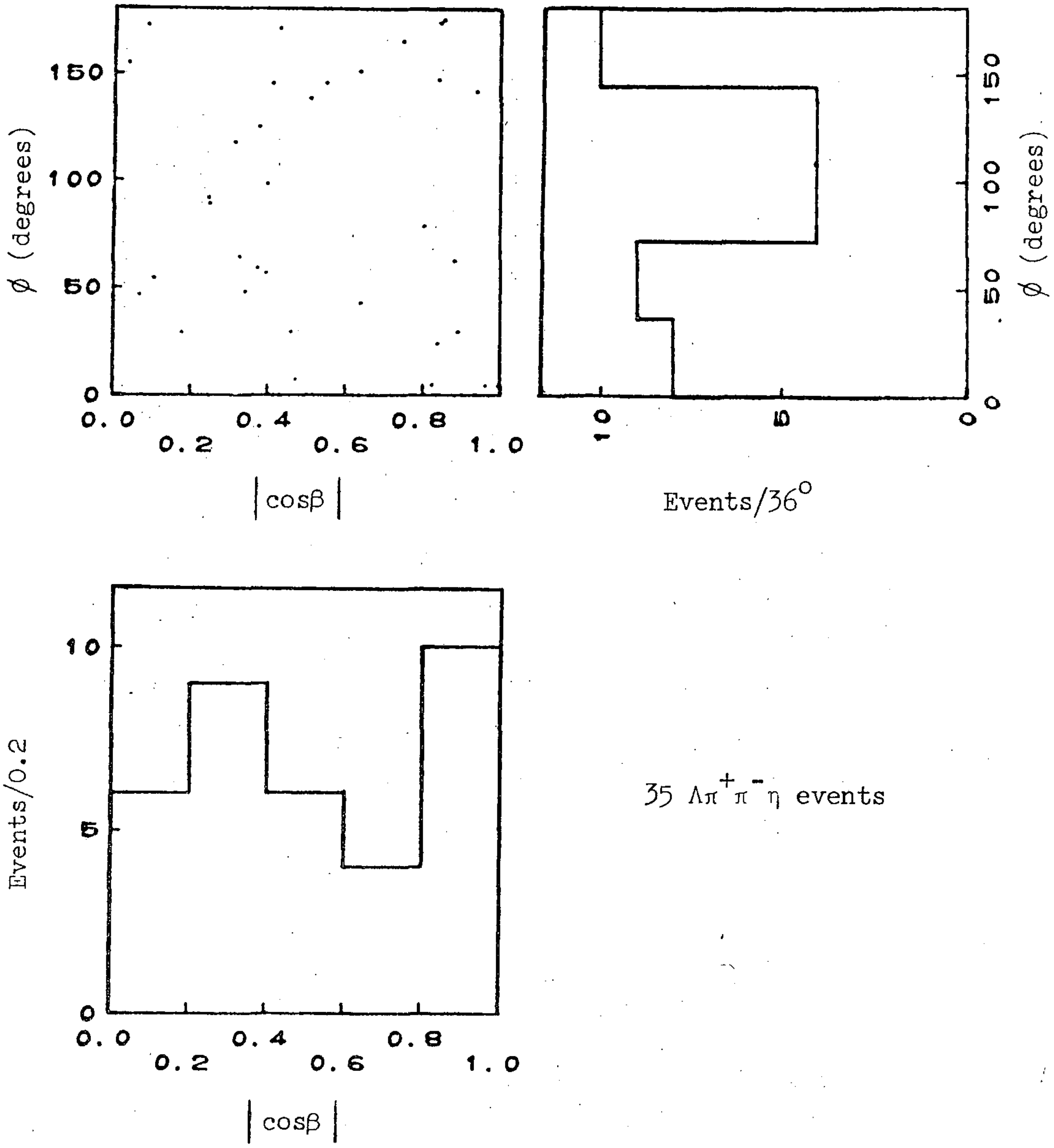

Figure 49. Decay correlations for the η' at 2.47 Gev/c. Only low Δ^2 $\pi^+\pi^-\eta$ events with $945 \leq M_{\pi\pi\eta} \leq 975$ Mev have been used. The angles β and ϕ are defined in the text and in Figure 46; the plots have been folded about $\cos\beta = 0$ and $\phi = 180^\circ$.

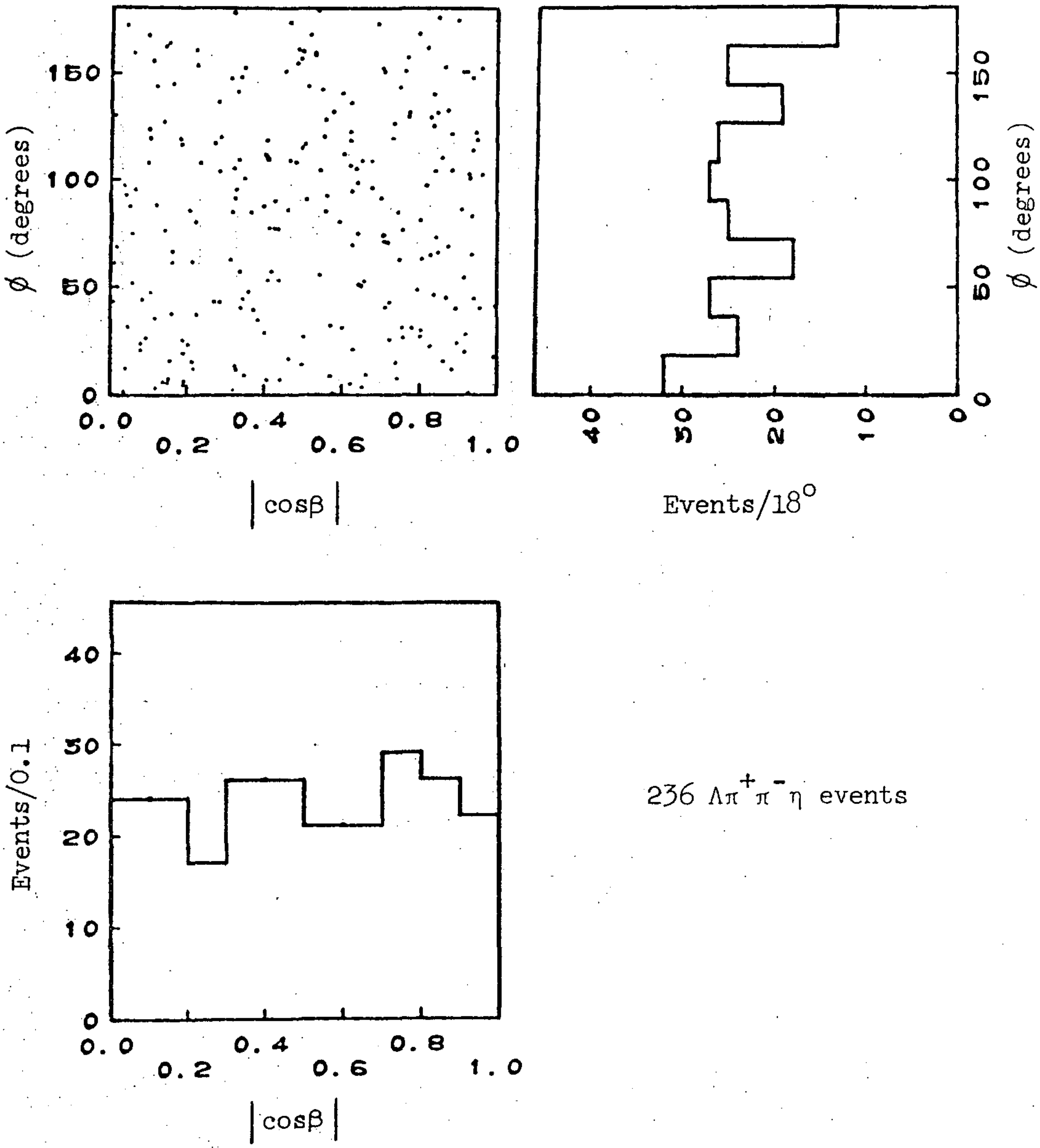

Figure 50. Decay correlations for the η' at 2.65 Gev/c. Only low Δ^2 $\pi^+\pi^-\eta$ events with $945 \le M_{\pi\pi\eta} \le 975$ Mev have been used. The angles β and ϕ are defined in the text and in Figure 46; the plots have been folded about cosβ = 0 and ϕ = 180°.

VIII. DEUTERIUM SEARCH FOR A CHARGED η'

The data to be presented here have essentially already appeared in published form,[28] and thus we will only summarize the arguments and bring some of the numbers up to date.

If the isospin of the η' were 1, then we should expect the negatively charged member of the multiplet to be produced in the reaction

$$K^- n \rightarrow \Lambda \eta'^- .$$

Further, since the $\Lambda\eta'$ final state would be pure $I = 1$, and since K^-n is also a pure $I = 1$ state while K^-p is an equal mixture of $I = 0$ and $I = 1$, we should expect

$$\sigma(K^-n \rightarrow \Lambda\eta'^-) = 2\sigma(K^-p \rightarrow \Lambda\eta'^0) .$$

We have used our deuterium film at 2.11 and 2.65 Gev/c to search for the reaction

$$K^- d \rightarrow p_s \Lambda \eta'^- ,$$

where p_s represents the spectator proton produced when the K^- interacts with the neutron within the deuteron via the impulse approximation. Since the postulated η'^- would be expected to decay primarily into $\pi^-\pi^0\eta$ ($\eta \rightarrow \pi^+\pi^-\pi^0$, $\pi^+\pi^-\gamma$, or all neutrals) and $\pi^-\pi^0\gamma$ ($\rho^-\gamma$), we should expect to find the η'^- in V-2 and -4 prong events when the spectator has sufficient energy to be visible, and in V-1 and -3 prong events when the spectator is not seen. We note that, in the decays under consideration, there are always two neutrals ($\pi^o\pi^o$ or $\pi^o\gamma$) in the final state, and thus the reactions of concern are

$$K^- d \rightarrow p_s \Lambda \pi^- MM$$

and $$K^- d \rightarrow p_s \Lambda \pi^+ \pi^- \pi^- MM \quad ,$$

where MM represents two or more missing neutrals. For that fraction of events, amounting to 70% of the total, where the spectator is not seen, we have assigned a momentum of zero to p_s. Since in fact, this momentum may have any value up to ~80 Mev/c, this means that our MM, π^-MM, and $\pi^+\pi^-\pi^-$MM distributions will be more smeared out, or have worse resolution, than would otherwise be the case. We have taken this into account in estimating the mass region where our η'^- events should fall.

How many η' events should we expect in our combined 2.11 and 2.65 Gev/c D_2 data? Using the cross sections of Table IX for H_2, the D_2 path lengths of Table I, and limiting ourselves to events where the Λ decays charged and where $\Delta^2_{n\to\Lambda} \leq 0.5$ $(\text{Gev/c})^2$, we should have a total of 798 ± 59 η' events produced (491 ± 53 at 2.11 Gev/c and 307 ± 27 at 2.65 Gev/c). However, there are four corrections to be applied to this result in order to obtain the number of η' events to be observed. First, in order to restrict ourselves to impulse events, we have required that the momentum of the spectator proton be ≤ 280 Mev/c. Using the Hulthen wave function for the momentum distribution of the spectator, this results in our losing 10 ± 1% of the events. The loss of short and escaping

Λ's amounts to a loss of 4 ± 1% of the events. Further, due to screening of the neutron in the deuteron, we must introduce a Glauber correction factor[29] of 0.96 ± 0.01. And finally, we must take account of our measuring efficiency. This introduces a problem: since our efficiencies are different for V-1 and -2 prongs as compared to V-3 and -4 prongs, we would have to know the branching fractions for one-charged-particle and three-charged-particle decay modes of the η'^-. We cannot ascertain these numbers on the basis of our hydrogen data, since we do not know what the all-neutrals and $\pi^+\pi^-$ + neutrals modes of the η'^o consist of and thus do not know what their charged counterparts, if any, would be. (Note that under the assumption of $I_{\eta'} = 1$, the all-neutrals mode of η'^o cannot be $\pi^o\pi^o\eta_N$.) To get around this difficulty, we will weight our V-3 and -4 prong events with a factor so as to bring their effective measuring efficiency down to that of the V-1 and -2 prong events. Combining the above correction factors, we then would expect to observe a total of 389 ± 35 η'^- events (253 ± 32 at 2.11 Gev/c and 136 ± 15 at 2.65 Gev/c).

Figure 51 shows a plot of the π^-MM effective mass and $\pi^+\pi^-\pi^-$MM mass (shaded) for the two reactions above. We show only those events with spectator momentum ≤ 280 Mev/c and with $\Delta^2 \leq 0.7$ $(\text{Gev/c})^2$. We have raised the Δ^2 cutoff from 0.5 $(\text{Gev/c})^2$ in order to take into account our poor resolution. If the only decay modes of an η'^- were $\pi^-\pi^o\eta$ and $\pi^-\pi^o\gamma$, we should have the full 389 ± 35 events in this plot, and they should all be contained within the mass region 920 to 1000 Mev. As can be seen, no such large number of events

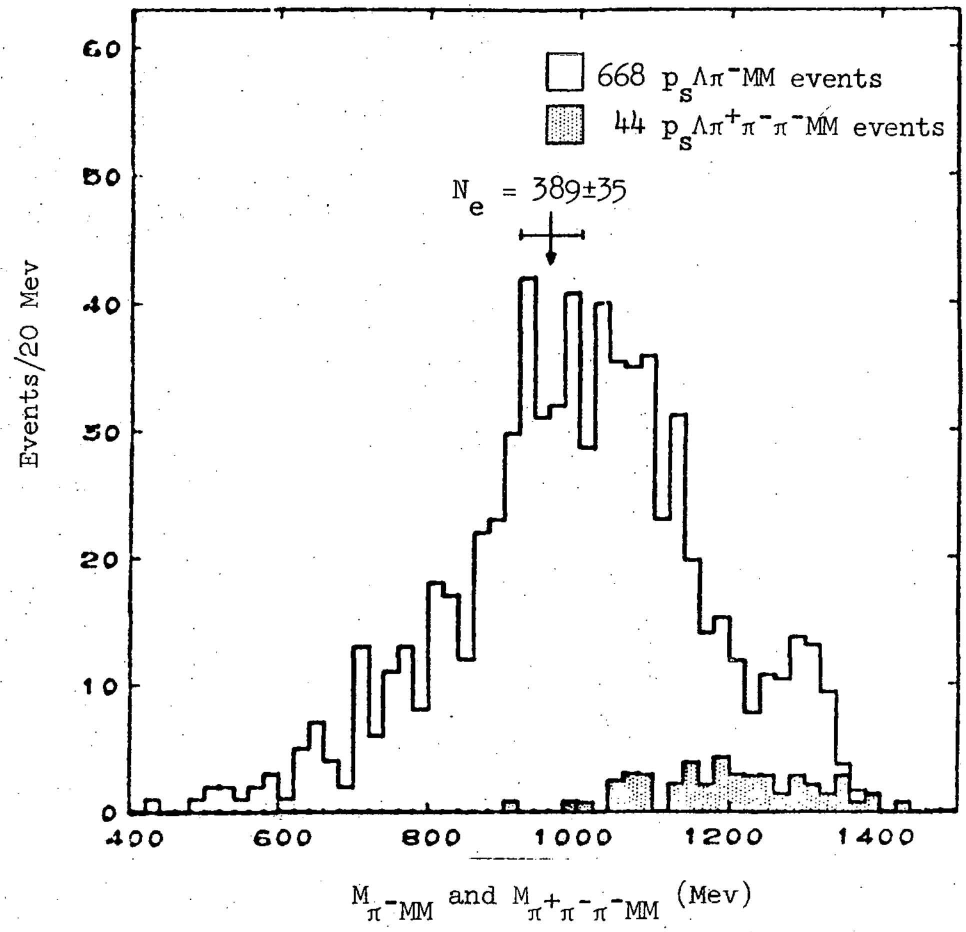

Figure 51. Plot of the π^-MM and $\pi^+\pi^-\pi^-$MM (shaded) mass spectra from $K^-d \rightarrow p_s\Lambda\pi^-$MM and $K^-d \rightarrow p_s\Lambda\pi^+\pi^-\pi^-$MM events, respectively. Only events having $\Delta^2_{n\rightarrow\Lambda} \leq 0.7$ (Gev/c)^2 have been plotted. The arrow and cross-bar indicate where the N_e expected η'^- events would appear if $I_{\eta'}$ were 1.

can be accommodated. The plot is consistent with there being no signal present, and we may set a one standard deviation upper limit of 15 events. Including neutral Λ decay and for $\Delta^2 \leq 0.5$ (Gev/c)^2, this would correspond to an average $K^- n \rightarrow \Lambda\eta'^-$ cross section at 2.11 and 2.65 Gev/c of $\sigma < 8$ μb, where 219 ± 15 μb would be expected for $I_{\eta'} = 1$.

We may reduce the background in Figure 51 by searching for a $\pi^-\pi^0\eta$ mode alone, for then we can restrict ourselves to those $p_s\Lambda\pi^-$MM events where MM $\geq m_\eta + m_{\pi^0}$ and to those $p_s\Lambda\pi^+\pi^-\pi^-$MM events where at least one $\pi^+\pi^-$ combination satisfies $M_{\pi^+\pi^-} \leq m_\eta$. We must, however, make an assumption as to the branching fraction for $\eta'^- \rightarrow \pi^-\pi^0\eta$. If we take this to be the same as that for $\eta'^0 \rightarrow \pi^+\pi^-\eta$, namely 0.44 ± 0.03, then we should observe 171 ± 19 events. Figure 52 shows the result of making the cuts outlined above, suitably adjusted to take errors into account. Again there is no signal in the η' region, and even the total background amounts to only 17 events.

There remains the possibility, however unlikely, that a charged η' could have some very heavily preferred decay mode open to it, with the corresponding neutral mode for the η'^0 being prohibited, or at least greatly suppressed. This could result from the fact that the decay of the η'^0 must conserve C, while there is no such selection rule for the decay of the charged members of a meson multiplet. For a strong decay, G parity conservation is equivalent to C conservation and thus would suppress any decay mode of an η'^- which was suppressed for η'^0. But we do not wish to rule out the possibility of an electromagnetic mode for the η'^- which would dominate over $\pi^-\pi^0\eta$ and $\pi^-\pi^0\gamma$.

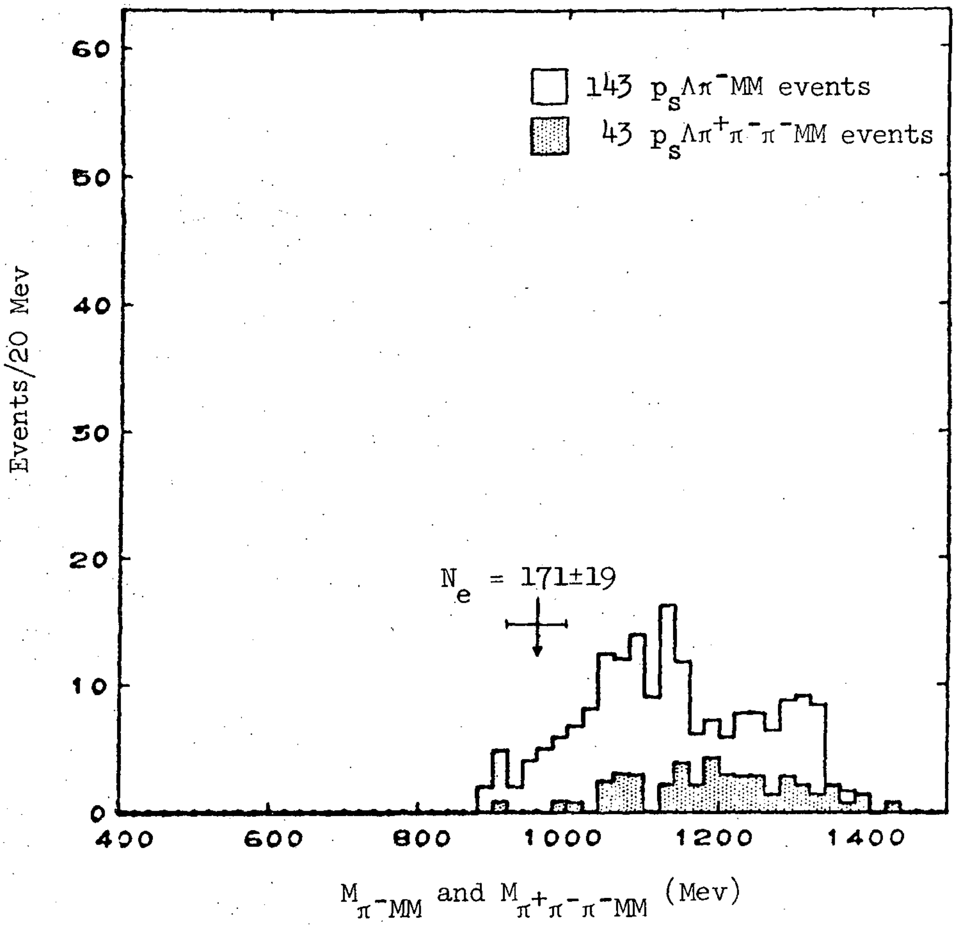

Figure 52. Plot of those events from Figure 51 which could be $\pi^-\pi^0\eta$ events: those π^-MM events with $MM \geq m_{\pi^0} + m_\eta$, and those $\pi^+\pi^-\pi^-MM$ events where at least one $\pi^+\pi^-$ mass combination satisfies $M_{\pi^+\pi^-} \leq m_\eta$. Again the arrow and cross-bar indicate where the N_e expected $\eta'^- \rightarrow \pi^-\pi^0\eta$ events would appear if $I_{\eta'}$ were 1.

Thus we present in Figure 53 histograms of the mass recoiling against the $p_s\Lambda$ system in the three reactions

$$
\begin{aligned}
K^- d &\rightarrow p_s \Lambda \pi^- \pi^o (\text{or } \gamma) \\
&\rightarrow p_s \Lambda \pi^+ \pi^- \pi^- \\
\text{and} \qquad &\rightarrow p_s \Lambda \pi^+ \pi^- \pi^- \pi^o (\text{or } \gamma) .
\end{aligned}
$$

These three reactions complete the possibilities for channels where an η'^- might be seen in conjunction with a Λ. It is clear from the plots that the 389 ± 35 η'^- events we would expect for $I_{\eta'} = 1$ are not present.

We conclude that, with a high degree of certainty, the isospin of the η' is zero.

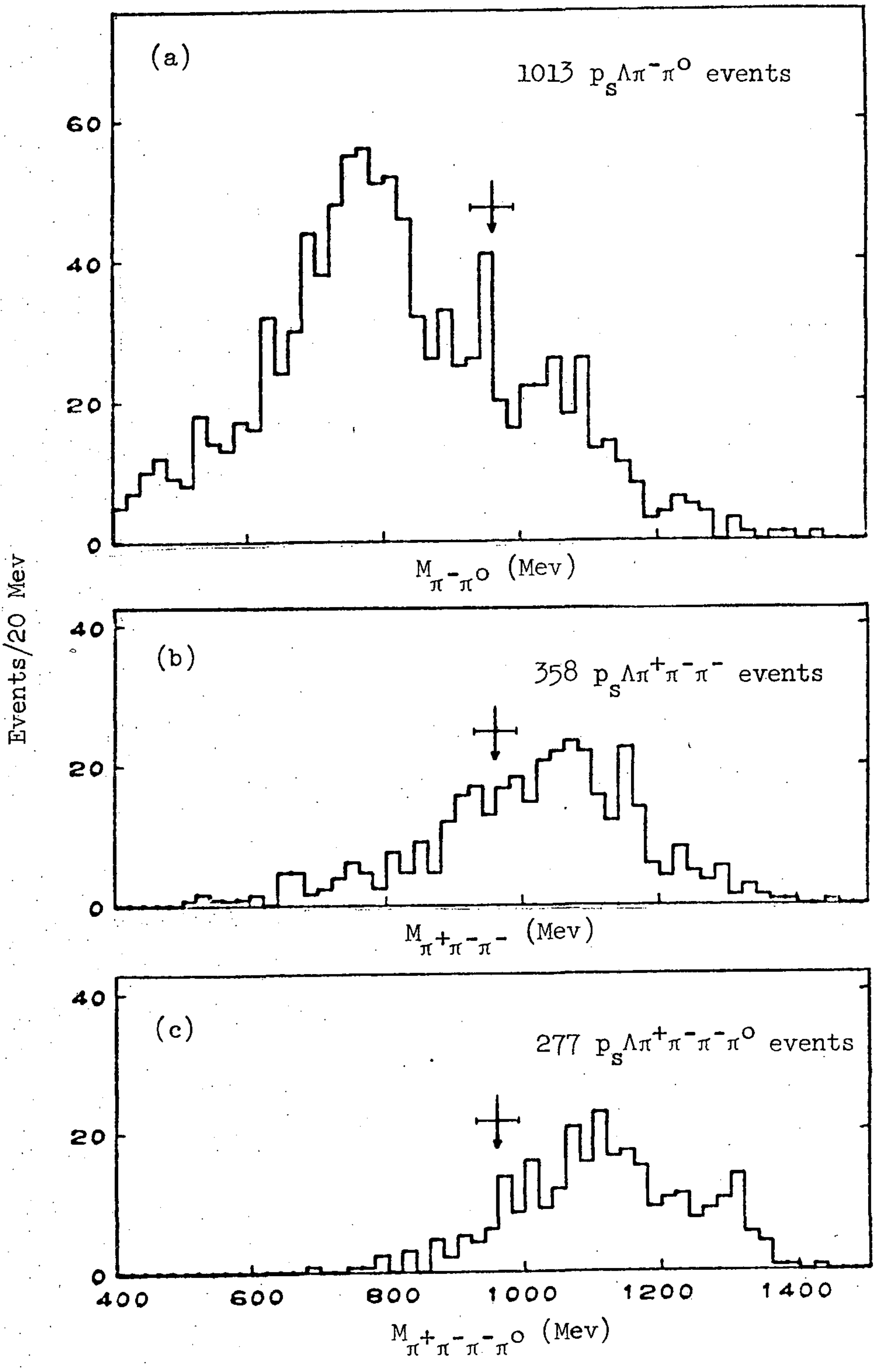

Figure 53. Plots of the mass recoiling against the $p_s\Lambda$ system in the deuterium final states (a) $p_s\Lambda\pi^-\pi^0$, (b) $p_s\Lambda\pi^+\pi^-\pi^-$, and (c) $p_s\Lambda\pi^+\pi^-\pi^-\pi^0$. Only events with $\Delta^2_{n\to\Lambda} \leq 0.7$ $(\text{Gev}/c)^2$ are shown. The arrows and cross-bars indicate where any η'^- events would appear.

IX. SU_3 CONSIDERATIONS

Assuming that our quantum number determination for the η' is correct, i.e., $I^G J^P = 0^+ 0^-$, the η' might then be considered as an SU_3 singlet, which would be expected to be mixed with the η, whose quantum numbers are the same. Using the masses $m_{\eta'} = 957$ Mev, $m_\eta = 548.8$ Mev, and $m_8 = 566.5$ Mev, where m_8 is the mass of the pure octet, $I = Y = 0$ pseudoscalar meson,[25] we would then have for the mass m_1 of the pure singlet, $I = Y = 0$ pseudoscalar meson

$$m_1 = \left[m_{\eta'}^2 + m_\eta^2 - m_8^2 \right]^{\frac{1}{2}} = 947 \text{ Mev} .$$

The mixing angle $\alpha_{\eta,\eta'}$ would then be

$$\alpha_{\eta,\eta'} = \tan^{-1} \left[\frac{m_8^2 - m_\eta^2}{m_{\eta'}^2 - m_8^2} \right]^{\frac{1}{2}} \cong 10^\circ .$$

This is to be contrasted with the much larger value $\alpha_{\phi,\omega} \cong 38^\circ$ involved in ϕ - ω mixing.[30]

It has been pointed out[25] that η - η' mixing, even if small, could have a significant effect on the radiative decay modes of the η'. In particular, it would perturb the branching ratio $(\eta' \rightarrow \omega\gamma)/(\eta' \rightarrow \rho\gamma)$ from the value of 0.08 which it would be expected to have if the η' were a pure SU_3 singlet and assuming that the electromagnetic field transforms like the T_3^3 member of an octet. Unfortunately we cannot measure this ratio very accurately because $\omega\gamma$ events would appear in the final state $\Lambda\pi^+\pi^-$MM, where, as pointed out earlier, the background is difficult to estimate. Further, the same final state contains the $\pi^0\pi^0\eta_C$ decay mode of the η'. Taking the latter events into account (by using isotopic spin conservation and the observed amount of $\eta' \to \pi^+\pi^-\eta$), we set a one standard deviation upper limit of $(\eta' \to \omega\gamma)/(\eta' \to \rho\gamma) < 0.04$.

We emphasize that this SU_3 discussion is purely speculative, since there is no direct experimental evidence that the η' is in fact a member of an SU_3 singlet. The situation is considerably muddied by the existence of the E(1420) meson, whose preferred quantum numbers are the same as those preferred for the η'.[31]

ACKNOWLEDGMENTS

This work would not have been possible without the large number of people who have contributed to the various phases of data production, reduction, and analysis. I would particularly like to thank Dr. Joseph J. Murray, who was primarily responsible for the beam design, Mr. Robert Watt and the members of the bubble chamber crew, and the corps of scanners, measurers, and librarians who were so necessary to the development of the data.

I would also like to thank Dr. George Kalbfleisch, who was largely responsible for the initial work on the η' in our data, and Dr. Angela Barbaro-Galtieri, who has been involved with the η' from the start and who has given me many useful suggestions. My thanks go to Dr. Donald Miller and Dr. Ronald Ross for their guidance, and to Dr. Luis Alvarez for his general encouragement given to the group.

This work was done under the auspices of the U. S. Atomic Energy Commission, and was supported in part by a National Science Foundation Fellowship.

FOOTNOTES AND REFERENCES

1. G. R. Kalbfleisch, L. W. Alvarez, A. Barbaro-Galtieri, O. I. Dahl, P. Eberhard, W. E. Humphrey, J. S. Lindsey, D. W. Merrill, J. J. Murray, A. Rittenberg, R. R. Ross, J. B. Shafer, F. T. Shively, D. M. Siegel, G. A. Smith, R. D. Tripp, Phys. Rev. Letters <u>12</u>, 527 (1964).
2. M. Goldberg, M. Gundzik, S. Lichtman, J. Leitner, M. Primer, P. L. Connolly, E. L. Hart, K. W. Lai, G. London, N. P. Samios, S. S. Yamamoto, Phys. Rev. Letters <u>12</u>, 546 (1964).
3. M. Goldberg, M. Gundzik, J. Leitner, M. Primer, P. L. Connolly, E. L. Hart, K. W. Lai, G. W. London, N. P. Samios, S. S. Yamamoto, Phys. Rev. Letters <u>13</u>, 249 (1964).
4. P. M. Dauber, W. E. Slater, L. T. Smith, D. H. Stork, H. K. Ticho, Phys. Rev. Letters <u>13</u>, 449 (1964).
5. G. R. Kalbfleisch, O. I. Dahl, A. Rittenberg, Phys. Rev. Letters <u>13</u>, 349a (1964).
6. J. Badier, M. Demoulin, J. Goldberg, B. P. Gregory, C. Pelletier, A. Rouge, M. Ville, R. Barloutaud, A. Leveque, C. Louedec, J. Meyer, P. Schlein, A. Verglas, D. J. Holthuizen, W. Hoogland, J. C. Kluyver, A. G. Tenner, Physics Letters <u>17</u>, 337 (1965).
7. J. J. Murray, J. Button-Shafer, F. T. Shively, G. H. Trilling, J. A. Kadyk, A. Rittenberg, D. M. Siegel, J. S. Lindsey, D. W. Merrill, UCRL-11426, 1964 (unpublished). See also D. W. Merrill, Alvarez Group Physics Memo 519, 1964 (unpublished), and S. M. Flatte, S. U. Chung, L. M. Hardy, R. I. Hess, Alvarez Group Physics

Memo 524, 1964 (unpublished).

8. M. Hutchinson, N. Joseph, M. Leavitt, Alvarez Group Programming Memo P-123, 1965 (unpublished).

9. The hydrogen path lengths are taken from P. M. Dauber, S. M. Flatte, J. H. Friedman, Alvarez Group Physics Memo 639, 1967 (unpublished).

10. For a description of the Franckensteins see M. Alston, J. V. Franck, L. T. Kerth, Chapter II of "Bubble and Spark Chambers", Vol. 2, Academic Press, New York (1967); for the SMP's, see W. E. Humphrey and R. R. Ross, UCRL-11425, 1964 (unpublished); for the Spiral Readers, see J. H Burkhard, L. J. Lloyd, G. R. Lynch, F. L. Hodgson, G. T. Armstrong, N. D. Travis, Proceedings of the 1965 International Conference on Programming for Flying Spot Devices, New York (1966) and J. Stedman, UCRL-16555, 1965 (unpublished).

11. G. R. Lynch, J. H. Burkhard, G. Armstrong, R. Carlson, F. T. Solmitz, The Group A POOH Scrapbook (unpublished); see also the Spiral Reader part of Reference 10.

12. M. Alston, J. P. Berge, J. Braley, J. Campbell, R. J. Harvey, M. Hutchinson, T. Schneider, Alvarez Group Memo 358, 1963 (unpublished).

13. For a description of PANG, the geometric reconstruction section of PACKAGE, see W. E. Humphrey, Alvarez Group Physics Memo 111, 1959 (unpublished); for KICK, the kinematic fitting section, see A. H. Rosenfeld and J. N. Snyder, Rev. of Sci. Instr. 33, 181 (1962).

14. O. I. Dahl, G. R. Kalbfleisch, A. Rittenberg, L. D. Jacobs, Alvarez Group Programming Memo P-54, 1965 (unpublished).

15. O. I. Dahl and D. Johnson, Alvarez Group Programming Memo P-5, 1963 (unpublished).

16. N. Barash-Schmidt, A. Barbaro-Galtieri, L. R. Price, A. H. Rosenfeld, P. Soding, C. G. Wohl, M. Roos, G. Conforto, Rev. of Modern Physics 41, 109 (1969).

17. C. Zemach, Phys. Rev. 140, B97 (1965).

18. W. E. Humphrey and B. J. Cottrell, Alvarez Group Programming Memo P-6, 1966 (unpublished).

19. L. Brown and P. Singer, Phys. Rev. Letters 8, 460 (1962); L. Brown and P. Singer, Phys. Rev. 133, B812 (1964).

20. Columbia-Berkeley-Purdue-Wisconsin-Yale Collaboration, Phys. Rev. 149, 1044 (1966).

21. The rules for formulating relativistically covariant electromagnetic decay matrix elements were obtained from a series of lectures given by Dr. D. Beder in a University of California Physics 245 course in February, 1967.

22. See Reference 16 for a compilation of data on the δ meson.

23. D. Bollini, A. Buhler-Broglin, P. Dalpiaz, T. Massam, F. Navach, F. L. Navarria, M. A. Schneegans, A. Zichichi, Nuovo Cimento 58A, 289 (1968).

24. S. K. Kundu and D. C. Peaslee, Nuovo Cimento 36, 277 (1965).

25. R. H. Dalitz and D. G. Sutherland, Nuovo Cimento 37, 1777 (1965).

26. G. W. London, R. R. Rau, N. P. Samios, S. S. Yamamoto, M. Goldberg, S. Lichtman, M. Primer, J. Leitner, Phys. Rev. 143, 1034 (1966). We have enlarged the η' cross section given in this reference by a factor of 1.14 to take account of events at large production angles (high Δ^2); for this purpose, we have used the $\pi\pi\eta$ production angular distribution given in Figure 19 of the reference and assumed

negligible background.

27. R. Davis, R. Ammar, J. Mott, S. Dagan, M. Derrick, T. Fields, Physics Letters 27B, 532 (1968).

28. A. Barbaro-Galtieri, M. Matison, A. Rittenberg, F. T. Shively, Phys. Rev. Letters 20, 349 (1968). Other deuterium searches for a charged η' have been reported by H. J. Martin Jr., R. R. Crittenden, L. S. Schroeder, Physics Letters 22, 352 (1966) and R. Barloutaud *et al.* (S.A.B.R.E. Collaboration), Physics Letters 26B, 674 (1968); these two searches also find $I_{\eta'} = 0$.

29. R. J. Glauber, Phys. Rev. 100, 242 (1955); V. Franco and R. J. Glauber, Phys. Rev. 142, 1195 (1966).

30. J. J. Sakurai, Phys. Rev. 132, 434 (1963).

31. See Reference 16 for a listing of the papers dealing with the E(1420) meson.